Fabrication and Properties Evaluation of CF/Al Composites for High Thermal Conductivity CF/Al

March 2012

Moonhee Lee

Fabrication and Properties Evaluation of CF/Al Composites for High Thermal Conductivity

Dissertation for the Degree of

Doctor of Philosophy

Department of Mechanical System Engineering
Graduate School of Engineering
Hiroshima University, Japan

Prof. Gen Sasaki, Advisor

Moonhee Lee

March 2012

CONTENTS

Chapter 1   Background and Objective

Chapter 2   Fabrication process and characterization of unidirectional CF preform by spark sintering method

Chapter 3   Fabrication process and characterization of unidirectional CF/Al composites by low pressure infiltration method

Chapter 4   Thermal and mechanical properties of the unidirectional CF/Al composites fabricated by LPI process

List of Figures

List of Tables

Chapter 1

Background and Objective

1.1 Introduction

In recent years, the fields of avionics, portable electronic devices, aerospace vehicles and automobiles have made remarkable development with the invention and innovation of the technologies. They have demanded the high performance components with the miniaturization and light weight. With the increase of the electric power levels, the developed electric and electronic components, in particular, became high heat generation parts which were needed the high performance thermal management materials called heat sink or thermal dissipation materials for the stable and efficient operation. The heat sink materials were basically required high thermal conductivity (TC) and coefficient of thermal expansion (CTE) matching to the heat generation components. The conventional heat sink materials were difficult to satisfy both of them. On the other hand, the newly developing composite materials can be attained the tailorable TC and CTE by controlling the addition of the reinforcement in matrix. Among the composite materials such as metal matrix composites (MMCs), ceramic matrix composites (CMCs) and plastic matrix composites (PMCs), the MMCs have been developed for the thermal management applications with the high TC, CTE matching and cost effective. Especially, the use of light metals as the matrix in composites was able to accomplish the weight saving in applications. The Al exhibited relatively high TC among metals and about 1/3 weight of steels, even if the CTE of Al was much higher than that of the electronic components such as semiconductors. Besides, the recently developed carbon fibers (CFs) have shown excellent TCs with low CTE, high strength and light weight. Therefore, the high thermal conductive CF/Al composites are expected to replace the conventional heat sink materials with high TC, tailorable CTE, light weight and good workability. Meanwhile, the development of the fabrication process for composites is one of the important parameter in terms of the productivity which is directly connected to the cost. The typical casting process for the MMCs limited the degree of freedom on the shape of composites and raised the

production cost by using high pressures. However, the casting process using low pressures for the MMCs enables the cost effective fabrication as well as the complex shape. Therefore, the CF/Al composites fabricated by the low pressure casting process can be competitive materials in the thermal management parts.

1.2 Trends of MMCs for thermal management

1.2.1 Applications for thermal management materials

In the electric and electronic component fields, the components have been becoming high power capacity according to increasing power consumption with the industrial development. Especially, with developing the hybrid electric vehicle (HEV) systems or electric vehicle (EV) systems in the transportation fields, the electric and electronic components have been required not only high power capacity of the components but also miniaturization and light weight.

Recently, many kinds of electrics or electronics related companies in the world have developed high power devices and their cooling systems [1-10]. In Japan, Mitsubishi Electric Corp. has produced many kinds of transistors such as metal oxide semiconductor field effect transistor (MOSFET), insulated gate bipolar transistor (IGBT), high voltage IGBT (HVIGBT) modules and intelligent power module (IPM) to apply the various power level ranges of the power devices [1]. Moreover, Denso Corp. has developed the battery electronic control unit (ECU) for HEV to maintain the desired state of charge levels and prevent over-charge or discharge of the main battery [2]. There also produces the converters for HEV. In the developing the power related systems, the development of the electric and electronic components is also in progress in republic of Korea. Hyundai MOBIS is producing the high power battery pack, converter and inverter for HEV [3] and KEC Holdings keep developing the IGBT and MOSFET products [4]. The representative components production companies for the transportation in the USA are Visteon Corp. and Delphi Automotive LLP. The Visteon Corp. [5] has manufacturing the high efficiency radiators for the optimized heat transfer, the heat exchangers for the high efficiency powertrain cooling systems and air conditioning systems. Besides, there has also developed the hybrid thermal management systems for the hybrid powertrain cooling systems in HEV and battery cooling modules for HEV or EV in order to maintain low temperature and improve the battery life. Delphi

Automotive LLP [6] is manufacturing not only air conditioning devices but also the newly developed powertrain systems including the inverter, converter, battery cooling system and power electronic cooling systems for HEV or EV. MAGNA International Inc. from Canada is giving force to develop the lithium-ion battery and HEV or EV modules including powertrain, power electronics and chargers [7]. In EU countries, SEMIKRON International GmbH from Germany has developed the IGBT, MOSFET and diode modules [8]. Robert Bosch GmbH from Germany also has produced the systems for EV including the inverter, battery charger and high voltage battery [9]. Besides, the GAIA Converter company from France, which is manufacturing the converter products mainly for aerospace, military and transportation applications, has developed various kinds of converters [10]. The applications for the thermal management are summarized in Table 1-1.

These kinds of newly developed electric and electronic related components usually face to inevitable high heat generation. Thus, the development of the high performance materials with high TC and stable range of CTE for the thermal management is required to replace the conventional heat sink materials. Besides, the innovative fabrication process on those materials has to be introduced for the improvement of productivity.

Table 1-1 Applications for the thermal management materials.

Company	Application	Country	
Denso	- Hybrid vehicle components: Battery ECU, DC-DC converter, Integrated starter generator, Electric compressor	Japan	Asia
Hyundai MOBIS	- Hybrid vehicle components: High power battery, Inverter, Converter, Engine, etc.	Korea	
KEC	- Electric components: MOSFET, IGBT, BJT, etc.	Korea	
Mitsubishi Electric	- Power related modules: IGBT modules, HVIGBT modules, Power MOSFET modules, IPM, etc.	Japan	
Delphi	- Thermal systems: Condenser, Evaporator, Heat pump coil - Hybrid & Electric vehicle systems(Power train systems): DC-AC inverter, DC-DC converter, Battery controller, High voltage bttery pack, Battery cooling (air, liquid), Power electronics cooling	United States	America
MAGNA	- Hybrid & Electric vehicle: Hybrid & Electric vehicle integration, Power battery packs, Energy battery packs	Canada	
Visteon	- Heat exchangers: Air conditioning, Power train cooling systems, High efficiency radiator - Hybrid & Electric vehicle: Battery cooling module, Hybrid powertrain cooling systems	United States	
GAIA Converter	- Various kind of converters for Aerospace, Military and Transport applications	France	Europe
Bosch	- Hybrid & Electric vehicle systems: Inverter, Battery charger, High voltage battery	Germany	
SEMIKRON	- Power related modules: IGBTmodules, IPM, CIB, MOSFET, Thyristor modules, etc.	Germany	

6

1.2.2 Development status of thermal management materials

The efforts to resolve the heat generation problems of the developing electric and electronic related components have been in progress from all over the world. In particular, some companies in the USA and Japan have concentrated on developing the thermal management materials. A.M. Tech Co., Ltd. [11], Hitachi Metal Admet, Ltd. [12], A.L.M.T. Corp. [13] and Nihon Ceratec Co., Ltd. [14] from Japan have developed and produced diverse composite materials with high performance thermal dissipation for the heat sink applications. Those companies mainly developed SiC/Al, C/Al and SiC/Si composites for the heat sink. The heat sink materials depending on the applications in Japanese companies are summarized in Table 1-2. Some companies in the USA also focused on developing the heat sink materials. CPS Technologies Corp. [15] has mainly manufactured various AlSiC series, which is made of the different composition between SiC and Al in SiC/Al composites, for the application fields such as the power modules and optoelectronics. Plansee, SE. [16] also has manufactured the heat sink materials such as W/Cu and Mo/Cu composites for optoelectronics, lasers, microwave applications and high performance chips. MMCC, LLC. [17] has mainly produced Al METGRAF^{TM}, Cu METGRAF^{TM} and AlGrp^{TM} by inserting the graphite fibers or platelets in Al or Cu matrix. The development status of heat sink materials in those companies is also summarized in Table 1-2.

7

Table 1-2 Development status of heat sink materials.

Company	Applications	Materials	Country
A. L. M. T.	- Automobile: IGBT substrate - IC parts: ceramic packaging substrate - Microwave parts: packaging substrate - Light emitting parts: heat sink	SiC/Al, SiC/Si composites	Japan
A. M. Tech.	- Heat sink for power devices, microwave devices, telecommunication devices, semiconductors, MPU, IGBT	SiC/metal(Al, Mg), C/metal(Al, Mg, Cu) composites	
Nihon Ceratec	- Heat sink of table or hand for LCD fabrication devices - Heat sink of structural materials for semiconductor fabrication devices	SiC/Al, SiC/Si composites	
Hitachi Metals Admet	- Heat sink for power devices, microwave devices, telecommunication devices, semiconductors, MPU, IGBT	SiC/metal (Al, Mg) composites	
CPS Technologies	- Flip chip lids, microwave packaging, opto-electronics, power applications (IGBT base plates, power substrates, power module coolers)	SiC/Al composites	United States
MMCC	- Heat sink for telecommunications, HEV, power semiconductor, opto-electronics, military and aerospace, heavy transportation, space systems, satellites	Gr/metal (Al, Cu) composites	
Plansee	- Heat sink for opto-electronics and lasers, microwave applications, high performance chips	W/Cu, Mo/Cu composites	

1.3 Previous studies on MMCs for thermal management

The many efforts have been made to manage the heat generation in newly developed electric and electronic devices in order to maintain the efficient operation conditions of those devices. Especially, the electric power related components generally contain the semiconductor materials. The semiconductors are the main cause of the heat generation when the electric and electronic devices operate, and have to be maintained their temperature ranges for the efficient operation. The thermal properties of the representative semiconductors are listed in Table 1-3. The semiconductors have various TC values and densities depending on the material types. However, there are needed to pay attention to the CTEs of semiconductors. The semiconductors have low CTEs with the range from 2.8 to $5.9 \times 10^{-6} \text{K}^{-1}$. Thus, the heat sink materials attaching directly to the semiconductors are required the CTE matching as well as the high TC.

Table 1-3 Thermal properties of several semiconductor materials.

Material	Density (Mgm^{-3})	CTE ($\times 10^{-6} \text{K}^{-1}$)	TC ($\text{Wm}^{-1}\text{K}^{-1}$)	Reference
Silicon (Si)	2.3-2.34	2.8-4.2	139-150	[18-22]
Silicon carbide (SiC)	3.1-3.21	2.8-5.0	80-490	[19-21]
Gallium arsenide (GaAs)	5.3	5.8-5.9	46-58	[19, 20]
Gallium nitride (GaN)	6.1	3.2	150	[20]

Many of monolithic thermal management materials have been developed and applied in the industrial field. However, the conventional heat sink materials had considerable difficulties to satisfy both CTE matching and high TC. As shown in Table 1-4, Cu and Al have high TCs but their CTEs cannot match to semiconductors. Meantime, Invar, Kovar, Al_2O_3, Mo and W have low CTEs but low TCs. AlN, SiC and BeO, however,

show good properties but those monolithic ceramics or oxide materials are hard to machining.

Table 1-4 Thermal properties of conventional electronic packaging materials [18-23].

Material	CTE at 273K ($\times10^{-6}$K^{-1})	TC (Wm^{-1}K^{-1})
Aluminum	22.3	237
Copper	16.5-17	398-400
Alumina	6.7	20-21
Beryllia	8	275
Aluminum nitride	3.3-4.5	125-250
Silicon carbide	2.8-5.0	80-490
Invar (Fe-36Ni)	1.6	10
Kovar (Fe-29Ni-17Co)	5.9	17
Molybdenum	5.0	140
Tungsten	4.5	168

On the other hand, the composite materials, especially MMCs, are considered for the promising heat sink materials due to their high TC and good cost performance, whereas the CMCs need high fabrication costs due to high temperature of the fabrication process and the PMCs have too low melting point of matrix to apply at the high heat generation objects. The candidate materials for the fabrication of MMCs are listed in Table 1-5. The most of the matrices excluding Al show the relatively high density with high CTEs. Besides, the most of reinforcements have relatively or extremely low CTEs with the low density. Especially, the carbon based materials such as diamond, CF, CNT and VGCF show excellent TCs with extremely low CTEs and densities.

The tailorable thermal or physical property is biggest advantages to use the composite materials. Therefore, the adequate composition ratio between the reinforcement and matrix is required to accomplish the high TC, CTE matching and light weight. Fig. 1-1 shows the TCs of the various heat sink materials used in electronic packaging as a function of their CTEs. Most CTEs of the MMCs such as Diamond/Cu, C/Cu, C/Al and SiC/Al composites matched to the CTEs of the semiconductors which were

approximately ranged from 4 to $7 \times 10^{-6}K^{-1}$. However, the MMCs show the wide range of TCs depending on the different composition of the materials. Table 1-6 shows the thermal properties of the diverse MMCs for heat sink applications. The MMCs are widely classified as SiC, diamond and CF reinforced composites.

Table 1-5 Thermal properties of various materials for the application of composite materials in electronic packaging materials.

Material	Density (Mgm^{-3})	CTE ($\times 10^{-6}$K^{-1})	TC (Wm^{-1}K^{-1})	Reference
Reinforcement				
Diamond	3.5	2.3	1300-1800	[20]
Silicon carbide (SiC)	3.1-3.21	2.8-5.0	80-490	[19-21]
Aluminum oxide (Al$_2$O$_3$)	3.9	6.7	20	[18, 20, 22]
Aluminum nitride (AlN)	3.26-3.3	3.3-4.5	125-250	[19, 20, 23]
Beryllium (Be)	1.85	12	194	[21]
Boron carbide	2.52	3.5	39	[21]
Carbon fiber (CF)	2.21	-1.2	800	Mitsubishi
Carbon nano tube (CNT)	2	-1	6600	[20]
Vapor grown CF (VGCF)	1.8-2	-1	1950	[20]
Tungsten	19.3	4.5	180	[20]
Matrix				
Aluminum	2.7	22.3-23	230-237	[18, 19, 22]
Copper	8.9	16.5-17	398-400	[18, 19, 22]
Silicon carbide (SiC)	3.1-3.21	2.8-5.0	80-490	[19-21]
Gold	19.3	14	316	[21]
Silver	10.5	19	431	[21]
Molybdenum	10.2	5	138	[21]

The diamond reinforced MMCs show high TC with low CTE due to the extremely high TC and low CTE properties of the diamond. In case of the SiC reinforced MMCs, the CTEs remarkably decreased by adding SiC in Al or Cu matrix in comparison with the monolithic Al or Cu. However, the high CTEs comparing to semiconductors

remains one of the problems to resolve. These kind of reinforcements have an disadvantage of bad workability, whereas carbon reinforcement shows excellent workability. The CF reinforced MMCs represented well matched CTEs to semiconductors because the extremely low CTEs of CFs could offset the high CTEs of matrix such as Al alloy or Cu. On the other hand, the TCs of CF reinforced MMCs did not improved comparing to Al or Cu. The problem can be expected to resolve by using newly developed CFs with high TCs.
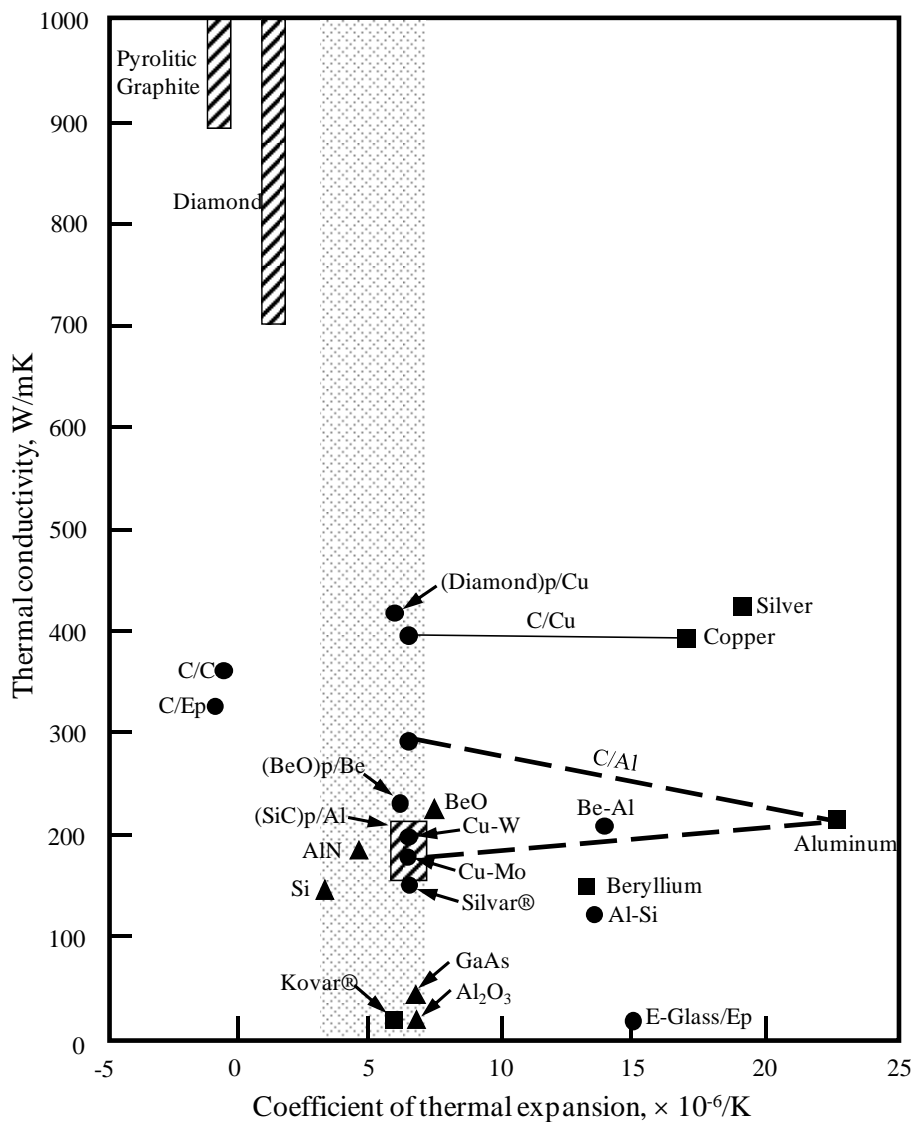
Fig. 1-1 Thermal conductivity as a function of CTE for materials used in electronic packaging [18, 24].

Table 1-6 Thermal properties of the various metal matrix composite materials.

Composite	Reinforcement	Vol.% of reinforcement	CTE ($\times 10^{-6} K^{-1}$)	TC ($Wm^{-1}K^{-1}$)	Reference
AlN/Al-Si alloy	AlN particle	56.5	8.9-10.8	95-110	[23]
SiCp/Cu	SiC particle	40	11.2-14.5	222-306	[25, 26]
SiCp/Cu	SiC particle	-	7.0-10.9	320	[27]
SiCp/Al	SiC particle	39-62	8.45-10.5	118-146	[28]
SiCp/Al	SiC particle	-	6.2-16.2	170-220	[27]
Dia/Al	Diamond	-	7.0-7.5	550-600	[27]
Dia/Cu	Diamond	-	5.8	600-800	[27]
Dia/Cu	Diamond	50	5.5	420	[20]
Dia/CuB	Diamond	60-80	-	300	[29]
CF/Al-Si alloy	Carbon fiber	55	2.8	131	[26, 30]
CF/Cu	Carbon fiber	28	6.5	290	[20]
Grp/Al-Si alloy	Graphite particle	67	11	118	[26, 30]
W/Cu	Tungsten	-	5.7-8.3	157-190	[27]

1.4 Fabrication processes of MMCs

Many fabrication processes for MMCs have been investigated to obtain high performance composites through the efficient fabrication route. The fabrication process of the MMCs is mainly divided into two routes: solid-state process and liquid-state process [31-40]. Fig. 1-2 represents the manufacturing processes for MMCs [31, 32].

Powder metallurgy (PM) is well known for the solid-state process. The PM process is generally introduced to the particles, flakes or short fibers reinforced metal composites [41-48]. Such reinforcements and metal powders are generally blended by ball milling or mixing. Subsequently, the mixture was sintered by pressureless sintering after cold pressing or sintered by hot pressing to consolidate each other and densification. The fabricated MMCs are subsequently treated by rolling, forging or extruding to final dimensions. The MMCs by PM process can be accomplished the high density by high pressurization. Moreover, the PM process enables the uniform dispersion of reinforcements in matrix by uniform blending of reinforcements and matrix powders before sintering. The PM process is suitable for the matrix of high melting point alloys which is difficult to use for the liquid-state process by their high melting point [26, 33]. In addition, the PM process is also appropriate for MMCs which contained too low volume fraction of reinforcements to make preform by liquid state process. In the industrial field, Plansee, SE. in USA [16] has developed the heat sink for the effective thermal management with high TC and low CTE which is close to semiconductors. The heat sink such as Mo/Cu composites was fabricated by PM process. The composites were rolled to give uniform CTE behavior in the sheet plane. However, the PM process has limitations: the high cost of matrix and reinforcement powders and not feasible for net-shape fabrication [26, 34].

On the other hand, the liquid-state process has been an attractive process for the MMCs fabrication. The process is mainly divided into two casting methods such as the stir casting and squeeze casting. Especially, the casting process for MMCs is generally introduced for the low melting point of matrix.
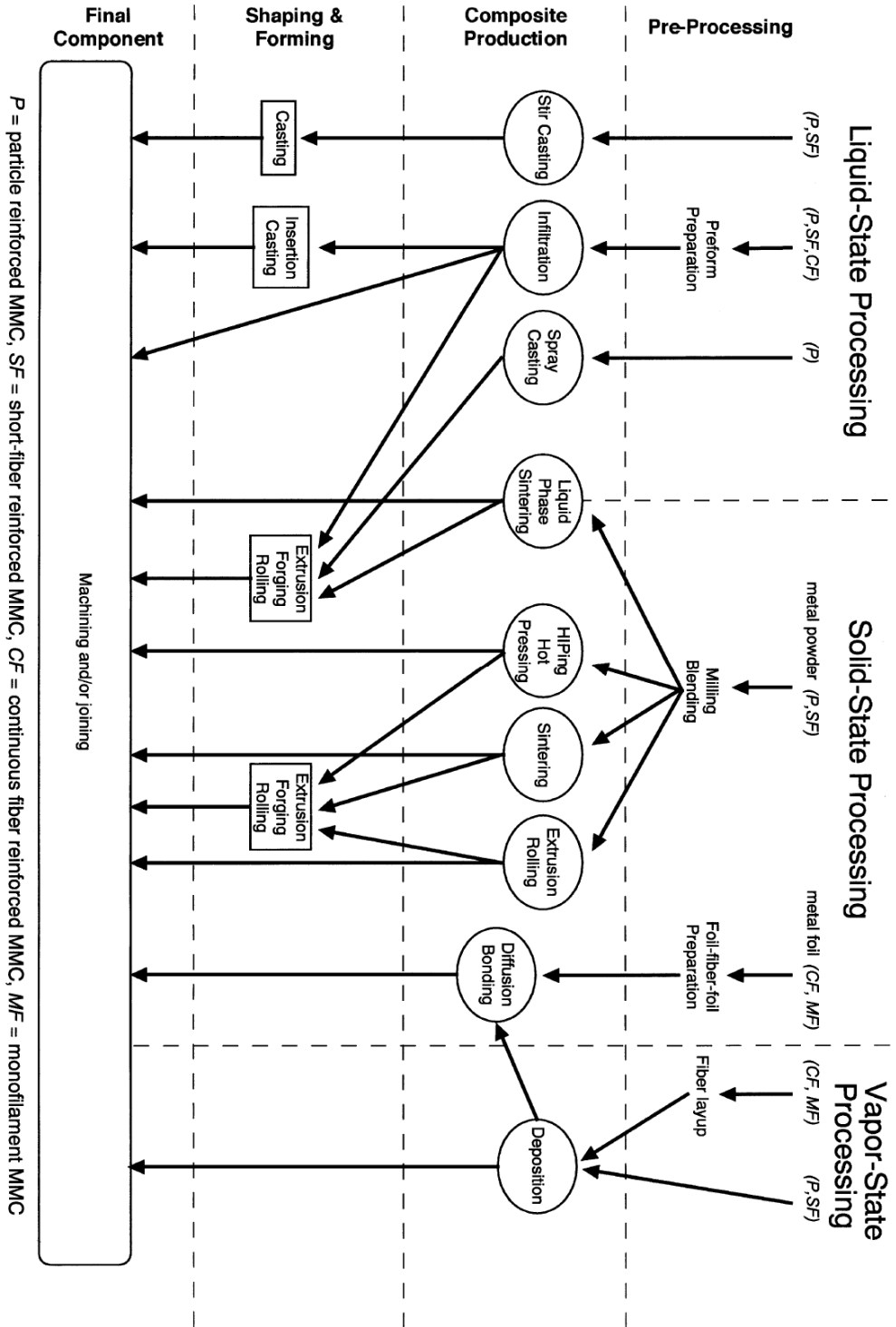
Fig.1-2 Manufacturing steps and different processes for the production of metal matrix parts [32]

The stir casting is one of the simple methods for the fabrication of MMCs: The reinforcements as the particles or short fibers are added into the molten metal and stirred without any additional pressures. This method has been adopted for wide applications such as automotive and other industrial fields due to the cost-effective fabrication [26, 34]. However, the stir casting has some disadvantages [26, 34, 35]: the high foundry and casting equipment cost, low ductility of the final product due to the agglomerated reinforcement in the matrix and lack of design information for use as engineered materials.

Many of the MMCs are difficult to fabricate without applied pressures by the bad wettability between the matrices and reinforcements [36-40]. The squeeze casting, recognized typical high pressure-assisted casting method have been used to the fabrication of MMCs through the pressure infiltration of molten metal as the matix into porous fiber preform as reinforcements [49-54]. A. M. Tech. Co., Ltd. [11] in Japan have manufactured the SiC/Al and F/Al composites by squeeze casting for the heat sink applications. Moreover, Nihon Ceratec Co., Ltd. [14] in Japan and MMCC, LLC. [17] in USA also employed the pressure casting method such as the squeeze casting to fabricate MMCs for heat sink materials. The squeeze casting enables the fast fabrication and high density of MMCs by using high pressures. Although such high pressure helps fast fabrication and densification of MMCs, the fabrication defects such as dimension instability or non-uniform distribution of fiber arrays when the infiltration is carried out. Moreover, the high pressure also disturbs the large or complex shape fabrication of MMCs.

1.5 Problems of previous studies and objective of this study

The previously studied MMCs in Table 1-6 for the heat sink in electric and electronic applications have mainly adopted the diamond, SiC and CF as reinforcement. Moreover, Cu and Al have usually used as matrix in order to exhibit their good properties in MMCs such as high TC of Cu and light weight and moderate TC of Al. However, there existed some defects to compensate. First of all, the diamond reinforced MMCs contained the high volume percent of reinforcement, even if there showed good TCs and CTEs by adding the diamonds of the extremely high TC and low CTE. Moreover, the diamonds of particle formation cannot exhibit their high TC enough in the composites due to loss of the thermal flow at many interfaces between diamonds and metals. Secondly, the SiC reinforced MMCs were required high volume fraction of SiC for the CTE matching to semiconductors of low CTEs, due to not so low CTE property of SiC. Besides, the TCs of the SiC reinforced MMCs showed not excellent TCs but similar to conventional TC ranges. Thirdly, the CF reinforced MMCs presented good CTEs because of the extremely low CTEs of CFs, but not good TCs. However, the disadvantage of low TC of the CF reinforced MMCs can be covered by using the newly developed pitch based unidirectional CFs in the MMC fabrication. On the other hand, the ceramic reinforcements such as diamond and SiC have too high hardness property to machining easily, whereas the CFs have good workability. In addition, the diamond is expensive, even if it has excellent thermal properties. In case of the decision of matrix, although the Cu as matrix in MMCs has showed higher TC than that of Al, the Cu has heavy weight.

The typical manufacturing process such as squeeze casting and PM for the fabrication of MMCs had some disadvantages by using high pressure. The high pressure limited the degree of freedom on the shape of the MMCs and raised the fabrication cost. Since many of the heat sink materials are required the complex fin structure, the MMCs fabricated by high pressure fabrication system are needed additional process such as

17

machining. Meanwhile, the manufacturing cost of MMCs also rose by using the complex and expensive high pressure apparatus and by high electricity cost to operate the high pressure apparatus. On the other hand, the fabrication process by LPI method is similar with the squeeze casting however it enables to fabricate the MMCs with extremely low pressure. It was reported that the low pressure casting also led to the complex and large shape fabrication of the MMCs [55-62]. Moreover, the low pressure-assisted apparatus was simple and helped keep the fabrication costs low. Therefore, the fabrication of MMCs with the newly developed unidirectional CFs of high TC and Al, in conjunction with the LPI process, can be competitive for the field of thermal management materials.

   In this study, the fabrication conditions for the unidirectional CF/Al composites by LPI process were investigated in the viewpoint of their optimization. Besides, the thermal and mechanical properties of the unidirectional CF/Al composites were characterized. Moreover, the suitability of the composites as heat sink materials was discussed.

1.6 Outline of this thesis

In Chapter 1, the trend of applications and the development status of the thermal management materials are reviewed. Moreover, from the problems of the previous studied thermal management materials, the direction of newly developing MMCs such as unidirectional CF/Al composites for heat sink is proposed.

Prior to fabricate the unidirectional CF/Al composites by LPI process, the fabrication process of the porous unidirectional CF preform for CF/Al composites is introduced in Chapter 2. In this chapter, the introduction of the bridging materials between CFs, fabrication route of the preform, characterization of the preform depending on the fabrication conditions and suitability of the preform for the fabrication of CF/Al composites are discussed.

In Chapter 3, the fabrication of the unidirectional CF/Al composites by LPI process is presented. Especially, the decision of the infiltration pressure of molten Al into porous unidirectional CF preform was carried out. Besides, the size control of the bridging material between CFs for high density and uniform fiber distribution are discussed.

The characterization of TC, CTE and mechanical properties on the unidirectional CF/Al composites is carried out in Chapter 4. The influences of the interfacial reactants between CF and Al on the TC of the composites are also studied. Finally, the suitability of the unidirectional CF/Al composites as heat sink materials is discussed.

The results from above mentioned investigation are summarized in Chapter 5.

References

[1] Mitsubishi Electric Corp., Japan, Available at. http://www.mitsubishielectric.co.jp (accessed 11.11.04).

[2] Denso Corp., Japan, Available at. http://www.globaldensoproducts.com/hvc/ (accessed 11.11.04).

[3] Hyundai MOBIS, Korea, Available at. http://www.mobis.co.kr/ (accessed 11.11.30).

[4] KEC Holdings, Korea, Available at. http://www.kec.co.kr/ (accessed 11.11.29).

[5] Visteon Corp., USA, Available at. http://www.visteon.com/products/climate.html (accessed 11.11.04).

[6] Delphi Automotive LLP, USA, Available at. http://delphi.com/manufacturers/auto/ (accessed 11.11.04).

[7] MAGNA International Inc., Canada, Available at. http://www.magnasteyr.com/ (accessed 11.11.04).

[8] SEMIKRON International GmbH, Germany, Available at. http://mobile.semikron.com/imps-semikron/ (accessed 11.11.04).

[9] Robert Bosch GmbH, Germany, Available at. http://www.bosch-automotive technology.com (accessed 11.11.04).

[10] GAIA Converter, France, Available at. http://www.gaia-converter.com/company/references.php (accessed 11.11.04).

[11] A.M. Tech Co., Ltd., Japan, Available at. http://www.amtech.co.jp/sitemap.htm (Accessed 11.11.04).

[12] Hitachi Metal Admet, Ltd., Japan, Available at. http://www.hitachi-m-admet.com/electro_material/mmc2.html / (Accessed 11.11.04).

[13] A.L.M.T. Corp., Japan, Available at. http://www.allied-material.co.jp/products/tungsten/heat sink/heatsync/ (Accessed 11.11.04).

[14] Nihon Ceratec Co., Ltd., Japan, Available at. http://www.ceratech.co.jp/product/01_03.html (Accessed 11.11.04).

[15] CPS Technologies Corp., USA, Available at. http://www.alsic.com/alsic-thermal -management-packaging.html (Accessed 11.11.04).

[16] Plansee, SE., USA, Available at. http://www.plansee-tms.com/Plansee_TMS_ MATERIALS.htm (Accessed 11.11.04).

[17] MMCC, LLC., USA, Available at. http://www.mmccinc.com/APIC.htm (Accessed 11.11.04).

[18] C. Zweben: JOM, **50** (1998) 47-51.

[19] S. Jin: JOM, **50** (1998) 46.

[20] J. Barcenaa, J. Maudes, M. Vellvehi, X. Jorda, I. Obieta, C. Guraya, L. Bilbao, C. Jimenez, C. Merveille, J. Coleto: Acta Astron., **62** (2008) 422-430.

[21] Chris H. Stoessel, J.C. Withers, C. Pan, D. Wallace, R.O. Loutfy: Surf. Coat. Tech., **76-77** (1995) 640-644.

[22] R. Lasky: Electronic Packaging and Production, **1** (1998) 64-66.

[23] R. Couturier, D. Ducret, P. Merle, J. P. Disson and P. Joubert: J. Euro. Cera. Soc., **17** (1997) 1861-1866.

[24] C. Zweben, Mechanical Engineers' Handbook, 2nd ed., ed. M. Kuntz, John Wiley & Sons, (1998).

[25] Th. Schubert, B. Trindade, T. Weisgärber, B. Kieback: Mater. Sci. Eng. A, **475** (2008) 39-44.

[26] S. Mallik, N. Ekere, C. Best, R. Bhatti: App. Therm. Eng., **31** (2011) 355-362.

[27] X. B. HE, X. H. Qu, S. B. Ren, C. C. Jia: Sci. China Ser. E-Tech. Sci., **52** (2009) 238-242.

[28] J. Liu, Z. Zheng, J. Wang, Y. Wu, W. Tang, J. Lü: J. Alloys. Compd., **465** (2008) 239-243.

[29] X. Yang, S. Yue-qing, L. Chen-guang, C. Shun, F. Zhen-zheng: Trans. Nonferrous Met. Soc. China, **19** (2009) 1161-1166.

[30] R. Prieto, J.M. Molina, J. Narciso, E. Louis: Scripta Mater., **59** (2008) 11-14.

[31] H. P. Degischer, P. Prader, C. S. Marchi: Composites A, **32** (2001) 1161-1166.

[32] A. Mortensen, C. San Marchi, H. P. Degischer: MMC-Assess Thematic Network, Vol.1, Available at. http://mmc-assess.tuwien.ac.at/public/v1_glossary.pdf (accessed 11.12.07).

[33] E. Delannay, C. Colin, Y. Marchal, L. Tao, F. Boland, P. Cobzaru, B. Lips, M.A.

Dellis: J. De Physique IV, **3** (1993) 1675-1685.

[34] Technologies Research Corporation, USA, Aluminium metal matrix composites technology roadmap, Available at. http://www.almmc.com/AlMMCRoadmapMay 2002.pdf (2002) (accessed 11.12.07).

[35] N.H. Babu, S. Tzamtzis, N. Barekar, J.B. Patel, Z. Fan: Solid State Phenomena, **141-14**3 (2008) 373-378.

[36] Ram B. Bhagat: Mater. Sci. Eng. A, **144** (1991) 243-251.

[37] A. Mortensen and J. A. Cornie: Metall. Trans. A, **18** (1987) 1160-1163.

[38] A. Mortensen, J. A. Cornie, M. C. Flemings: JOM, **40** (1988) 12-19.

[39] A. Mortensen, M. N. Gungor, J. A. Cornie and M. C. Flemings: JOM, **38** (1986) 30-35.

[40] S. Nourbakhsh, E L. Liang and H. Margolin, Adv. Mater. Manuf. Proc., **3** (1988) 57-78.

[41] L. Jiang, Z. Li, G. Fan, D. Zhang: Scripta Mater., **65** (2011) 412–415.

[42] Z.Y. Liu, Q.Z. Wang, B.L. Xiao, Z.Y. Ma, Y. Liu: Mater. Sci. Eng. A, **527** (2010) 5582-5591.

[43] M. F. Moreno, C. J. R. González Oliver: Powder Technology, **206** (2011) 297–305.

[44] S. T. Mileiko, A. A. Khvostunkov, V. M. Kiiko, M. V. Gelachov: Compo. Sci. Tech., **59** (1999) 873-877.

[45] A. Olszówka-Myalska, J. Szala, J. Cwajna: Mater. Char., **46** (2001) 189-195.

[46] S. F. Moustafa, S. A. El-Badry, A. M. Sanad, B. Kieback: Wear, **253** (2002) 699-710.

[47] Q. C. Jiang, H. Y. Wang, B. X. Ma, Y. Wang, F. Zhao: J. Alloys. Compd., **386** (2005) 177-181.

[48] H. Wang, R. Zhang, X. Hu, C. -A. Wang, Y. Huang: J. Mater. Proc. Tech., **197** (2008) 43-48.

[49] T. Shalu, E. Abhilash, M. A. Joseph: J. Mater. Proc. Tech., **209** (2009) 4809-4813.

[50] S. Ravi Kumar, M. K. Panigrahi, S. K. Thakur, K. U. Kainer, M. Chakraborty, B. K. Dhindaw: Mater. Sci. Eng. A, **415** (2006) 207-212.

[51] B. Moser, A. Rossoll, L. Weber, O. Beffort and A. Mortensen: Composites A, **32**

(2001) 1067-1075.

[52] B. Wielage and A. Dorner: Surf. Coat. Tech., **108-109** (1998) 473-478.

[53] R. J. Sample, R. B. Bhagat and M. F. Amateau: J. Compo. Mater., **23** (1989) 1021-1028.

[54] J. M. Molina, R. Prieto, J. Narciso and E. Louis: Scripta Mater., **60** (2009) 582-585.

[55] Y. B. Choi, G. Sasaki, K. Matsugi, O. Yanagisawa: Mater. Trans., **46** (2005) 2156-2158.

[56] Y. B. Choi, G. Sasaki, K. Matsugi, N. Sorida, S. Kondoh, T. Fujii, O. Yanagisawa: JSME A, **49** (2006) 20-24.

[57] Y. B. Choi, K. Matsugi, G. Sasaki, K. Arita, O. Yanagisawa: Mater. Trans., 47 (2006) 1227-1231.

[58] Y. B. Choi, K. Matsugi, G. Sasaki, S. Kondoh: Mater. Trans., **49** (2008) 390-392.

[59] K. Matsugi, Y. B. Choi, K. Arita, O. Yanagisawa, G. Sasaki: J. Jpn. Inst. Light Met., **58** (2008) 71-80.

[60] A. Daoud: Mater. Sci. Eng. A, **391** (2005) 114-120.

[61] E. Carreño-Morelli, T. Cutard, R. Schaller and C. Bonjour: Mater. Sci. Eng. A, **251** (1998) 48-57.

[62] J. M. Molina, M. Rheme, J. Carron and L. Weber: Scripta Mater., **58** (2008) 393-396.

23

Chapter 2

Fabrication process and characterization of unidirectional CF preform by spark sintering method

2.1 Introduction

Recently, many kinds of metal matrix composites (MMCs) have been developed for the thermal management applications with the tailorable coefficient of thermal expansion (CTE), thermal conductivity (TC) and cost effectiveness [1-14]. Meanwhile, the pitch based carbon fibers (CFs) are one of the excellent reinforcement materials to manufacture the MMCs because of their high TC, low coefficient of thermal expansion, excellent mechanical properties and light weight [15-19]. In addition, the unidirectional long CFs facilitate the high performance of thermal conduction in the composites with the efficient thermal flow through the CFs of high TC. As a result, pitch based unidirectional CFs reinforced Al matrix composites are one of the promising materials for the thermal management applications.

In order to fabricate unidirectional CF/Al composites, the low pressure infiltration (LPI) process has many advantages such as simple facilities, cost effective and complex shape fabrication using low applied pressure [20-27]. Under LPI process, the unidirectional CF/Al composites are fabricated by means of molten Al infiltration to porous CF preform. Therefore, prior to the fabrication of unidirectional CF/Al composites by the LPI process, the unidirectional CF preform has to be prepared. However, the porous preform with unidirectional fibers is hard to fabricate because of the difficulty of controlling the long fibers without fiber clustering. Moreover, the unidirectional CF preform is required not only to maintain the uniform or proper conduit size between CFs for the smooth flow of molten Al but also to exhibit the higher compressive strength than the applied infiltration pressure. In order to obtain well dispersed CFs and maintain the porous and aimed strength property of CF preform, the introduction of the fiber-bridging can be considered in this study. Besides, the preparation route such as the selection of the bridging materials, the way to disperse them uniformly into the CF arrays and fabrication conditions by sintering to play a role

of bridging between CFs has to be established to obtain high performance unidirectional CF preform. On the other hand, the examination of the compressive strength on the unidirectional CF preform is needed to evaluate the suitability for the LPI process.

In this study, the fabrication process for unidirectional CF preform with the addition of Cu particles as bridging materials has been investigated, in conjunction with the adoption of the spark sintering method. Especially, the effect of sintering temperature on the sintering phenomena and the roles of bridging materials into the unidirectional CF bundles also discussed, in conjunction with the observation of the microstructure of the preform. Besides, the compression strength property of the CF preform has been evaluated by compression test in order to confirm the suitability on the durability against the infiltration pressure range of below 1 MPa at the LPI process.

2.2 Experimental procedure

2.2.1 Raw materials

In order to fabricate unidirectional CF preform by spark sintering process, CFs and bridging materials have to be prepared. The coal tar pitch based unidirectional CFs, K13D2U CFs, were used in this study which have purchased from Mitsubishi Plastics, Inc. The K13D2U CFs have high tensile strength and low CTE with excellent TC [28]. However, there are too many candidates to decide the bridging materials between unidirectional CFs, such as ceramics and metals. The ceramics have bad workability, even if they have light weight. Thus, the ceramics were excluded from the candidates as bridging materials. The important factors to determine the metal elements as bridging materials are classified as TC, melting temperature and reactivity to CFs. Especially, the TC of Al-X alloys (X: bridging materials in this study) [29-35] is more important than that of the original bridging materials because the matrix of unidirectional CF/Al composites consists of the element of Al and bridging material by infiltrating Al into unidirectional CF preform. The TC of various Al alloys was shown in Fig. 2-1. The industrial pure Al (A1 1000 series) had high TC of about 240 $Wm^{-1}K^{-1}$. In addition, the Al alloys containing the composition elements of Cu, Mn, Mg and Zn had relatively low TC ranged from 132 to 191 $Wm^{-1}K^{-1}$ because of the influence of each intermetallic compounds of low TC. However, their thermal conductivities were not big difference.

As a result, the reactivity to CFs and the melting temperature of the bridging materials can be an important factor to determine the bridging materials for unidirectional CF preform. The generation of the reactants between CFs and bridging materials on the fabrication stage of the unidirectional CF preform enables to degrade the mechanical and thermal properties of CFs on the viewpoint of CF degradation. Moreover, the lower melting temperature of the bridging materials than Al (933 K) or the infiltration temperature is able to lead to deform the whole CF preform by melting

the bridging materials on the preheating stage before infiltration. Both Cu and Mg do not react to CFs, whereas both Mn and Zn react well to CFs and generate reactants, as shown in Table 2-1. However, Mg has too low melting point of 923 K to use in the LPI process for unidirectional CF/Al composites even though Mg is hard to react with CFs.
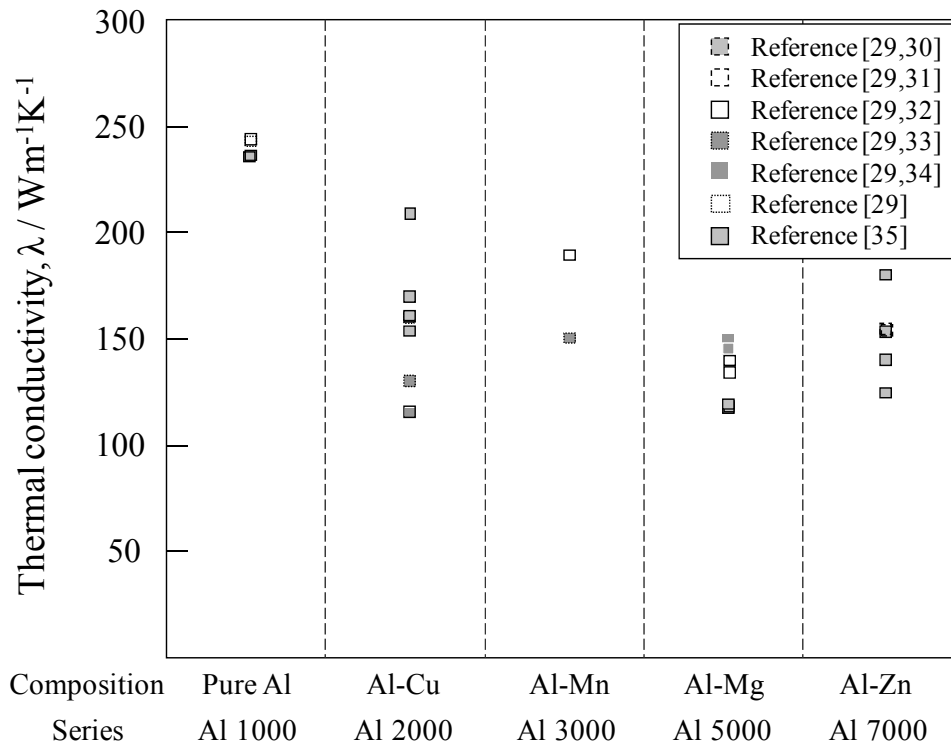
Fig. 2-1 Thermal conductivity of various aluminum alloys.

Meanwhile, Cu has high melting temperature without the reaction to CFs. Therfore, Cu particle is selected as a bridging materials for the unidirectional CF preform, even if it showed high density.

Table 2-1 Candidates for bridging materials between CFs in unidirectional CF preform

Material	Density (Mgm^{-3})	Melting point (K)	Reactivity to carbon
Copper	8.93	1357	×
Manganese	7.21	1519	○ (Mn$_3$C)
Magnesium	1.74	923	×
Zinc	6.52	2128	○ (ZrC)

Table 2-2 Properties of raw materials for unidirectional CF/Al composites

Material	Density (Mgm^{-3})	Tensile strength (MPa)	CTE (×10^{-6}K^{-1})	TC (Wm^{-1}K^{-1})
CF (K13D2U)	2.21	3700	-1.2	800
Atomized Cu	8.93	225	16.5	400
Al (A1070)	2.7	70	24	234

   Table 2-2 shows the physical and mechanical properties of the selected raw materials for the unidirectional CF preform and CF/Al composites. The CFs have light weight, low CTE, high TC and excellent tensile strength, as mentioned above. The Al has high CTE, whereas it and its alloys have relatively good TC and light weight in the field of metal. Therefore, the addition ratio of CF and Al alloy has to be calculated for demanding properties of aimed thermal management applications. In addition, the addition amount of Cu particle has to be little because it has heavy weight and degrade the TC of matrix. Fig. 2-2 shows the images of CFs and Cu particles, used in the fabrication of unidirectional CF preform.
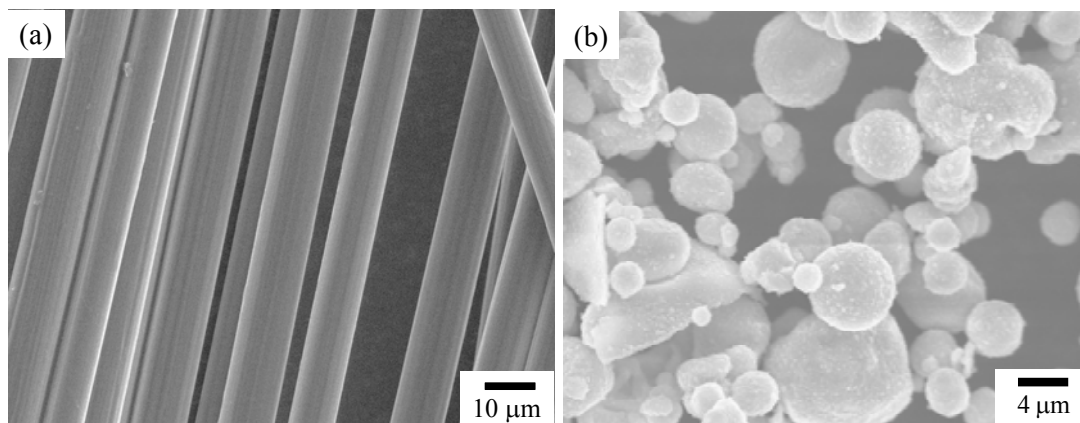
Fig. 2-2 Microstructure of (a) K13D2U carbon fibers and (b) atomized copper powders used in porous CF preform.

2.2.2 Preparation of fiber mixture for unidirectional CF preform

In order to infiltrate the molten Al into porous unidirectional CF preform easily by the LPI process, the uniform distribution of CFs with securing the spaces of the conduit for Al flow in the unidirectional CF preform was required. The clustered CFs usually make hard to infiltrate the Al between clustered CFs because of too narrow spaces to infiltrate [36]. Prior to fabricate the unidirectional CF preform by spark sintering process, the unidirectional CF mixture has been prepared by dispersing Cu particles into CF bundles. The utilized atomized Cu powders (Fukuda metal, foil & powder Co, LTD.) have an average particle size of about 2.55 μm. The unidirectional CF mixture was prepared as follows: The inherent sizing treatment on the CFs surface by company was removed in acetone for 40 min with ultrasonic cleaning. Subsequently, Cu powders mixed with a dispersant such as polyethylene glycol (PEG) were dispersed into the CF bundles by rolling process to avoid CFs clustering. The graphite rod was rolled to the parallel direction of unidirectional CFs with Cu powders and PEG mixture on the unidirectional CF bundles, as shown in Fig. 2-3. The load and speed of rolling were 9.8 N and 15 mms^{-1}.
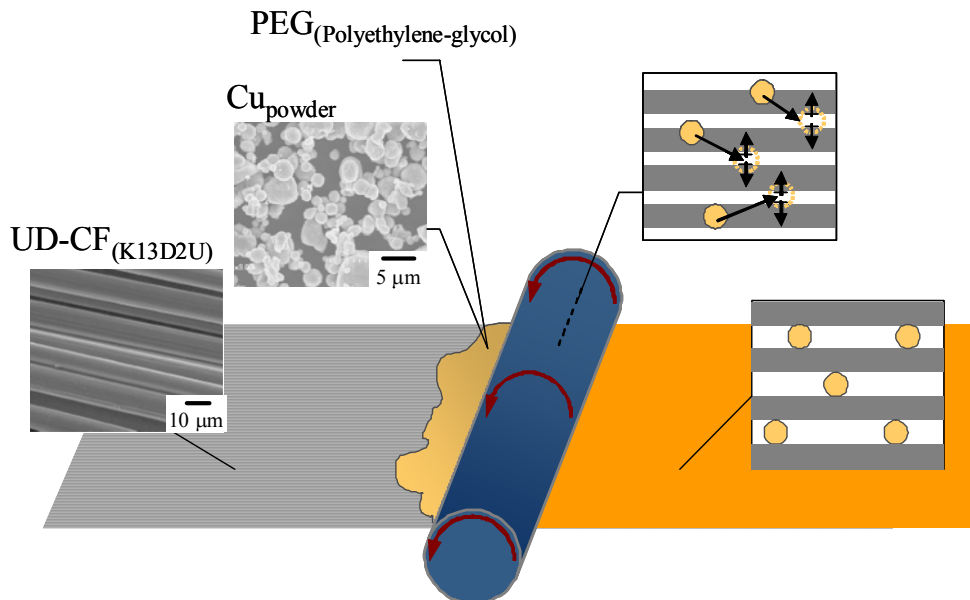
Fig. 2-3 Preparation of unidirectional CF mixture.

2.2.3 Preparation of unidirectional CF preform by spark sintering method

The unidirectional CF preform was fabricated by spark sintering the unidirectional CF mixture. The tailored unidirectional CF mixture in length of 10 mm was stacked and put into the cylindrical graphite mold and sintered by spark sintering method. The schematic illustration of spark sintering apparatus and fabricated CF preform were shown in Fig. 2-4. The volume fraction of CF, Cu and PEG was 0.3, 0.1 and 0.6, respectively. The CF mixture was sintered by direct electrical current flow from upper punch to lower punch. The sintering temperature was measured at the center of the graphite die where was 2.0 mm far from the perimeter of the CF mixture. The PEG in the CF mixture was removed at the temperature of 873 K during 600 s, before heating up to sintering temperature. The sintering temperatures were from 1073 to 1173 K during 1800 s with the constant voltage of 4 V and electrical current of form 380 to 410 A under vacuum environment of 2.7×10^{-2} Pa. The dimension of the CF preform was ø10 × L10 mm^3. The fabrication condition of unidirectional CF preform by spark sintering was summarized in Table 2-3.

Table 2-3 Fabrication condition of unidirectional CF preform by spark sintering.

Materials	Sintering Temp.(K)	Current (A)	Voltage (V)	Holding Time (min)	Environment
Carbon fiber 30Vol%, Cu powder 10Vol%	1073	380			
	1123	390	4	30	Vacuum, 2×10^{-3} Torr
	1173	410			
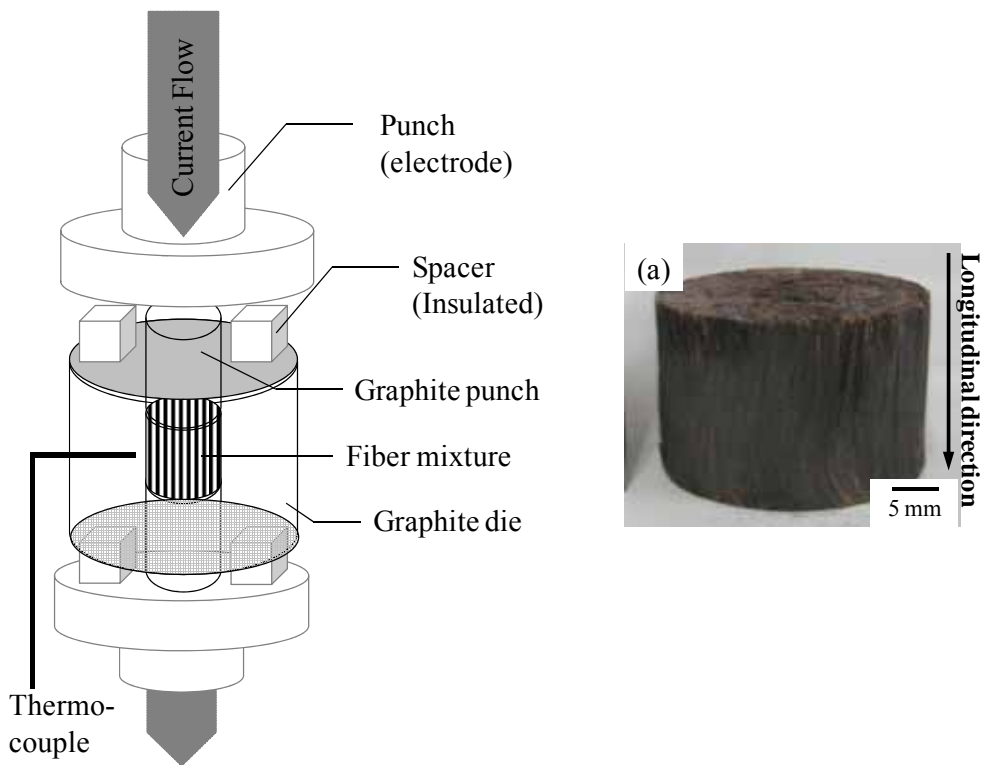
Fig. 2-4 Schematic illustration of spark sintering apparatus and (a) external image of unidirectional CF preform.

2.2.4 Evaluation equipment

2.2.4.1 Observation of microstructure

The microstructure and fracture surface of unidirectional CF preform was observed by a scanning electron microscope (SEM; Hitachi S-3000H2, Japan). The image analysis on the microstructure of both CFs and Cu bridging particles from the unidirectional CF preform has been carried out to calculate the occupied area of Cu deposition particles and the contact area of Cu bridging particles on CFs by image analyzer (Media Cybernetics Image-Pro Plus, Inc., USA).

2.2.4.2 Compression test

The universal testing machine (Shimadzu corp. DSC-R-5000, Japan) was utilized in compression test of unidirectional CF preform. The crosshead speed of the compression test was 0.5mm/min at room temperature.

2.3 Results and discussion

2.3.1 Microstructure of unidirectional CF preform
2.3.1.1 Microstructure of Cu bridging material

The microstructures of unidirectional CF preform by spark sintering are shown in Fig. 2-5 which was fabricated at the different sintering temperatures of 1073, 1123 and 1173 K, respectively. The microstructures represented that the CFs are well dispersed with maintaining the proper spaces between CFs to infiltrate the molten Al easily. Besides, there are observed two kinds Cu particles: Cu bridging particles between CFs and Cu deposition on the CF surfaces. In the previous studies of spark sintering process [37, 38], the powder compact with extremely small contact area between powders proceeds mass transport by high local current densities and occurs melt and vaporization of adjacent particles under spark sintering conditions. In case of this study, the addition of Cu powders is able to play a role of not only the Cu bridging between CFs, but also deposition on CFs by melt and vaporization under spark sintering process. It was also reported that Cu coatings by deposition on CFs facilitated the wettability with the molten Al [39-44].

As shown in Fig. 2-5(a), the CF preform consists of CFs and well dispersed Cu particles between CFs. However there are little amount of Cu bridging between CFs and Cu deposition on CFs. The little amount of Cu bridging can be expected lower compression strength level of CF preform due to the easier debondings between CFs and Cu particles than well bridged preform by compression loading. The fiber bridging is essential to produce the preform shape formation with the expected dimension by bonding fibers each other and possess the strength of CF preform against the infiltration pressure. The CF preform fabricated at 1123K (Fig. 2-5(b)) shows significant Cu bridging between CFs by coalescence of contact particles. The coalescence phenomena of Cu particles are considered that the particles moved to adjacent particles by boiling in

accordance with the high heat generation of CFs contacted with the graphite punch. Besides, the Cu deposition on CFs remarkably increased in accordance with the increase of current density conditions. Fig. 2-5(c) also shows the significant Cu deposition on CFs and bridging between fibers into the CF preform at the sintering temperature of 1173 K. However, the Cu bridging particles formed enlarged shape by bonding the adjacent particles continuously. It is possible that the infiltration of molten Al can be disturbed by enlarged Cu particles when the molten Al flows into the inter fiber region by LPI process. Therefore, the CF preform with the fabrication temperature of 1173 K can be said as 'over sintering'.
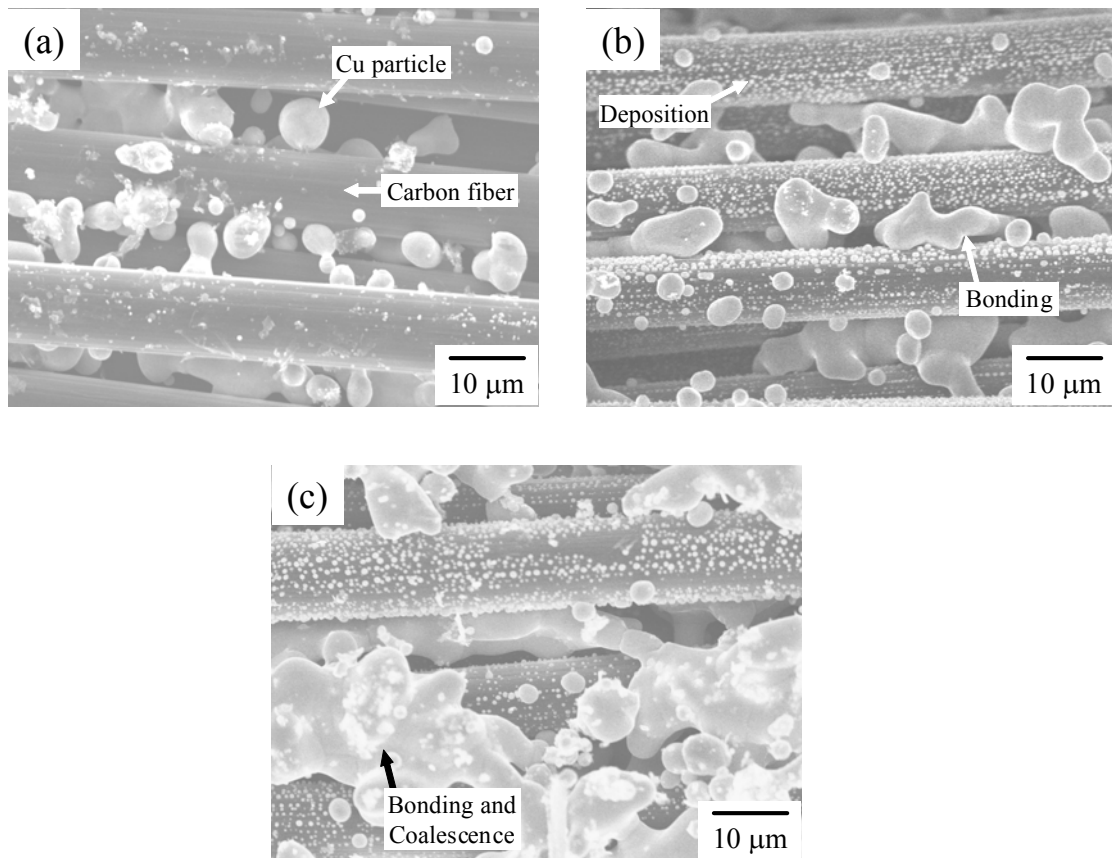
Fig. 2-5 Microstructure of unidirectional CF preform depending on the sintering temperature of (a) 1073, (b) 1123 and (c) 1173 K, respectively.

Fig. 2-6 represents the contact area between Cu bridging particles and CFs depending on the fabrication temperatures. The contact area increased such as 2.95, 6.32 and 10.81 mm^2 with the increase of the fabrication temperature of 1073, 1123 and 1173 K, respectively. It means that the Cu particles grow up their sizes in accordance with the elevation of the fabrication temperature and bridge the CFs by continuous bonding and coalescence of adjacent Cu particles each other, as shown in Fig. 2-7. In addition, the increase of contact area was expected to improve the compression strength properties of CF preform with a role of resistance to the fiber deformation by direct compression loading.
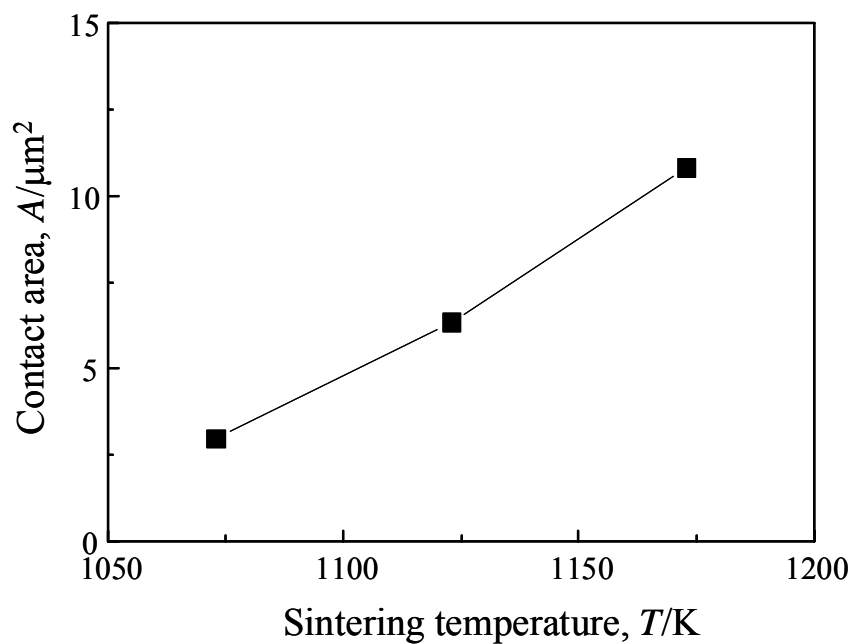
Fig. 2-6 Size variation of contact area between Cu bridging particles and CFs depending on the fabrication temperature.
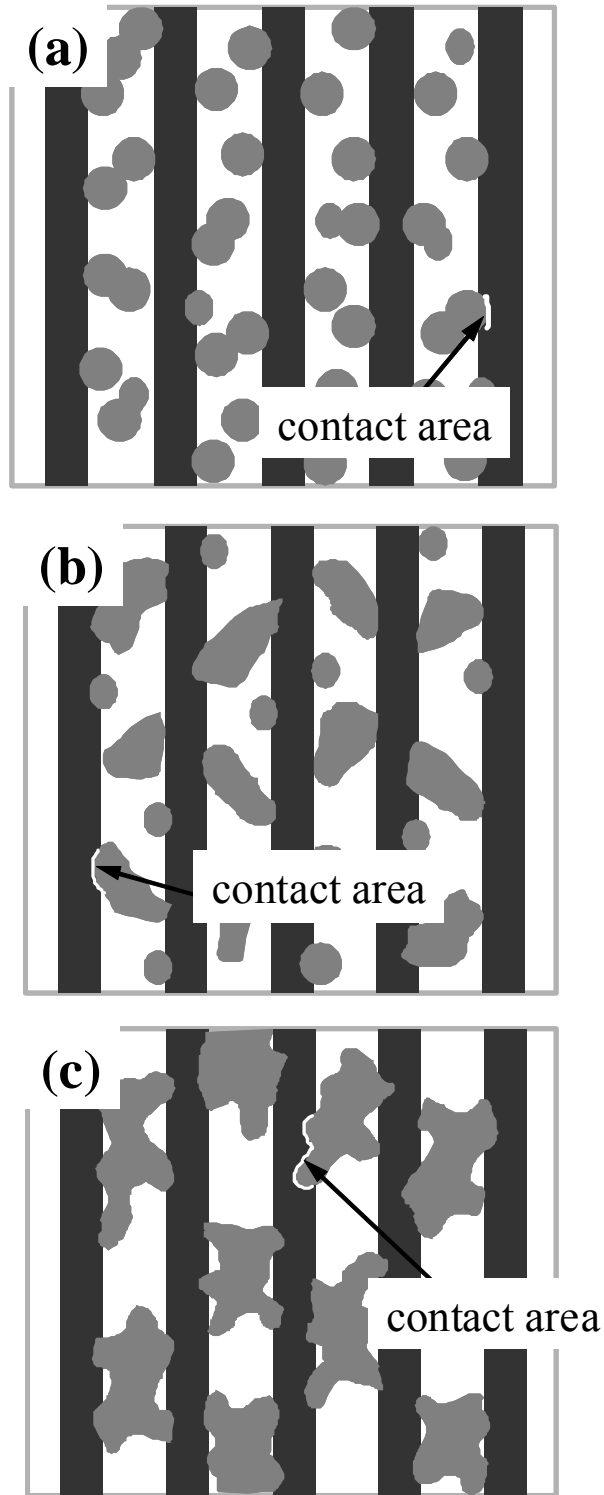
Fig. 2-7 Schematic illustration of unidirectional CF preform depending on the sintering temperature of (a) 1073, (b) 1123 and (c) 1173 K, respectively.

2.3.1.2 Microstructure of Cu deposition particle

In the LPI process, the bad wettability between CFs and Al is one of difficulties to infiltrate the molten Al into the unidirectional CF preform smoothly. In other words, it can be a kind of resistance force to flow the liquid Al into a carbon capillary tube. Therefore, the Cu coating on CF surface is one of the solutions in order to encourage the infiltration of molten Al into the CF preform easily because of the good wettability between Cu and molten Al. Fortunately, the Cu deposition was occurred locally on the CF surfaces during spark sintering, as shown in Fig. 2-5. The Cu deposition on the CF surface is expected to improve the wettability when the molten Al flows into the CF preform in the stage of LPI process. Accordingly, the microstructure of Cu deposition was observed under magnification in Fig. 2-8. However, it seems that the amount of Cu deposition was different depending on the sintering temperatures. The Cu deposition was activated by increasing the current density. The occupied area of Cu deposition on the CF surface depending on the each fabrication temperature is indicated in Fig. 2-9. The CF preform fabricated at 1073 K shows low deposition ratio on the CF surface of about 2.87 %, whereas the CF preform fabricated at 1123 K shows high percent of deposition of about 32.19 % with increasing current density. However, the Cu deposition ratio in the CF preform fabricated at 1173 K decreased to about 16.49 %. In the detailed observation of Fig. 2-8(c), the bonding and coalescence of adjacent deposition particles was occurred. It is considered to be a main reason to decrease the deposition ratio.
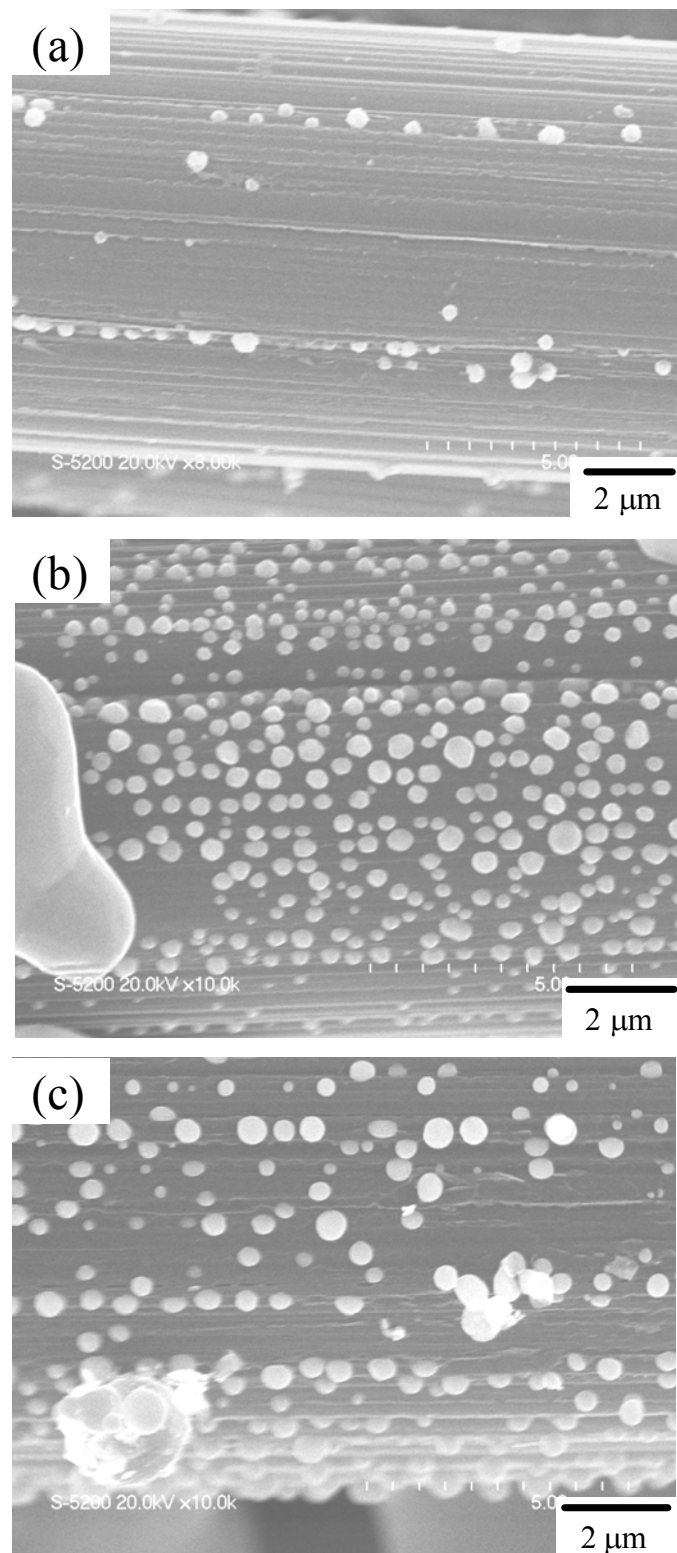
Fig. 2-8 Microstructure of Cu deposition on CF surface depending on the CF preform sintering temperature of (a) 1073, (b) 1123 and (c) 1173 K, respectively.
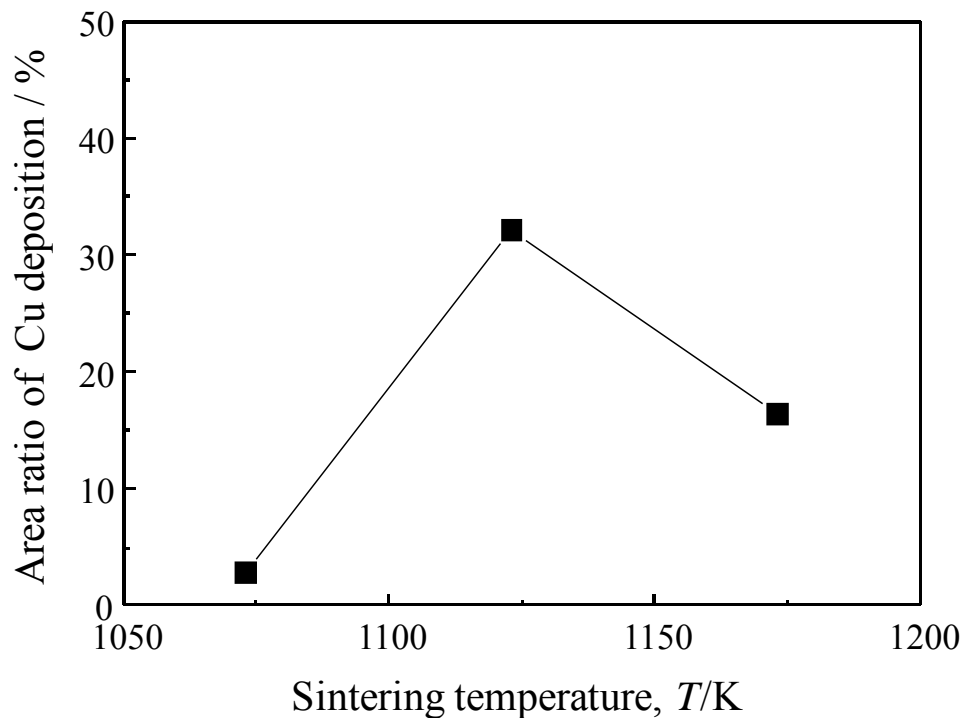
Fig. 2-9 Magnitude of Cu deposition area on CF surface depending on the fabrication temperature.

2.3.2 Sintering phenomena in unidirectional CF mixture

The sintering phenomena in the unidirectional CF preform such as Cu bridging particles between CFs and Cu deposition on CF surfaces can be explained from the spark sintering mechanism. The spark sintering process has been well known as a rapid densification process of a powder compact by means of the direct resistance heating employing the direct current flow through the powder compact or surrounded mold [37, 38, 45-50]. From the vigorous studies on the characterization of spark sintering process with experiments and simulations [37, 38, 46, 47, 49], the current distribution in a graphite mold (die and punch) and the powder compact came out into two systems for the sintering of electrically conducting and non-electrically conducting powder compacts. Typically, the electrically conducting powder compact such as Cu or Ti was sintered with the generation of the Joule heating in the powder compact by the internal current flow through the compact and conducting high current density at locally small contact area in

the particle contacts. The heat flow was mainly caused in the mold from the punch near the compact to the die, compact and the punch far from the compact and from the compact to die. The non-electrically conducting powder compact such as Al_2O_3, in contrast, was sintered by the external heat from die and punch even though the Joule heating did not occur at the compact. The heat flow was caused from the punch near the compact to the die and compact and from the die to the compact. The schematic diagrams of heat flow on two systems were described in Fig. 2-10. Moreover, the applied pressure helps the densification of the compact to be a high density material in spark sintering process. However, the pressure was not applied, in this study, by spacing the insulated ceramic spacer between die and upper/lower electrodes as shown in Fig. 2-4, in order to obtain the desired height of the CF preform and to prevent the fiber deformation. The illustration description of internal structure of the graphite mold for the unidirectional CF preform was shown in Fig. 2-11. The temperatures of the upper punch (punch position) and the CF mixture (fiber mixture position) were measured when the sintering temperature (die position) were 1073, 1123 and 1173 K, as shown in Fig. 2-11(a).
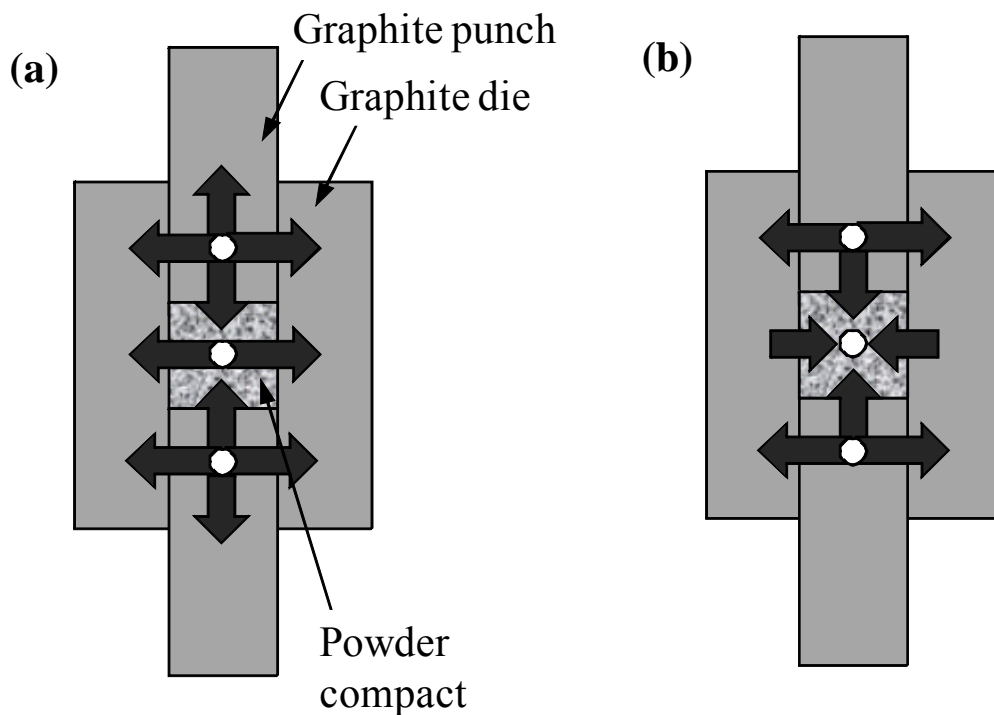
Fig. 2-10 Schematic diagrams of heat flow for (a) electrically conducting and (b) non-electrically conducting powder compacts.

The measured temperatures at each point in Table 2-4 represented that the fiber mixture position is highest temperature in each sintering temperature. Moreover, the temperature of fiber mixture position is higher than that of die position. It is deduced that the high heat generation occurred by Joule heating in CF mixture such like the spark sintering process in electrically conducting powder compact. Thus, the heat flow is anticipated both from upper punch to die and from the CF mixture to die as mentioned in Fig. 2-5 (a). Although the temperature of CF mixture is higher than that of die, the temperature was still lower than melting point of Cu (1357 K). In the step of preparation of the unidirectional CF with 10 mm in height, the dimension of CF was not accurate 10 mm experimentally. Thus the various dimensions around 10 mm existed as illustrated in Fig. 2-6 (b). The CFs above or exactly 10 mm in height make contact with the graphite punch and are able to occur extremely high local temperature by Joule heating, in accordance with the increase of the current density through CFs because of their extremely small diameter of 11 μm. Such high local heat generation at long CFs can melt or boil the contacting Cu particles. Thus the Cu particles are expected to move to bond each other and vaporize by boiling. On the other hand, the short CFs below 10 mm in height are expected relatively lower temperature than contacted CFs to the upper punch without direct joule heating from the upper punch. Thus, the small Cu particles from evaporation of boiled Cu particles are also considered to deposit on the surface of the short CFs.

Table 2-4 Temperature distribution in the graphite mold and CF mixture as a function of the sintering conditions of spark sintering process.

Temperature (K)				
Die position (*F.T)	Punch position	Fiber mixture position	Voltage (V)	Current (A)
1073	1079	1193		380
1123	1126	1250	4	390
1173	1174	1296		410

*F.T means fabrication temperature for unidirectional CF preform in this study
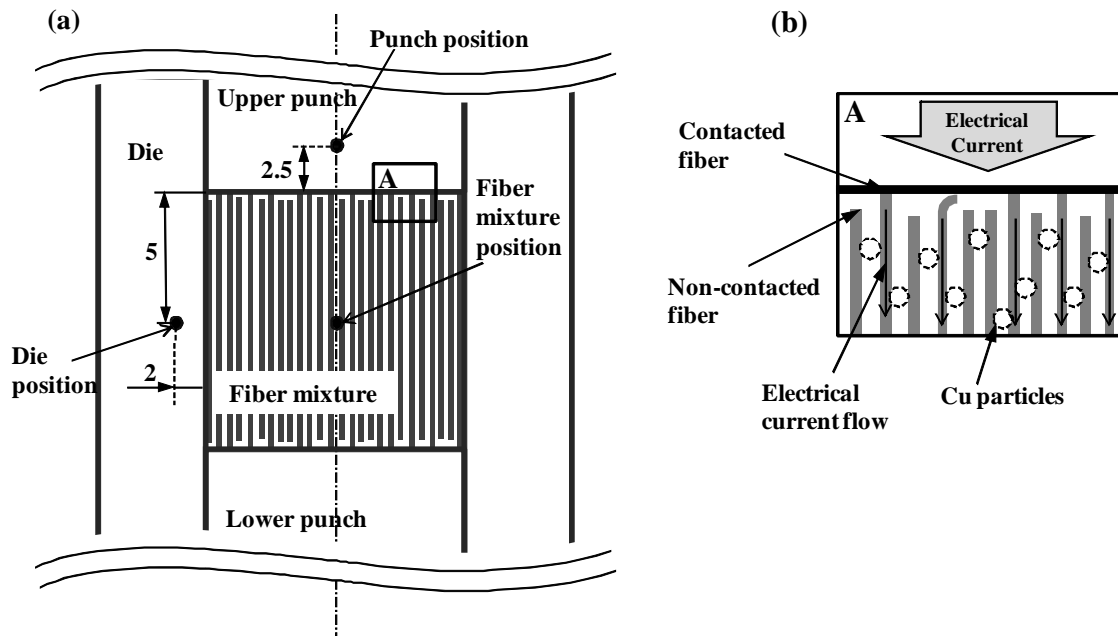
Fig. 2-11 Schematic illustration of (a) internal structure of sintering mold (die) for unidirectional CF preform and (b) electrical current flow at the contact area between graphite upper punch and CF front.

2.3.3 Compressive strength of unidirectional CF preform

The compression test by direct axial loading to the unidirectional CF preform was carried out to identify the compressive behavior of the preform and determine the infiltration pressure of the molten Al. Fig. 2-12 shows the compressive stress-strain curves of the unidirectional CF preform depending on the fabrication temperature. The curves of the CF preform represent the similar behavior with those of common porous foam materials [51-53]. It is divided to 3 stages such as 'compression elastic stage' until initial maximum compressive stress, 'plateau stage' which is plastic deformation region with energy absorption against the applied compressive load and subsequent 'densification stage'. In this compression behavior, the compression strength of the unidirectional CF preform is determined by initial maximum compressive strength. The initial maximum strength of CF preform fabricated at 1073, 1123 and 1173 K was evaluated as 0.56, 1.67 and 2.15 MPa, respectively. In other words, the initial maximum

stress of the preform increased with the increasing fabrication temperature. Meanwhile, the porous unidirectional CF preform is able to appear the fiber micro-buckling [54] or fiber kinking [55] phenomenon instead of the typical plastic deformation on the porous foam materials after the initial maximum stress.
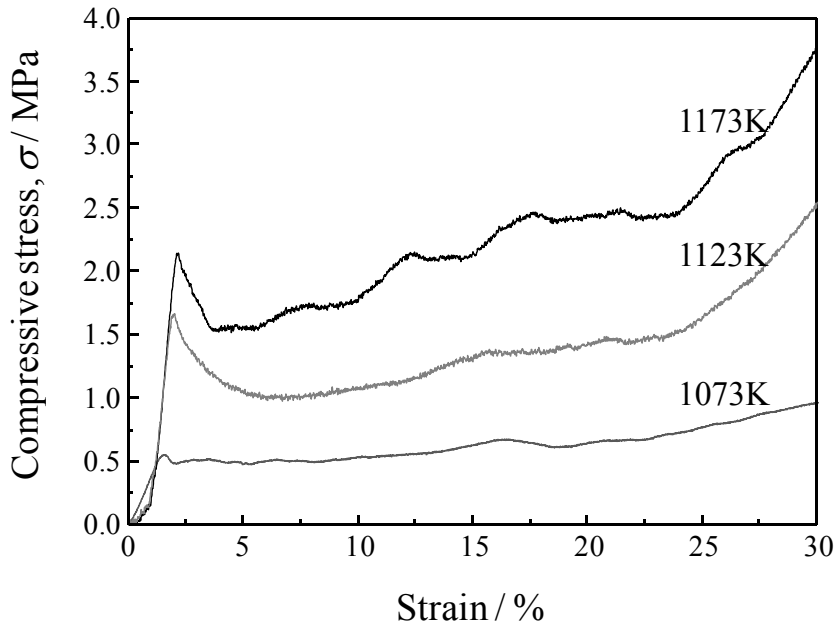
Fig. 2-12 S-S curves of unidirectional CF preform by compression test.

The increase of the initial maximum stress can be considered that the relatively wide bonding area of Cu particles between CFs, as shown in Fig. 2-5, which delays the deformation such like micro-buckling or kinking of CFs by preventing from the fiber bending. The cross section images of the CF preform after compression strain of 10 % were shown in Fig. 2-13. Indeed, the CF preform undergone plastic deformation shows the fiber micro-buckling (Fig. 2-13 (a)) and fiber kinking (Fig. 2-13 (b), (c)) phenomena by different bonding sizes of Cu bridging.

The CF preforms fabricated with the sintering temperature above 1123 K were satisfied the expected strength (> 1 MPa) for the LPI process. However, the CF preform fabricated with that of 1073 K did not exceed the expected strength because of lack of Cu bridgings between CFs. Besides, the enlarged Cu bridgings between CFs at the sintering temperature of 1173 K are able to obstacles to flow the molten Al when the

infiltration is carried out. Therefore, the unidirectional CF preform with the sintering temperature of 1123 K, which represented stable size of the Cu bridgings between CFs, excellent Cu deposition on CF surfaces and suitable compressive strength can be expected to be used for the fabrication of the unidirectional CF/Al composites by LPI process.
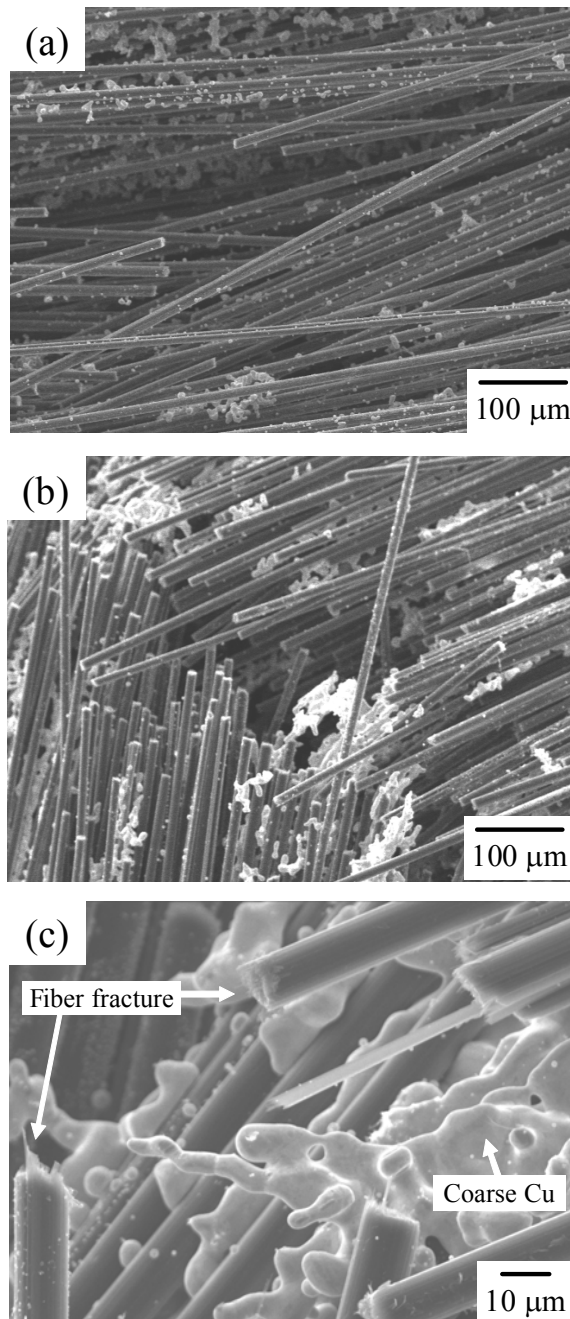
Fig. 2-13 Microstructure of CF preform fabricated at (a) 1123, (b) 1173 K and (c) magnification of (b) after compression strain of 10%.

2.4 Summary

(1) The unidirectional CF preform was prepared by spark sintering, in conjunction of the introduction of the Cu particles as bridging materials between CFs. The Cu particles between the CFs transformed to fiber bridging and deposition on CF surfaces by spark sintering.

(2) The contact area between CFs and Cu particles and the deposition area of Cu particles on CF surface increased with increasing fabrication temperature. The CF preform with the fabrication temperature of 1123 K was observed excellent Cu bridging without enlarged Cu particles and Cu deposition on the CF surfaces.

(3) The maximum compressive strength of the CF preform increased depending on the increasing fabrication temperature. The CF preforms with the sintering temperature above 1123 K were satisfied the expected strength for the LPI process. The CF preform with the sintering temperature of 1073 K had lower strength than expected one, due to the lack of Cu bridgings. However, the preform with the fabrication temperature of 1173 K which showed the highest level of compression strength exhibited the enlarged Cu particles between CFs.

(3) From the viewpoint of the appropriate Cu bridgings between CFs, Cu deposition on CF surfaces and compressive strength, the unidirectional CF preform with the sintering temperature of 1123 K can be suitable for the fabrication of the unidirectional CF/Al composites by LPI process.

References

[1] C. Zweben: JOM, **44** (1992) 15-23.

[2] C. H. Stoessel, J.C. Withers, C. Pan, D. Wallace, R.O. Loutfy: Surf. Coat. Tech., **76-77** (1995) 640-644.

[3] R. Couturier, D. Ducret, P. Merle, J. P. Disson and P. Joubert: J. Euro. Cera. Soc., **17** (1997) 1861-1866.

[4] C. Zweben: JOM, **50** (1998) 47-51.

[5] G. Korb, J. Koráb, G. Groboth: Composites A., **29** (1998) 1563-1567.

[6] K. J. Euh, S. B. Kang: Mater. Sci. Eng. A, **395** (2005) 47-52.

[7] C. Zweben: Power El. Tech., **32** (2006) 40-47.

[8] J.M. Molina, J. Narciso, L. Weber, A. Mortensen, E. Louis: Mater. Sci. Eng. A, **480** (2008) 483-488.

[9] J. M. Molina, M. Rhême, J. Carron, L. Weber: Scripta Mater., **58** (2008) 393-396.

[10] Th. Schubert, B. Trindade, T. Weißgärber, B. Kieback: Mater. Sci. Eng. A, **475** (2008) 39-44.

[11] H. Uozumi, K. Nakanishi, K. Inoue, T. Tsukada, N. Fuyama, T. Fujii, M. Yoshida: J. Jpn. Inst. Light Met., **59** (2009) 562-568.

[12] X. B. HE, X. H. Qu, S. B. Ren, C. C. Jia: Sci. China Ser. E-Tech. Sci., **52** (2009) 238-242.

[13] Y. Xia, Y. Q. Song, C. G. Lin, S. Cui, Z. Z. Fang: Trans. Nonferrous Met. Soc. China, **19** (2009) 1161-1166.

[14] S. Mallik, N. Ekere, C. Best, R. Bhatti: Appl. Therm. Eng., **31** (2011) 355-362.

[15] P. M. Adams, H. A. Katzman, G. S. Rellick, G. W. Stupian: Carbon, **36** (1998) 233-245.

[16] D. D. Edie: Carbon, **36** (1998) 345-362.

[17] T. Suzuki, H. Umehara: Carbon, **37** (1999) 47–59

[18] L. Laffont, M. Monthioux, V. Serin: Carbon, **40** (2002) 767-780.

[19] K. Naito, J. M. Yang, Y. Xu, Y. Kagawa: Carbon, **48** (2010) 1849-1857.

[20] Y. B. Choi, G. Sasaki, K. Matsugi, O. Yanagisawa: Mater. Trans., **46** (2005) 2156-2158.

[21] Y. B. Choi, G. Sasaki, K. Matsugi, N. Sorida, S. Kondoh, T. Fujii, O. Yanagisawa: JSME A, **49** (2006) 20-24.

[22] Y. B. Choi, K. Matsugi, G. Sasaki, K. Arita, O. Yanagisawa: Mater. Trans., **47** (2006) 1227-1231.

[23] Y. B. Choi, K. Matsugi, G. Sasaki, S. Kondoh: Mater. Trans., **49** (2008) 390-392.

[24] K. Matsugi, Y. B. Choi, K. Arita, O. Yanagisawa, G. Sasaki: J. Jpn. Inst. Light Met., **58** (2008) 71-80.

[25] A. Daoud: Mater. Sci. Eng. A, **391** (2005) 114-120.

[26] E. Carreño-Morelli, T. Cutard, R. Schaller and C. Bonjour: Mater. Sci. Eng. A, **251** (1998) 48-57.

[27] J. M. Molina, M. Rheme, J. Carron and L. Weber: Scripta Mater., **58** (2008) 393-396.

[28] Mitsubishi Plastics, Inc., DIALEAD data sheet. (2009) Available at. http://www.mpi.co.jp/products/industrial_materials/pitch_based_carbon_fiber/pbcf 001.html (accessed 11. 12. 09).

[29] A. Woodcraft: Cryogenics, **45** (2005) 421–431.

[30] A. Woodcraft, R. V. Sudiwala, R. S. Bhatia: Cryogenics, **41** (2001) 603-606.

[31] J. G. Hust, D. H. Weitzel, R. L. Powell: J. Res. Natl. Bur. Stand. Sec. A, **75** (1971), 269.

[32] R. L. Powell, W. J. Hall, H. M. Roder: J. Appl. Phys., **31** (1960) 496-503.

[33] Y. S. Touloukian, P. E. Liley, S. C. Saxena: Thermophysical properties of matter, Plenum (1970).

[34] R. W. Klaffky, N. S. Mohan, D. H. Damon: Phys. Rev. B, **11** (1975) 1297-1307.

[35] A. F. Clark, G. E. Childs, G. H. Wallace: Cryogenics, **10** (1970) 295-305.

[36] A. Mortensen: Mate. Sci. Eng. A, **135** (1991) 1-11.

[37] K. Matsugi, H. Kuramoto, T. Hatayama, O. Yanagisawa: J. mater. Proc. Tech., **146**

(2004) 274-281.

[38] U. Anselmi-Tamburini, S. Gennari, J. E. Garay, Z. A. Munir: Mater. Sci. Eng. A, **394** (2005) 139-148.

[39]S. Abraham, B. C. Pai, K. G. Satyanarayama: J. Mater. Sci. **27** (1992) 3479-3486.

[40] R. Asthana, P. K. Rohatgi: Compo. Manuf., **3** (1992) 119-123.

[41] Y. Z. Wan, Y. L. Wang, G. J. Li, H. L. Luo, G. X. Cheng: J. Mater. Sci. Letter., **16** (1997) 1561-1563.

[42] J. F. Silvain, A. Proult, M. Lahaye, J. Douin: Composites A, **34** (2003) 1143-1149.

[43] M. Sánchez, J. Rams, A. Ureña: Oxid. Met., **69** (2008) 327-341.

[44] Y. Tang, L. Liu, W. Li, B. Shen, W. Hu: Appl. Surf. Sci., **255** (2009) 4393-4400.

[45]L. G. Yu, K. A. Khor, G. Sundararajan: Surf. Coat. Tech., **157** (2002) 226-230.

[46] H. Kuramoto, K. Matsugi, O. Yanagisawa: J. Jpn. Inst. Met., **66** (2002) 621-626.

[47] K. Matsugi, H. Kuramoto, O. Yanagisawa, M. Kiritani: Mater. Sci. Eng. A, **354** (2003) 234-242.

[48] B. Prawara, H. Yara, Y. Miyagi, T. Fukushima: Surf. Coat. Tech., **162** (2003) 234-241.

[49]K. Vanmeensel, A. Laptev, J. Hennicke, V. Vleugels, O. Van der Biest: Acta Mater., **53** (2005) 4379-4388.

[50] D. Salamon, Z. Shen, P. Šajgalík: J. Euro. Cera. Soc., **27** (2007) 2541-2547.

[51]I. Jeon, T. Asahina: Acta Mater., **53** (2005) 3415-3423.

[52] E.Andrew, W. Sanders, L. J. Gibson: Mater. Sci. Eng. A., **270** (1999) 133-124.

[53] Method for compressive test of porous metal, JIS H 7902 (2008).

[54] P. Berbinau, C. Soutis, I. A. Guz: Compos. Sci., **59** (1999) 1451-1455.

[55] A. Jumahat, C. Soutis, F. R. Jones, A. Hodzic: Compos. Struct., **92** (2010) 295-305.

Fabrication process and characterization of unidirectional CF/Al composites by low pressure infiltration method

3.1 Introduction

There are lots of fabrication processes which have been introduced in the field of MMCs, in order to manufacture the high performance composite materials [1-31]. The fabrication of MMCs was widely divided into two main routes such as powder metallurgy (PM) [2-7] and casting methods [8-24, 26-31], by means of solid state or liquid state processes. In case of PM, the metal powders blended with the fiber or particle state reinforcements were mainly sintered to form the composite materials. The MMCs containing long fiber reinforcements have usually fabricated by casting processes with the infiltration of molten metal into fiber preform. However, the conventional casting processes such as squeeze casting [8-13, 22, 23] and gas infiltration [14-23] methods had some disadvantages for long fiber reinforced MMCs such as the limiting degree of freedom in shape, fiber fracture and deformation of the fiber preform by applying high pressure of composites. Especially, the deformation of the fiber preform led to the imperfect infiltration of molten metal into fiber bundles because of the formation of narrow space between fibers by fiber clustering. Meanwhile, the low pressure infiltration (LPI) process [27-31], among the casting processes, enabled to fabricate complex and/or large size composites with the simple apparatus and cost-effective fabrication by applying low pressure of some atmospheric pressures (≥ 1 MPa).

In order to optimize the LPI process for the densification of unidirectional CF/Al composites, the determination of infiltration pressure and the fiber distribution have to be considered. From the viewpoint of the decision of infiltration pressure, the infiltration of molten Al into unidirectional CF arrays is mainly influenced by the bad wettability between Al and CFs with following resistance pressures such as the capillary resistance, internal viscous friction, gravity and back pressure [22, 27, 32]. On the other hands, the fiber distribution is one of the important factors for the uniform infiltration of the molten Al into whole of the CF preform. The fiber clustering is able to disturb the infiltration of molten Al into unidirectional CF preform because of the narrow space between CFs.

In this study, the unidirectional CF/Al composites were fabricated by LPI process. Especially, this chapter mainly aimed at the fabrication of dense CF/Al composites by using low pressure below 1.0 MPa. In order to obtain the dense composites, the decision of the infiltration pressure was carried out. Moreover, the size decision and control of Cu particles, were carried out by avoiding the CF clustering

3.2 Experimental procedure

3.2.1 Preparation of fiber mixture and unidirectional CF preform

The unidirectional CF preform was fabricated by sintering of the unidirectional CF mixtures. The CF mixtures were prepared by blending with 30 vol % of coal tar pitch based K13D2U carbon fibers (Mitsubishi Plastics, Inc., Tokyo, Japan), 10 vol % of the Cu powder (Fukuda Metal, Foil & Powder Co, LTD, Kyoto, Japan) and polyethylene glycol (PEG) as a dispersant. The Cu powders were dispersed into the CF bundles by passing CF mixtures through a graphite roller and play a role such as spacing and bridging between CFs. The Cu powders added with different particle size conditions, such as average particle sizes of 2.55, 11.79, 12.44, 28.86 μm and bimodal particles. Especially, the bimodal powder was gained by blending the average Cu particle sizes of 2.55 and 11.79 μm. The average particle size of the bimodal Cu powder was 6.89 μm. The CF mixtures were put into the cylindrical graphite mold and sintered under the SPS process by the direct electrical current discharge into the CF mixtures under a vacuum of 2.7×10^{-2} Pa. The sintering conditions for CF preform by the SPS process were sintering temperatures of 1123 K in accordance with the applied electrical current and voltage of 390 A and 4 V. The temperature was directly measured at the center of the graphite mold. The dimension of the CF preform was ø10 × L10 mm^3.

3.2.2 Preparation of unidirectional CF/Al composites by LPI process

The unidirectional CF/Al composites were fabricated under the LPI process by means of the infiltration of molten Al (A1070) into unidirectional porous CF preform.
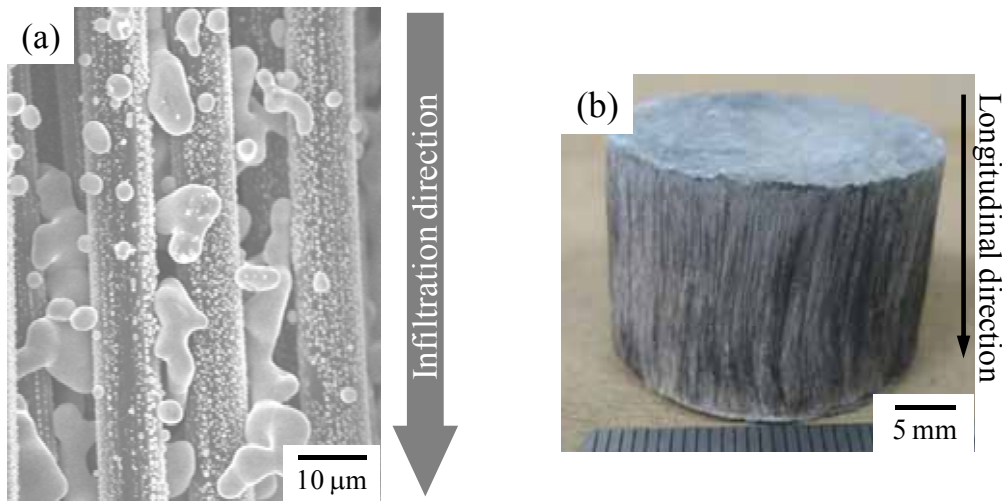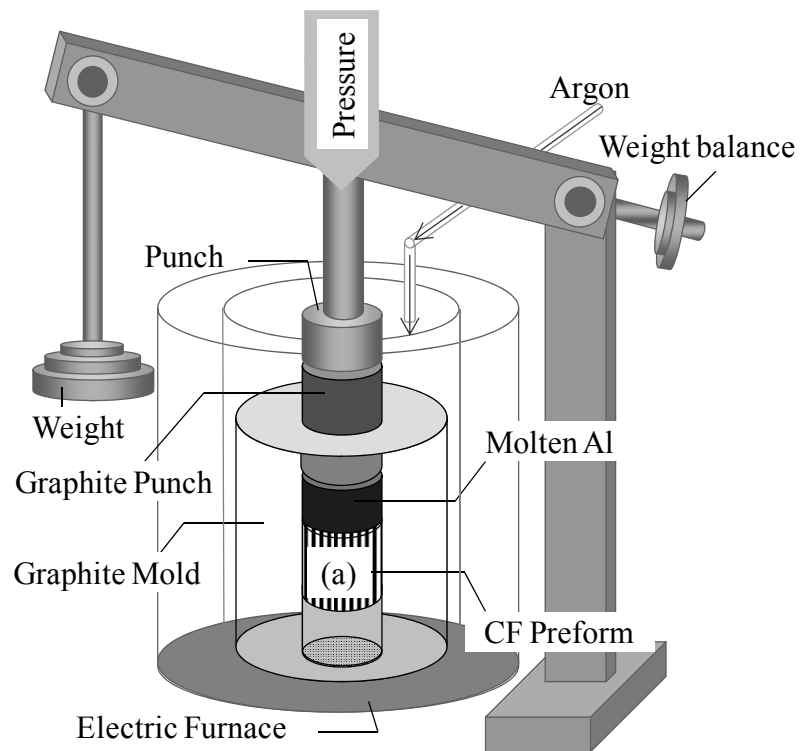
Fig. 3-1 Schematic illustration of LPI apparatus, (a) the magnification of the unidirectional CF preform and (b) external image of unidirectional CF/Al composites.

Fig. 3-1 shows the schematic illustration of LPI apparatus. The LPI apparatus was simply designed without complex and large hydraulic pressure device. The CF preform was set into the cylindrical graphite mold and heating up to infiltration temperature. Subsequently, the molten Al was poured upon the CF preform and pressurized by

graphite punch. The infiltration pressure was applied by the iron weight with a lever. The infiltration pressure and temperature conditions of LPI process were from 0.2 to 0.8 MPa and 1073 K, respectively. The environment for LPI process was argon in order to avoid the oxidation of Al, Cu and CFs. The fabrication conditions were summarized in Table 3-1. The dimension of the CF/Al composites was ø10 × L10 mm^3.

Table 3-1 Fabrication conditions of LPI process for unidirectional CF/Al composites

	Materials	Volume fraction	Infiltration pressure (MPa)	Environment
Preform	K13D2U CFs	0.3		
	Cu powders	0.1	0.2 - 0.8	Ar
Matrix	Al 1070	0.6		

3.2.3 Evaluation equipment

3.2.3.1 Observation of microstructure

The microstructure of unidirectional CF/Al composites was observed by a scanning electron microscope (SEM; Hitachi S-3000H2, Japan). The image analysis was carried out to calculate the size of the initial Cu by an image analyzer (Media Cybernetics Image-Pro Plus, Inc., USA).

3.2.3.2 Measurement of CFs dispersion

The degree of CFs distribution was examined by computer modeling which quantified the 2-dimensional spatial distribution.

3.2.3.3 Measurement of density

The densities of unidirectional CF/Al composites were measured with the water immersion method by Archemedes' principle.

3.3 Results and discussion

3.3.1 Decision of infiltration pressure in LPI process

The infiltration of liquid metal into the porous reinforcement preform in casting process depended on several physical phenomena [33]. It is considered that the liquid metal infiltrate in the capillary tube between reinforcements. The infiltration types, in particular, are divided into two systems by wettability between the liquid metal and capillary tube. The schematic of liquid metal drop on the reinforcement substrate is described in Fig. 3-2. The contact angle θ is defined with the two surface tensions and fiber-liquid interfacial energy σ_{fl} by Young's equation as follows [33, 34]

$$\sigma_{lv} \cos \theta = \sigma_{fl} - \sigma_{fv} \qquad\qquad 3\text{-}1$$

The contact angle of more than 90 degree is non-wetting system whereas that of less than 90 degree is spontaneous wetting system.

(a) $\theta > 90^{\circ}$ (b) $\theta < 90^{\circ}$
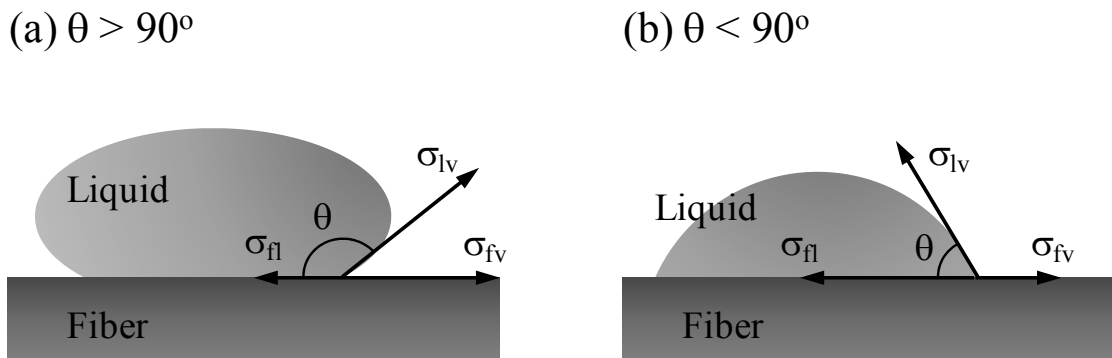
Fig. 3-2 Schematic description of liquid metal drop on a fiber substrate: (a) non-wetting and (b) spontaneous wetting system, where σ_{lv}, σ_{fv} and σ_{fl} are liquid-vapor surface tension, fiber-vapor surface tension and fiber-liquid interfacial energy.

Moreover, the curved liquid front in a capillary tube generally called a meniscus. The existence of liquid-vapor surface tension σ_{lv} at the meniscus causes the pressure

difference between both side of meniscus. The capillary pressure by the pressure difference was defined by Laplace equation [35, 36],

$$\Delta P_c = \frac{2\sigma_{lv}\cos\theta}{r_c} \tag{3-2}$$

where, ΔP_c is the pressure difference between both side of meniscus and r_c is the radius of the capillary tube. In case of the molten Al-CFs system in a capillary tube, the externally applied infiltration pressure is required because of its non-wetting system between Al and C with the contact angle of about 135 degree [37]. However, the infiltration initiation pressure was not determined by only capillary pressure. The Schematic diagram of flowing liquid in a capillary tube by exert forces was considered, as shown in Fig. 3-3 [22]. There is a stress field consisted of the capillary resistance P_{cap}, internal viscous friction f, gravity G, back pressure P_{back} and externally applied pressure P_{ram}.
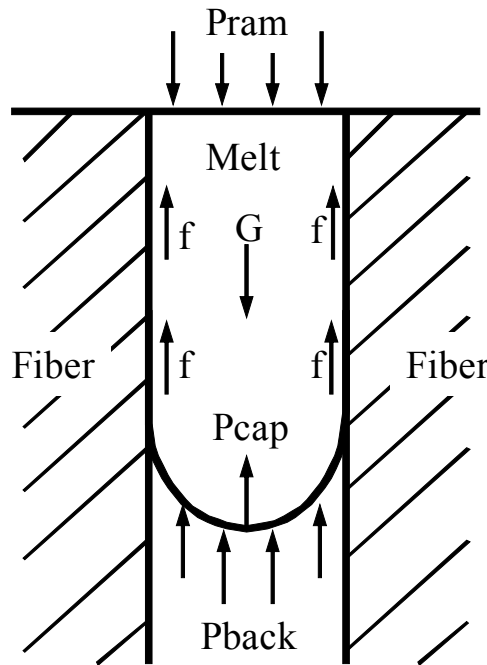
Fig. 3-3 Schematic description of the forces exerted on the flowing melt in a capillary tube, where P_{ram}, P_{cap}, P_{back}, f and G are externally applied pressure, capillary resistance pressure, back pressure, internal viscous friction of the melt and gravity, respectively [22].

A mathematical model for the infiltration of liquid metal into the unidirectional fiber array has been established [32]. For an incompressible viscous Newton fluid, constant infiltration speed, no solidification during the process and no chemical reaction between liquid metal and the fiber array, the mathematical model was expressed as follows: [22, 32]

$$P_{ram} = \frac{2\sigma_{lv}V_f \cos\theta}{(1-V_f)R_f} + \frac{32\eta\overline{V}V_f^2}{(1-V_f)^2R_f^2}Z - \rho gZ + P_{back} \qquad (3.3)$$

where, P_{ram} is the externally applied pressure, σ_{lv} is the liquid-vapor surface tension, V_f is the volume fraction of the fiber, θ is the contact angle, R_f is the fiber radius, η is the coefficient of viscosity of the liquid metal, $\overline{V}$ is the average flow viscosity, Z is the infiltration depth, ρ is the density of liquid metal, g is the gravity and P_{back} is the back pressure caused by air at the liquid metal front.

The Eq. (3-3) consisted of the capillary resistance of static character, internal viscous friction of hydrodynamic character, gravity and back pressure which were represented by from first to fourth term in the right hand of the equation, respectively. The infiltration of liquid metal into the fiber array is able to initiate when the P_{ram} overcomes the resistances. The externally applied infiltration pressure meant the P_{ram} in this study.

Table 3-2 Required properties for infiltration of liquid Al into unidirectional CF preform.

Parameter	Value	References
Liquid-vapor interfacial energy, σ_{lv} (MPa)	837×10^{-3}	[37]
Contact angle, θ (deg)	135	[37]
Dynamic viscosity of Al, η (Pa·s)	0.947×10^{-3}	calcuated from [38]
Infiltration rate, $\overline{V}$ (m·s^{-1})	0.45×10^{-3}	experiment
Infiltration length, Z (m)	10×10^{-3}	experiment

Table 3-2 indicates the physical properties between molten Al and CFs which are required in Eq. (3-3). From these values, the infiltration initiation pressure was calculated depending on the CF volume fraction, as shown in Fig. 3-4. The required infiltration pressure increased with increasing CF volume fraction. However, the

internal viscous friction, gravity and back pressure had not an influence on the different volume fraction of CFs. In addition, the gravity and internal viscous friction were not a decisive factor to determine the infiltration pressure because of their insignificant pressure level. The resistance pressure by internal viscous friction was calculated at 0 to 1425 Pa according to the CF volume fraction range of 0 to 0.5. The gravity was also small that was constant 265 Pa regardless of CF volume fraction. Meantime, the back pressure affects to determine the infiltration pressure with the constant pressure of 0.1 MPa by atmospheric pressure at the rear space before infiltration regardless of CF volume fraction. The capillary resistance, in particular, is most sensitive to the CF volume fraction. The volume fraction of CFs, in this study, was determined 0.3 by the prediction of thermal conductivity. When the CF volume fraction is 0.3, the capillary resistance pressure was calculated about 0.1 MPa. The threshold pressure for the infiltration was calculated to approximately 0.2 MPa.   The practical LPI process was carried out with the applied infiltration pressure of 0.2, 0.4, 0.6 and 0.8 MPa. The results were indicated in Fig. 3-5, in terms of the densification of the unidirectional CF/Al composites depending on the applied infiltration pressure. The average
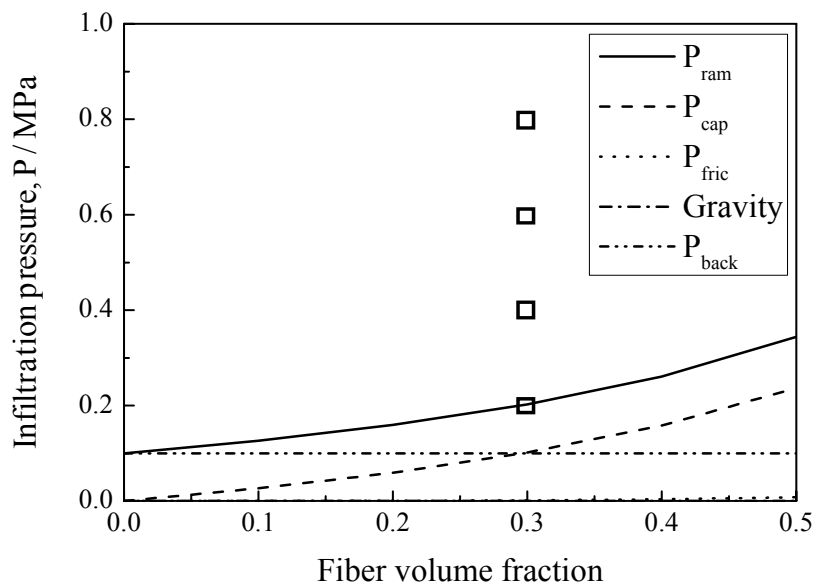
Fig. 3-4 Calculated infiltration pressure as a function of the CF volume fraction: □ is experimentally applied pressure.

Cu particle size used in unidirectional CF preform as bridging materials was 12.44 μm. The density of CF/Al composites were 1.4, 2.4, 2.6 and 2.7 Mg·m^{-3} in accordance with the applied pressure of 0.2, 0.4, 0.6 and 0.8 MPa, respectively. The CF/Al composites with the infiltration pressure of 0.2 MPa had very low relative density of about 45 % whereas the composites with the infiltration pressure of 0.8 MPa showed high relative density of about 84 %. It can be supposed that the radius of the capillary tube between CFs had different sizes by non-uniform fiber distribution. The non-uniform CF distribution means that the local volume fraction of CF arrays is different. In addition the required infiltration pressure to the different size of each tube was also different. The infiltration pressure of 0.2 MPa had extremely low ability to infiltrate into the CF preform. In other words, the size of the capillary tube to be infiltrated at 0.2 MPa might be very little amount when the infiltration started at LPI process.
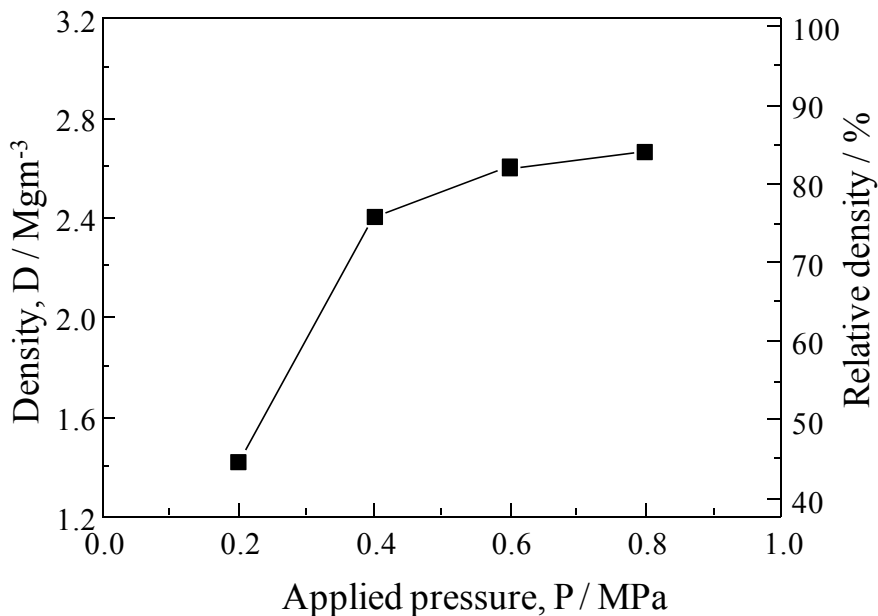
Fig. 3-5 Influence of applied infiltration pressures on the density of unidirectional CF/Al composites.

Fig. 3-6 showed the CF/Al composites with different applied infiltration pressure of 0.2 and 0.8 MPa. There are clearly divided into the infiltrated region by Al and clustered CFs region in case of the applied infiltration pressure of 0.2 MPa. The molten Al seemed to flow at the large spaced region between CFs and the other space such as imperfect infiltration region remained pores by the fiber clustering. However, the CFs distribution between Fig. 3-6 (a) and (b) represented quite different formation by different applied infiltration pressure. It is supposed that the molten Al with the applied infiltration pressure of 0.2 MPa preferentially infiltrated in largely spaced region between CFs. At the same time, the infiltrated Al pressurized to the sideways of the adjacent CFs because of their bad wettability. Meantime, the intermetallic compound such as $CuAl_2$ created by chemical reaction between molten Al and the Cu bridging material. However, the intermetallic compound mainly formed around the clustered CFs and it alluded that the Cu particles which were initially formed at the center between CFs melted by molten Al and moved to the sideways of the CFs by flowing molten Al to the sideways of CFs. As a result, the non-infiltrated region with narrow space and the adjacent CFs became narrower than before, such like fiber clustering. The broad clustering region of CF arrays encouraged an infiltration defect such as the imperfect infiltration. On the other hand, Fig. 3-6 (b) showed well distributed CFs with the Al infiltration into the quite narrow spaces by relatively high applied infiltration pressure of 0.8 MPa. It meant that the initial infiltration was extensively and simultaneously occurred at diverse sizes of the capillary tubes when the infiltration started. The LPI process aimed at the infiltration pressure below 1.0 MPa. Therefore, infiltration pressure of 0.8 MPa was decided at LPI process at the CF volume fraction of 0.3 in this study. However, there also existed some imperfect infiltration region by CFs clustering phenomena as-mentioned in Fig. 3-6 (a). These could be known that not only the determination of the infiltration pressure but also uniform distribution of unidirectional CF array is an important factor for the densification of unidirectional CF/Al composites. In order to prevent imperfect infiltration region, the initial CF array have to be designed the uniform distribution at the fabrication stage of the unidirectional CF preform. As an

effective measure, the sizes of the Cu particles were controlled for the uniform distribution of CFs.
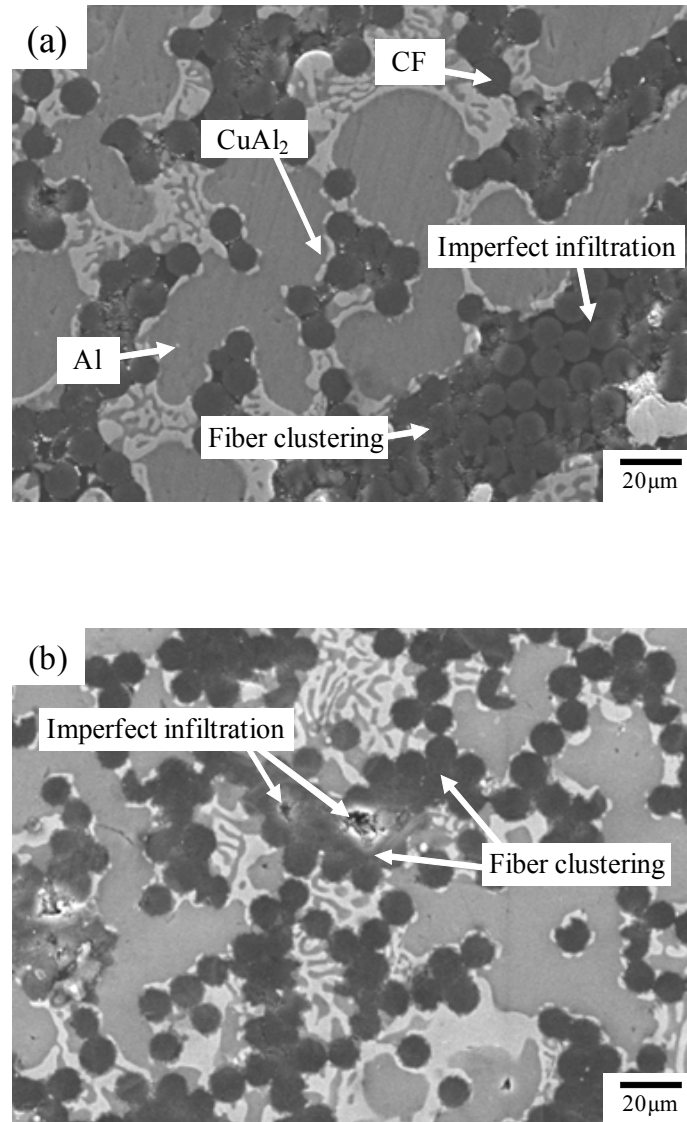
Fig. 3-6 Microstructure of unidirectional CF/Al composites fabricated by applied infiltration pressure of (a) 0.2 and (b) 0.8 MPa.

3.3.2 Decision of copper particle size in unidirectional CF preform

There were considered many kinds of formations of CF arrays in unidirectional CF preform. From the viewpoint of the basic formations of fiber arrays, they are classified into two groups such as square fiber array and hexagonal fiber array. The geometrical description and following equations (Eq. (1) and (3)) for the theoretical square and hexagonal fiber arrays have been proposed in the reference [32]. It was known that the space between theoretical fiber arrays was influenced by the volume fraction and radius of fibers. The Cu bridging material in unidirectional CF preform can play a crucial role as a spacer to maintain the theoretical fiber arrays with the suitable flow space of the molten Al in the unidirectional CF array. In addition, the control of the Cu size helps the size of the space uniformly over whole of the CF arrays.
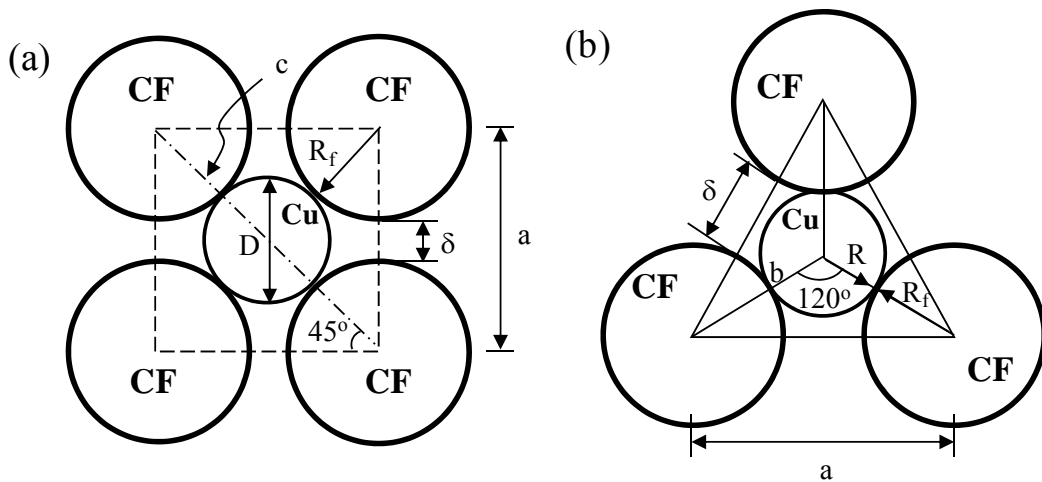
Fig. 3-7 Schematic description of theoretical fiber array base on the Ref. [32] with Cu spacer for: (a) square fiber distribution and (b) hexagonal fiber distribution.

The new geometrical schematics based on a reference [32] were considered in Fig. 3-7, in order to calculate the theoretical size of the Cu particles between CFs for the uniform fiber distribution. The sizes of Cu particles on the square fiber array and hexagonal fiber array depended on the volume fraction and the radius of the fibers. The theoretical sizes

of Cu particles for the uniform square and hexagonal fiber arrays can be calculated by following equations.

For square fiber array:

$$a = \sqrt{\frac{\pi}{V_f}}\, R_f \qquad (3\text{-}4)$$

$$D = c - 2R_f = \sqrt{2}a - 2R_f \qquad (3\text{-}5)$$

For hexagonal fiber array:

$$a = \left(\frac{2\pi}{\sqrt{3}V_f}\right)^{1/2} R_f \qquad (3\text{-}6)$$

$$D = 2R = 2(b - R_f) = 2\left(\frac{a/2}{\cos 30^\circ} - R_f\right) \qquad (3\text{-}7)$$

where a, b and c are the distance between each center of adjacent CFs, each center of Cu and CF and each center of the distant CFs. D and R are the diameter and radius of Cu. R_f and V_f are radius and volume fraction of CF, and δ is the distant of the gap between adjacent CFs.

Table 3-3 Various kinds of Cu powders for fabrication of unidirectional CF preform.

Products	Cu HWQ -5µm	Cu HWQ-20µm with 20µm sieving	+ (: =50:50%)	Hukuda Metal 25~45µm
Fab. process	Atomization	Atomization	Atomization	Electrolysis
Ave. particle size (µm)	2.55	11.79	Bimodal	28.86
Volume fraction (%)	10	10	10	10

In the present study, the D were calculated to be about 14.17 and 11.08 μm for the uniform square and hexagonal fiber arrays when the V_f and R_f were 0.3 and 5.5 μm, respectively. The four kinds of the Cu powders were used for the fabrication of the unidirectional CF preform, as shown in Table 3-3. The product of Cu HWQ-20 μm, in particular, had high degree of scattering on particle sizes. Thus, the Cu powder was filtered by 20 μm-net sieve and became the average particle size of 11.79 μm without most of the particle sizes over 20 μm. The bimodal particle contained average particle size of 2.55 and 11.79 μm with the same addition ratio of 50 : 50 %. The images of the initial Cu powders used in CF preform are shown in Fig. 3-8. The average particle size of 2.55 and 11.79 μm represented the spherical form produced by the atomization method whereas the average particle size of 28.86 μm showed the rough form produced by electrolysis method. Fig. 3-9 represented the degree of scattering of the particle size on each kind of the Cu powder. Each kind of Cu powder also had especially high percent of the particle size range. The average particle size of 2.55 μm was measured the range of the particle size from 0.6 to 5.9 μm. Moreover, a largest number of the particles ranged between 1.0 and 2.0 μm. The average particle size of 11.79 μm had their size ranges from 2.4 to 22.4 μm and a largest number of the size ranged from 12.0 to 15.0 μm. The bimodal particles showed the mixed range with the average particle size of 2.55 and 11.79 μm. In case of the average particle size of 28.86 μm, most of the particle ranged from 20.0 to 35.0 μm. Among these particles, the average particle size of 11.79 μm was the nearest to the theoretical Cu size from the results of the Eg. (3-5) and (3-7). Therefore, the particles were expected the most to improve the densification of the unidirectional CF/Al composites maintaining with the uniform CFs distribution.
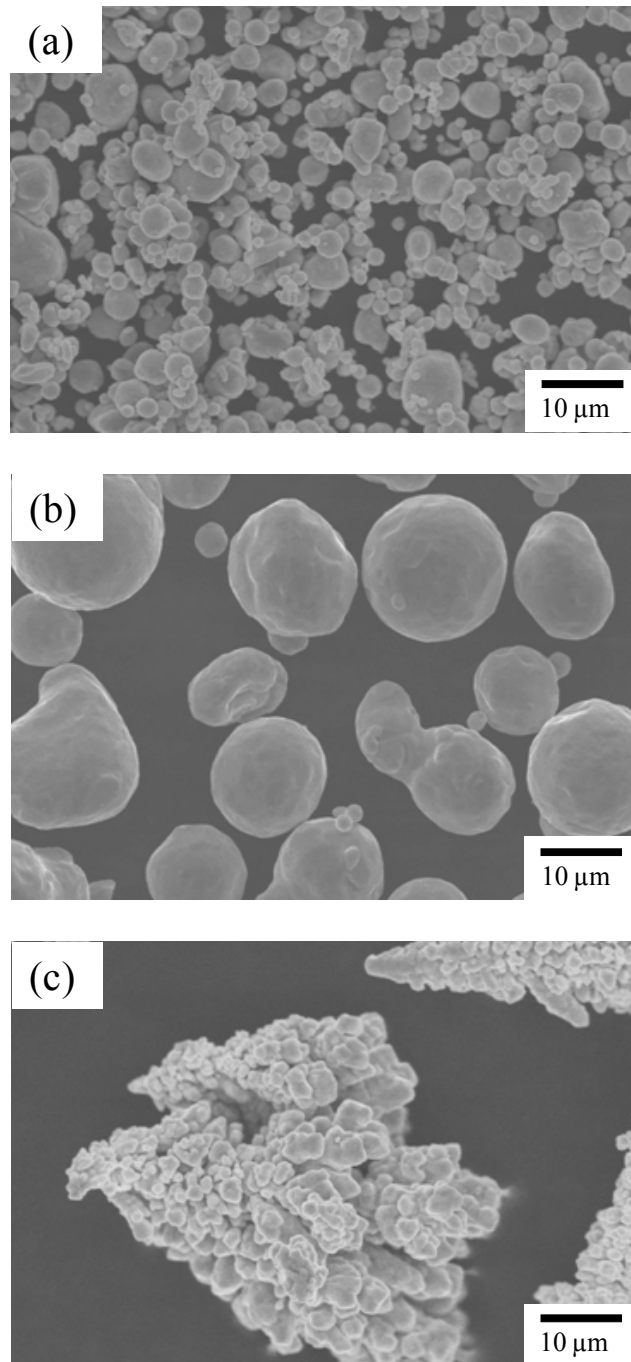
Fig. 3-8 Microstructure of initial Cu particles with the average particle size of (a) 2.55, (b) 11.79 and 28.86 μm.
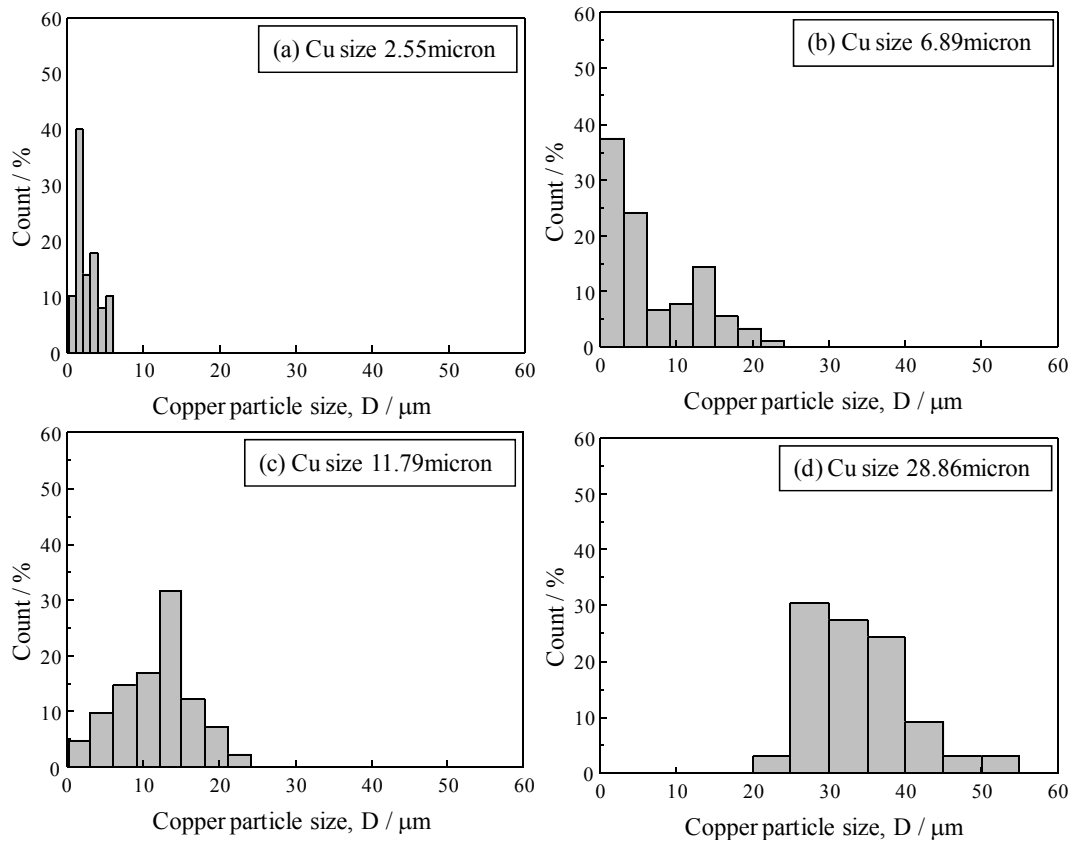
Fig. 3-9 Size distribution diagrams of the various kinds of Cu particles used in the fabrication of unidirectional CF preform.

3.3.3 Microstructure and density of unidirectional CF/Al composites

The influence of added Cu particle sizes on the microstructure of CF/Al composites is shown in Fig. 3-10. The applied infiltration pressure for the fabrication of CF/Al composites was 0.8 MPa. In the case of Fig. 3-10 (a), the microstructure of CF/Al composites shows both the CF clustering and the large spaces in the matrix. It was supposed that the addition of the 2.55 μm Cu particles, smaller than the theoretical size for uniform fiber array, generate large margin between CFs. As a result, the molten Al infiltrated preferentially into large margin of the spaces with relatively low volume
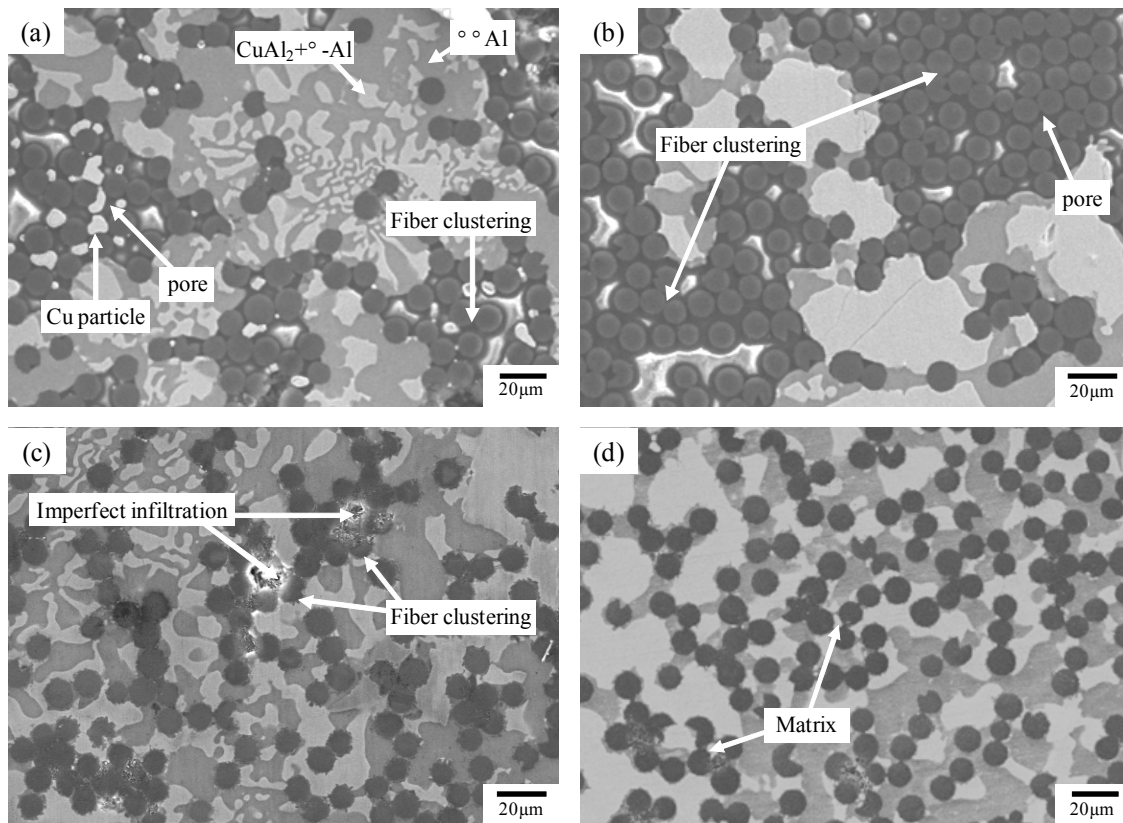
Fig. 3-10 Microstructure of CF/Al composites depending on the added average Cu particles size of; (a) 2.55, (b) 28.86, (c) 11.79 μm and (d) bimodal Cu particles, respectively.

fraction of CFs during the initial infiltration. Subsequently, the molten Al pressurized to the sideways of the CFs and the pressurized CFs clustered each other. Therefore, the molten Al was hard to infiltrate into the narrow spaces because the relatively high volume fraction between clustered CFs, even if there existed some Cu particles. In other words, the narrow spaces became pores because they were too narrow to infiltrate the molten Al with the applied infiltration pressure of 0.8 MPa. Fig. 3-10 (b) also shows the non-uniform fiber distribution such as fiber clustering and large space of matrix region. It was assumed that 28.86 μm Cu particles, relatively larger than theoretical size, were dispersed locally between the CFs and enlarged the spaces between the CFs. Thus, most of the molten Al infiltrated into those large spaces between CFs, whereas the narrow

66

space between clustered CFs remained pores, as shown in Fig. 3-10 (a). It was reported in [27] that a smaller or larger particle size than the theoretical size has an adverse effect on homogeneity of the fiber distribution. On the other hand, Fig. 3-10 (c) shows well dispersed fiber array in comparison with Fig. 3-10 (a) and (b). Since the added Cu particles had the average particle size of 11.79 μm, which were close to the theoretical size, the homogeneity of fiber arrays improved with decreasing fiber clustering.
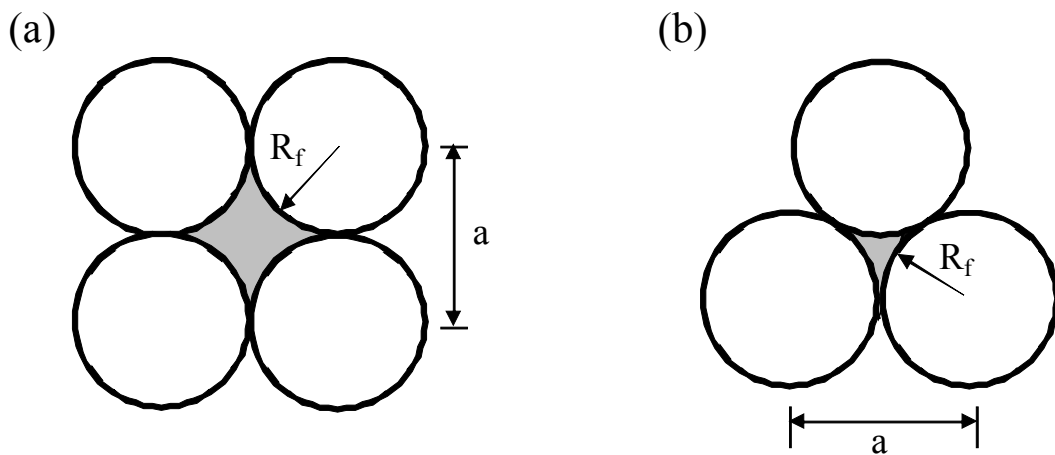
Fig. 3-11 Schematic description of closest packed fiber arrays: (a) square fiber distribution and (b) hexagonal fiber distribution.

However, some imperfect infiltration regions were observed in the closed CF arrays without Cu spacers. The schematics of Fig. 3-11 represented the common imperfect infiltration regions by CF clustering as shown in Fig. 3-10 (a), (b) and (c). The closest packed fiber arrays showed the narrowest spaces between fibers as well as highest fiber volume fraction. In these cases, the distance between each center of adjacent CFs 'a' equals to '$2R_f$'. In addition, the fiber volume fraction was able to be calculated to high volume fraction of 0.79 and 0.91 on the uniform square and hexagonal fiber distribution, respectively by using the Eq. (3-4) and (3-6). Thus, the required infiltration pressures on the uniform square and hexagonal fiber arrays were also recalculated to 0.95 and 2.63 MPa when the R_f was 5.5 μm. Since the required infiltration pressures at the clustered CF arrays were higher than the applied infiltration pressure, the narrow spaces remained

pores. As a countermeasure to prevent such CF clustering, the small Cu particles of 2.55 μm added with the nearly theoretical size of 11.79 μm. As a result, the CF/Al composites in Fig. 3-10 (d) show nearly homogeneous CF arrays without CFs clustering and infiltration defects mostly. The added small particles of 2.55 μm might have acted as spacers to prevent the formation of fiber clustering. The CF/Al composites of Fig. 3-10 (d) were expected to exhibit excellent mechanical properties without referred defects in the microstructure.

The distribution of the CFs in CF/Al composites can be quantitatively evaluated by computer analyzing the 2-dimensional spatial distribution. In the Ref. [39, 40], the distribution of second phase particles in matrix was examined by calculating the relative frequency distribution of the 2-dimensional local number (LN2D). Especially, variance of LN2D, $LN2D_{var}$ was a criterion for the degree of particle distribution. Fig. 3-12 shows the variance of LN2D versus area fraction of the particles. The line in Fig. 3-12 meant the theoretical and uniform random dispersion of the particles in matrix depending on the area fraction [40]. Moreover, the larger variance of particles than the line meant 'non-uniform' dispersion or 'clustering' and close to the line meant 'ordering'. Fig. 3-12 also represents $LN2D_{var}$ of CF/Al composites with different Cu particle sizes of 2.55, 11.79, 28.86 μm and bimodal. It is confirmed that the CF/Al composites with the bimodal Cu particles show excellent CFs distribution comparing with others.

Fig. 3-13 represents the influence of the addition of various Cu particles sizes for the fabrication of CF preform on the density of CF/Al composites. The densities of CF/Al composites were 1.88, 2.86, 2.09 and 3.00 Mg·m^{-3} in accordance with the addition of the average Cu particle sizes of 2.55, 11.79, 28.86 μm and bimodal Cu particles, respectively. Especially, CF/Al composites into which were added the bimodal Cu particles, have a high density level corresponding to about 95 % of relative density with the nearly homogeneous fiber distribution in the microstructure. In other words, the degradation of the density property of the CF/Al composites was significantly influenced on the creation of fiber clustering. From these results, the unidirectional

CF/Al composites with high density and excellent fiber distribution could be obtained by the LPI process with the applied pressure of 0.8 MPa.
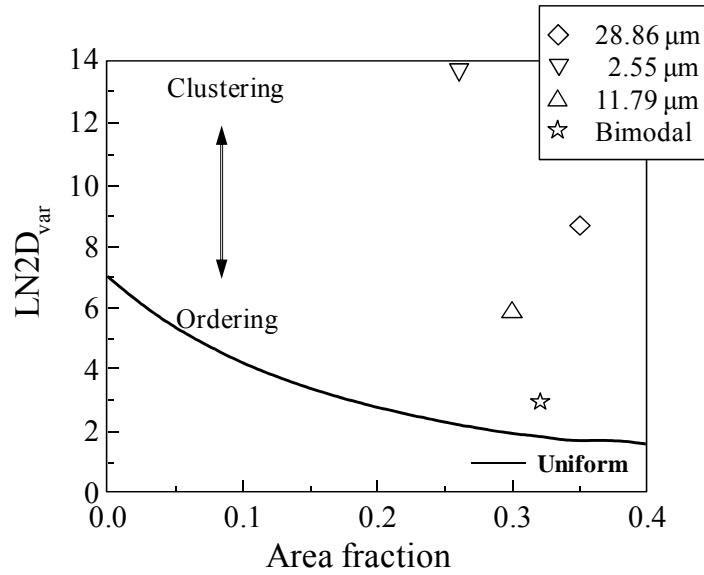
Fig. 3-12 Variance of LN2D depending on the area fraction of CFs in CF/Al composites.
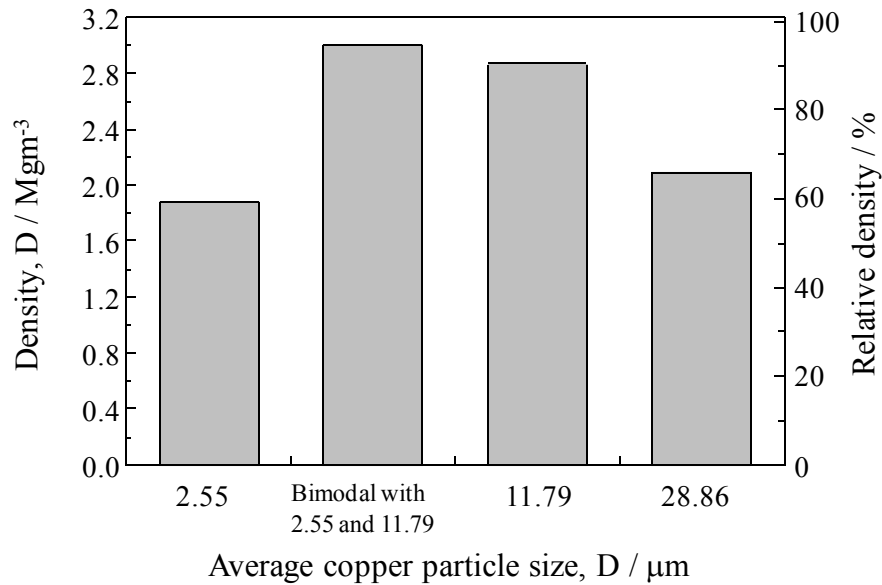
Fig. 3-13 Effect of the added Cu particle sizes on the density of unidirectional CF/Al composites.

3.4 Summary

(1) The unidirectional CF/Al composites were fabricated by LPI process, in conjunction with the decision of the applied infiltration pressure and control of the uniform CF array distribution for the densification of the composites.

(2) The theoretical infiltration initiation pressure for the fabrication of the unidirectional CF/Al composites was calculated to 0.2 MPa as a function of the capillary resistance, internal viscosity, gravity and back pressure when the CF volume fraction and radius were 0.3 and 5.5 μm. Although the increase of the applied pressure above calculated infiltration initiation pressure improve the density of the composites, there were generated imperfect infiltration region.

(3) The imperfect infiltration region around the CF clustering was occurred by non-homogeneity of CF arrays. Thus the theoretical sizes of the Cu particles were calculated and used for the uniform CF distribution.

(4) The unidirectional CF/Al composites with the addition of the nearly theoretical Cu particle size exhibited high density and relatively well dispersed CFs. However, there was also existed some of the clustered CFs and the pores. As a countermeasure to prevent such CF clustering, the small Cu particles added with the nearly theoretical size. As a result, the CF/Al composites exhibited the highest relative density of 95% without CF clustering mostly because the small size of Cu particles acted as spacers to prevent the formation of fiber clustering. From these results, the unidirectional CF/Al composites could be fabricated by the LPI process with the applied pressure of 0.8 MPa with high density and excellent fiber distribution.

References

[1] S. Mallik, N. Ekere, C. Best, R. Bhatti: App. Therm. Eng., **31** (2011) 355-362.

[2] S. Zhou , X. Zhang, Z. Ding, C. Min, G. Xu, W. Zhu: Composites A, **38** (2007) 301-306.

[3] A. M. K. Esawi, K. Morsi, A. Sayed, A. Abdel Gawad, P. Borah: Mater. Sci. Eng. A, **508** (2009) 167-173.

[4] C. L. Xu, B. Q. Wei, R. Z. Ma, J. Liang, X. K. Ma, D. H. Wu: Carbon, **37** (1999) 855-858.

[5] Th. Schubert, B. Trindade, T. Weißgärber, B. Kieback: Mater. Sci. Eng. A, **475** (2008) 39-44.

[6] Z. F. Xu, Y. B. Choi, K. Matsugi, D. C. Li and G. Sasaki: Mater. Trans., **50** (2009) 2160-2164.

[7] Z. F. Xu, Y. B. Choi, K. Matsugi, D. C. Li and G. Sasaki: Mater. Trans., **51** (2010) 510-515.

[8] J. Wang, T. Hong, G. Li and P. Li: Composites A, **28** (1997) 943-948.

[9] T. Shalu, E. Abhilash, M.A. Joseph: J. Mater. Proc. Tech., **209** (2009) 4809–4813.

[10] F. Boland, C. Colin, and F. Delannay: Metall. Mater. Trans. A, **29** (1998) 1727-1739.

[11] J. I. Song, Y. C. Yang, K. S. Han: J. Mater. Sci., **31** (1996) 2615-2621.

[12] H. Uozumi, K. Nakanishi, K. Inoue, T. Tsukada, N. Fuyama, T. Fujii and M. Yoshida: J. Jpn. Inst. Light Met. **59**   2009   562–568.

[13] S. Ravi Kumar, M.K. Panigrahi, S.K. Thakur, K.U. Kainer, M. Chakraborty, B.K. Dhindaw: Mater. Sci. Eng. A, **415** (2006) 207-212.

[14] A. J. Cook and P. S. Werner: Mater. Sci. Eng. A, **144** (1991) 189-206.

[15] L. Weber, J. Dorn, A. Mortensen: Acta Materialia **51** (2003) 3199-3211.

[16] H. Ouyang, H. Li, L. Qi, Z. Li, T. Fang, J. Wei: J. Mater Sci., **43** (2008) 4618-4624.

[17] E. Carreño-Morelli , T. Cutard, R. Schaller, C. Bonjour: Mater. Sci. Eng. A, **251** (1998) 48–57.

[18] A. Daoud: Mater. Sci. Eng. A, **391** (2005) 114–120.

[19] W. Hufenbach, M. Andrich, A. Langkamp, A. Czulak: J. Mater. Proc. Tech., **175** (2006) 218–224.

[20] R. Prieto, J. M. Molina, J. Narcisoa and E. Louis: Scripta Materialia, **59** (2008) 11-14.

[21] G. Requena, G. Fiedler, B. Seiser, P. Degischer, M. D. Michiel, T. Buslaps: Composites A, **40** (2009) 152–163.

[22]   Z. Zhang, S. Long and H. M. Flower: Composites, **25** (1994) 380-392.

[23] B. Moser, A. Rossoll, L. Weber, O. Beffort, A. Mortensen: Composites A, **32** (2001) 1067-1075.

[24] B. Bhav Singh, M. Balasubramanian: J. Mater. Proc. Tech., **209** (2009) 2104-2110.

[25] T. Matsunaga, K. Matsuda, T. Hatayama, K. Shinozaki, M. Yoshida: Composites A, **38** (2007) 1902–1911.

[26] A. A. Baker: Mater. Sci. Eng., **17** (1975) 177-208.

[27] M. Mizumoto, Y. Kaneko, A. Kagawa: J. Jpn. Inst. Metals, **68** (2004) 1047-1052.

[28] Y. B. Choi, G. Sasaki, K. Matsugi and O. Yanagisawa: Mater. Trans., **46** (2005) 2156-2158.

[29] Y. B. Choi, G. Sasaki, K. Matsugi, N. Sorida, S. Kondoh, T. Fujii and O. Yanagisawa: JSME International Journal A, **49** (2009) 20-24.

[30] Y. B. Choi, K. Matsugi, G. Sasaki, K. Arita and O. Yanagisawa: Mater. Trans., **47** (2006) 1227-1231.

[31] Y. B. Choi, K. Matsugi, G. Sasaki and S. Kondoh: Mater. Trans., **49** (2008) 390-392.

[32] S. Long, Z. Zhang, H. M. Flower: Acta Metall. Mater. **42** (1994) 1389-1397.

[33]   A. Mortensen and J. A. Cornie: Metall. Trans. A, **18** (1987) 1160-1163.

[34] S. Suresh, A. Mortensen and A. Needleman: Fundamentals of Metal-Matrix

Composites, Copyright © 1993 by Butterworth-Heinemann, ISBN 0-7506-9321-5.

[35] P. S. Laplace: Mechanique Celeste, Paris, 1806.

[36] A. W. Adamson: Physical Chemistry of Surfaces 5th edition, 1990, Wiley, ISBN 0-4716-1019-4.

[37] K. Landry, S. Kalogeropoulou, N. Eustathopoulos, Y. Naidich and V. Krasovsky: Scripta Mater., **34** (1996) 841-846.

[38] L. Battezzati and A. L. Greer; Acta Metall., **37** (1989) 1791-1802.

[39] K. Sugio, Y. Momota, D. Zhang, H. Fukushima and O. Yanagisawa: Mater. Trans., **48** (2007) 2762-2767.

[40] K. Sugio, G. Sasaki and O. Yanagisawa: 18th International Conference on Composite Materials (ICCM-18), 2011

Chapter 4

Thermal and mechanical properties of the unidirectional CF/Al composites fabricated by LPI process

4.1 Introduction

In the thermal management material fields, the composite materials with high thermal conductivity (TC) and light weight have been expected to utilize as heat sink materials for high heat generation parts [1, 2]. Recently, the metal matrix composites (MMCs) reinforced with SiC have been widely developed as the heat sink materials. However, the high volume of SiC reinforcement was required to accomplish for the desired TC and coefficient of thermal expansion (CTE) because the TC and CTE of SiC has not excellent thermal properties as shown in Table 1-4. In addition, the composite materials reinforced with SiC are difficult to machining because of the high hardness property. On the other hand, the coal-tar pitch based carbon fibers (CFs) possess high thermal and electrical conductivity, extremely low CTE and good mechanical properties through the longitudinal direction. In addition, the coal-tar pitch based CF reinforced Al composites can be one of the promising materials for the heat sink components with high TC, light weight and good workability. Moreover, the low pressure infiltration (LPI) method is the useful fabrication process for composite materials with cost saving and possibility of large or complex structure [3-7].

The unidirectional CF/Al composites fabricated by LPI process are required to investigate the thermal and mechanical properties in order to evaluate the suitability as heat sink materials. However, the CF/Al composites inevitably contain Al_4C_3 at the fiber-matrix interface by chemical reaction between the CF and Al. The Al_4C_3 is able to give a bad effect to the TC of CF/Al composites. Many attempts have been made to characterize the Al_4C_3 in both chemical and mechanical fields [8-26]. It was known that the generation and growth of Al_4C_3 happened at the temperature above 773 K with holding time. In the LPI process for CF/Al composites, Al_4C_3 could easily generate where the molten Al infiltrated into the porous CF preform. Therefore, the effect of the

generation of Al_4C_3 on the TC of the unidirectional fiber reinforced composites has to be characterized.

In the present study, the TC of the coal-tar pitch based unidirectional CF/Al composites by LPI process have been characterized, in conjunction with the discussion of the improvement way of the TC of the composites. Especially, the influence of the interfacial reactants on the TC of CF/Al composites was discussed attention being paid to the damage of CFs. Besides, the CTE and flexural strength of the CF/Al composites were evaluated. From these investigations, the suitability of the unidirectional CF/Al composites as heat sink was discussed.

4.2 Evaluation methods

4.2.1 Thermal conductivity

The thermal conductivity of unidirectional CF/Al composites was evaluated by laser flash method thermal constants measuring system (TC-700, ULVAC-RICO Inc., Japan) at the room temperature in air. The schematic illustration was shown in Fig. 4-1. The specimen size of transverse and longitudinal direction of unidirectional CF/Al composites was ø 10 × H 1 and ø 10 × H 2 mm^3, respectively. One side (front side) of the thin circular disc specimens were placed in the laser flash apparatus was irradiated with instantaneous heat source by laser beam and the temperature was detected by thermocouple at the other side (back side). The thermal conductivity is calculated as follows:

$$\lambda = \alpha \cdot \rho \cdot C_p \qquad\qquad (4\text{-}1)$$

where λ, α, ρ and C_p are thermal conductivity (Wm^{-1}K^{-1}), thermal diffusivity (m^{2}s^{-1}), density (Mgm^{-3}) and specific heat (Jg^{-1}K^{-1}) of the sample, respectively. The thermal diffusivity is also calculated as follows:

$$\alpha = 1.37 \cdot L^2 / (\pi^2 \cdot t_{1/2}) \qquad\qquad (4\text{-}2)$$

where L is specimen thickness and $t_{1/2}$ (ms) is the half of the time which reaches to maximum temperature of specimen after irradiation by laser. The $t_{1/2}$ of the CF/Al composites was measured by the laser flash apparatus.
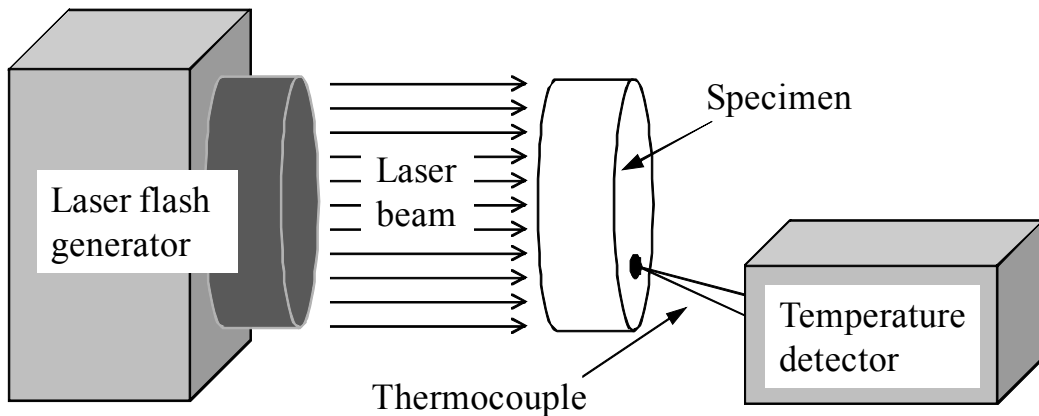
Fig. 4-1 Schematic diagram of laser flash method.

4.2.2 Coefficient of thermal expansion

The CTE is one of the important properties on the composite materials for heat sink materials to avoid thermal stress with objects such as the heat generation parts by matching the CTE. Typically, many of studies have introduced various kinds of dilatometers as the measurement method of CTE for several materials [27-45]. The dilatometer enables to measure the CTE accurately in the broad range of temperature. However, the specimens have to be precisely worked for the desired size and roughness in order to reduce errors. In addition, the measurement by the dilatometer can only be performed on the straightforward geometries of specimen [46]. Few papers introduced a strain gage method as the alternate method for the measurement of CTE. The strain gage method is able to measure the CTE on the arbitrary geometries of specimens with easily and quite accurately measuring by strain gage [46-49]. Therefore, the strain gage method can be utilized in in-situ experiment. In this study, the CTE of unidirectional CF/Al composites was also investigated with the reliability of the newly designed and fabricated CTE measuring equipment by strain gage method, as described in Fig. 4-2.

The thermal strain on longitudinal and transverse direction of the unidirectional CF/Al composites was simultaneously measured by 0/90° type strain gage (Type; KFG-

3-120-D16-11L3M2S, Kyowa Electronic Instruments Co., LTD., Japan) at the exposed temperature range from room temperature to 393 K.

Although the CTE measurement by a strain gage looks different in several studies [46, 47], they used same principle [46]. That is, the strain of a sample is compared to the strain of a reference material, which was well known CTE. The calculation of CTE was expressed as followed equation:

$$\alpha_s = \alpha_r + (\varepsilon_s - \varepsilon_r) / \Delta T \qquad (4\text{-}3)$$

where α_s and α_r are the CTE of the specimen and reference material, ε_s and ε_r are the strain of the specimen and reference material at the test temperature, ΔT is variation of the test temperature. The test temperature was from 300 to 393 K. The extremely low CTE material such as titanium silicate (CTE= 0) was preferred mostly as a reference material to measure accurately. However, the reference material was replaced in soda-lime glass (CTE= $9.2 \times 10^{-6}\,K^{-1}$ [48]) in this study. The strain of the soda-lime glass at the test temperature was measured to -392 and -402 μmm^{-1}, in which the gage length was 2 and 3 mm, respectively.
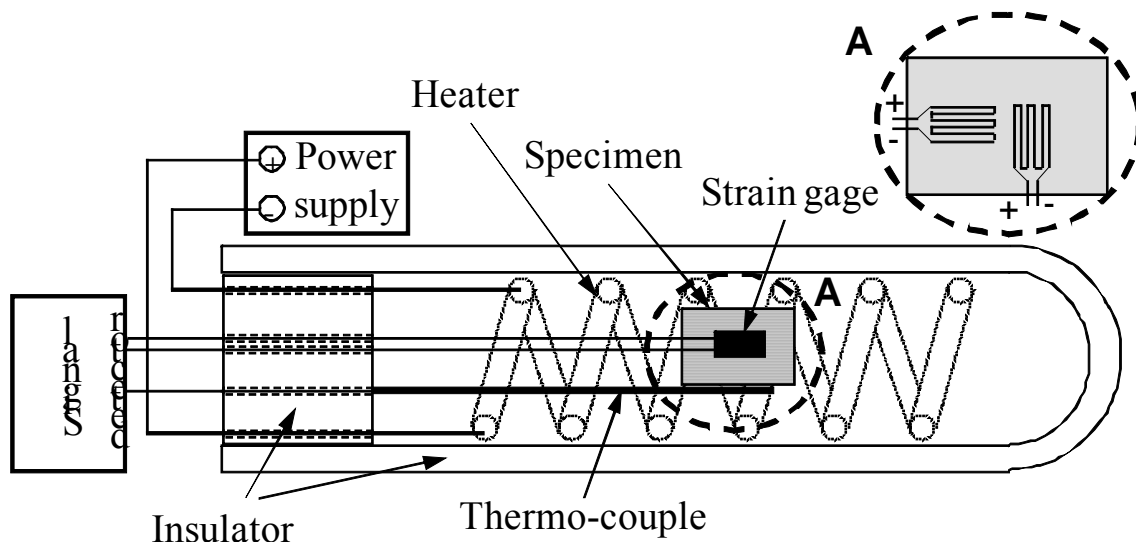
Fig. 4-2 Measurement apparatus of coefficient of thermal expansion by strain gage method.

4.2.3 Flexural strength

The flexural strength of unidirectional CF/Al composites was evaluated by universal testing machine (Shimadzu corp. DSC-R-5000, Japan). The 3-point bending test was carried out for the evaluation of the flexural strength. The support span and the crosshead speed were 16 mm and 0.0083 mms^{-1}, respectively. The dimension of a specimen was W4.0 × T2.0 × L20 mm^3.

4.2.4. Quantification of Al_4C_3

The interfacial reaction between Al-C interfaces is occurred in unidirectional CF/Al composites over fabrication stages of LPI process. The chemical reaction is expressed as followed:

$$4Al + 3C \rightarrow Al_4C_3 \qquad (4\text{-}4)$$

On the other hand, Al_4C_3 is able to react with water and then generate CH_4 gas as below,

$$Al_4C_3(s) + 12H_2O(l) \rightarrow 3CH_4(g) + 4Al(OH)_3(s) \qquad (4\text{-}5)$$
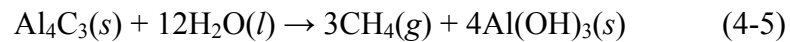
The generation amount of Al_4C_3 in CF/Al composites can be estimated by a water immersion test as shown in Fig. 4-3, in conjunction with the measurement of generated gas or weight loss of CF/Al composites after venting CH_4 gas and use of the Eq. (4-5). Moreover, the weight loss of CFs in CF/Al composites can be also measured by using Eq. (4-5) and (4-5). In the present study, the weight loss of the CF/Al composites was measured in order to estimate the amount of Al4C3. In addition, the weight loss of CFs was also measured in the viewpoint of the degradation of CFs by the interfacial reaction.
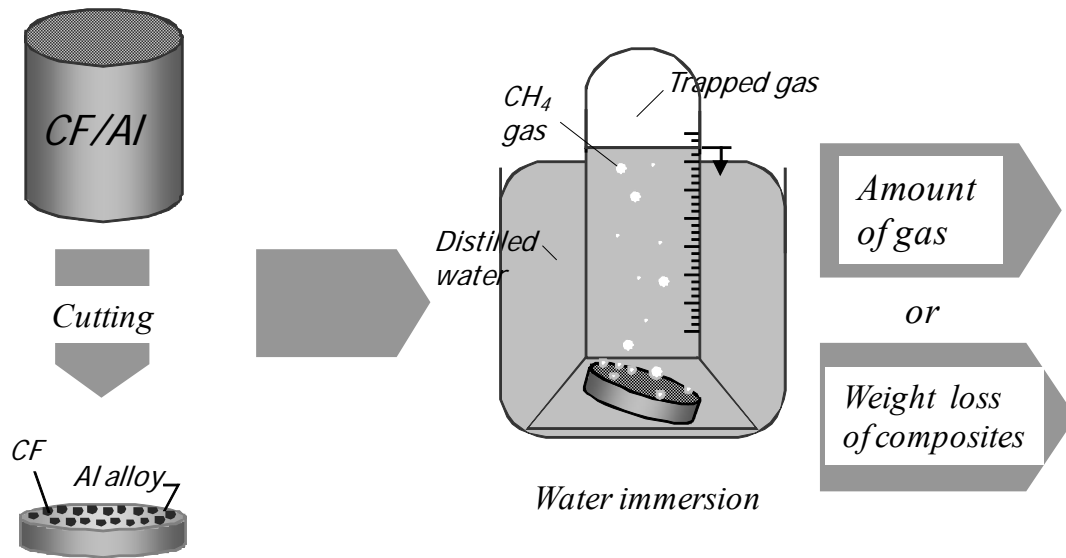
Fig. 4-3 Water immersion test for measurement of Al_4C_3 amount.

4.2.5 Extraction of CFs from CF/Al composites

The CFs was extracted by immersing in aqueous 2N HCl solution of CF/Al composites. The matrix was corroded and the Al_4C_3 in the interfacial was removed by the chemical reaction with HCl as below:

$$Al_4C_3 + 12HCl \rightarrow 3CH_4(g) + 4AlCl_3 \qquad (4\text{-}6)$$
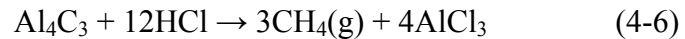
The CFs was extracted from the CF/Al composites by ultrasonic vibration in the HCl solution and then filtered from the HCl solution. Fig. 4-4 shows the schematic diagram for the extraction process of CFs from CF/Al composites.

4.2.6 Microstructure

The observation of surface microstructures of CFs extracted from CF/Al composites was carried out by scanning electron microscope (SEM; Hitachi S-3000H2, Japan). Especially, the surface damages of those CFs by interfacial reaction was intensively discussed. Moreover, the radius reduction of damaged CFs was measured from those microstructures.
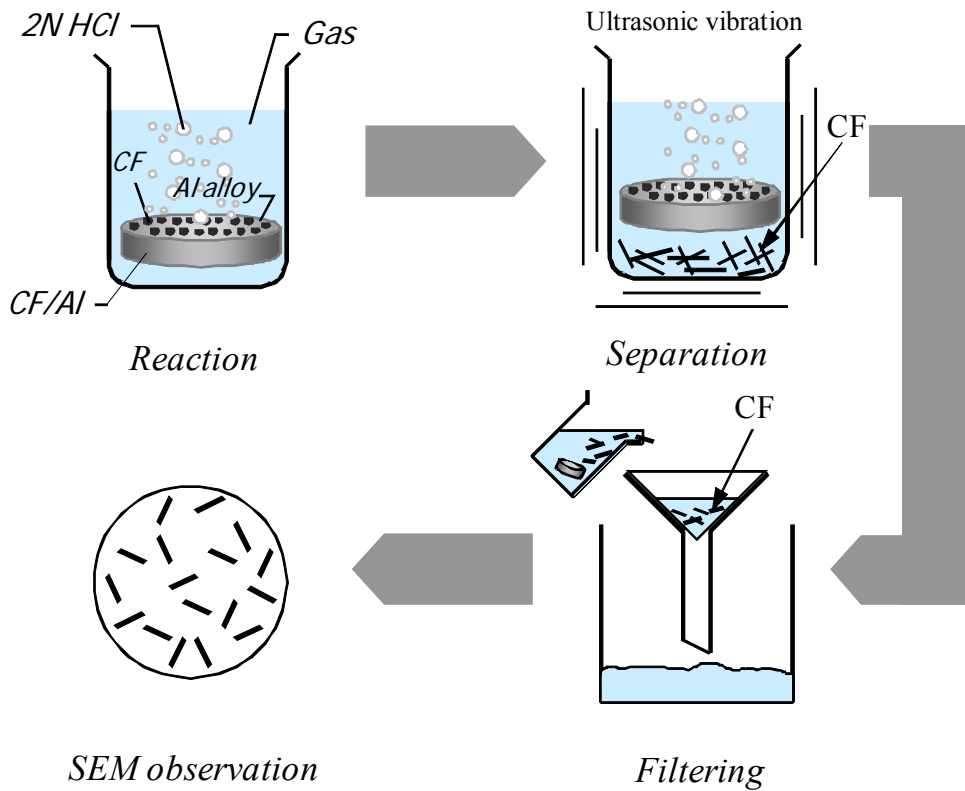
Fig. 4-4 Extraction process of CFs from CF/Al composites.

4.3 Results and discussion

4.3.1 Influence of Al$_4$C$_3$ on the TC of unidirectional CF/Al composites

The creation of the interfacial reactant between CFs and Al matrix was inevitable after the infiltration in the LPI process. It has been reported that the nucleation and growth of the interfacial reactant Al$_4$C$_3$ initiate at the exposure temperature above 773 K [8]. The temperature versus holding time at the LPI process was shown in Fig.4-5. The infiltration of the molten Al into the unidirectional CF preform initiated at the temperature of 1073 K, after then the infiltrated body was cooled in the electrical furnace. The infiltration was carried out during 1 min at 1073 K, and the cooling time from the infiltration temperature to reach 773 K was controlled every 10 min from 30 to 10 min by increasing the Ar flow into the electrical furnace. The generation of Al$_4$C$_3$ is expected during those 'infiltration process' and 'cooling process' until 773 K. Moreover, the generation amount of Al$_4$C$_3$ has to be investigated in order to confirm which one is predominant between those two processes.
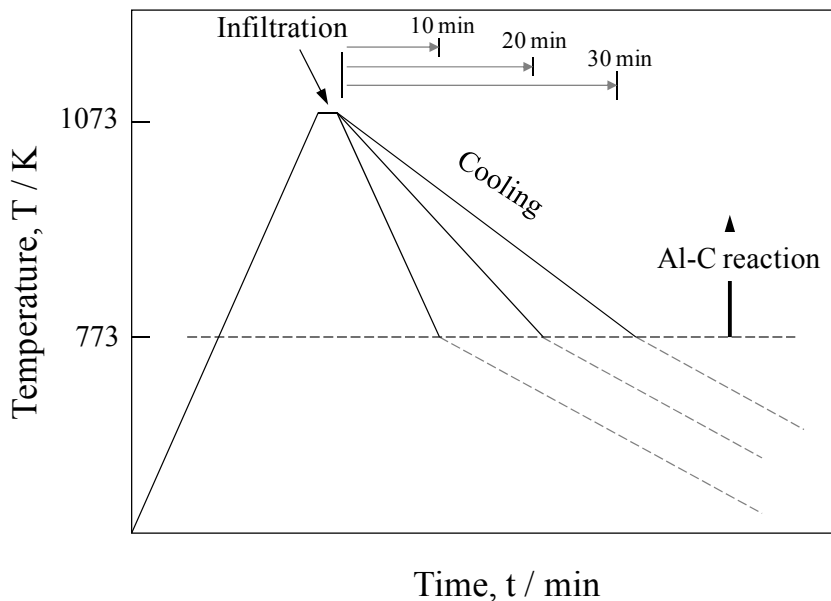
Fig. 4-5 Cooling conditions of unidirectional CF/Al composites after infiltration in LPI process.

Meanwhile, the amount of Al_4C_3 can be calculated from the weight loss of CF/Al composites by venting CH_4 gas as mentioned before. The weight loss of CF/Al composites by a water immersion test can transform the amount of vented CH_4 gas. Using the ratio of atomic weight between Al_4C_3 and $3CH_4$ of 144:48 with the Eq. (4-5), the amount of Al_4C_3 is calculated. Furthermore, the growth rate of Al_4C_3 can be calculated which is based on the Ref. [10] as follows:

$$dw / dt = K / t \qquad\qquad (4\text{-}7)$$

$$w^2 / 2 = Kt + C \qquad\qquad (4\text{-}8)$$

$$w = \sqrt{2Kt} \qquad\qquad (4\text{-}9)$$

where w, K and t are weight of Al_4C_3, rate constant and holding time, respectively. Moreover, the K can be expressed by Arrhenius' law as

$$K = k \exp(-Q/RT) \qquad\qquad (4\text{-}10)$$

Taking logarithms,

$$\ln(\sqrt{2K}) = \ln(2k)/2 - Q/(2RT) \qquad\qquad (4\text{-}11)$$

where k, Q and R are a constant, activation energy ($kJmol^{-1}$) and a gas constant (8.31 kJ $K^{-1}mol^{-1}$), respectively. The activation energy Q is calculated from the gradient of the straight line in a graph of ln(2K) versus 1/T.

The growth of Al_4C_3 at the 'infiltration process' is able to be derived by calculating the activation energy. The heat treatment with the temperature of 783, 823 and 873 K of the unidirectional CF/Al composites has been carried out to calculate the activation energy. After heat treatment, the growth amount of Al_4C_3 is calculated by measuring the weight loss of CF/Al composites, in conjunction with the equations from Eq. (4-7) to (4-9). Fig. 4-6 represents the growth amount of Al_4C_3 as a function of the temperature and holding time of the heat treatment. Each gradient of linear fitting is $(2K)^{1/2}$ on each

temperature in accordance with the Eq. (4-9). The rate constant of $(2K)^{1/2}$ can be expressed by Arrhenius plot, as shown in Fig. 4-7. From the gradient of the plot, the activation energy Q is calculated as 127.31 kJmol^{-1}, in accordance with the Eq. (4.11). Such activation energy Q of the K13D2U CF is close to that of the graphite fiber (147.19 kJmol^{-1})[8], while the high strength CF[10] showed low activation energy as 53 kJmol^{-1}. The calculated activation energy can derive the growth amount of Al$_4$C$_3$ from the Eq. (4-11) and (4-9). As a result, the growth amount of Al$_4$C$_3$ at the 'infiltration process' is calculated as 0.279 wt% at the infiltration temperature of 1073 K. The infiltration of Al into the CF preform is possible at the temperature above Al melting point of 933 K. If the infiltration temperature decreased such as 1023 and 973 K, the average thickness of Al$_4$C$_3$ also decreases to 0.197 and 0.134 wt%, respectively.
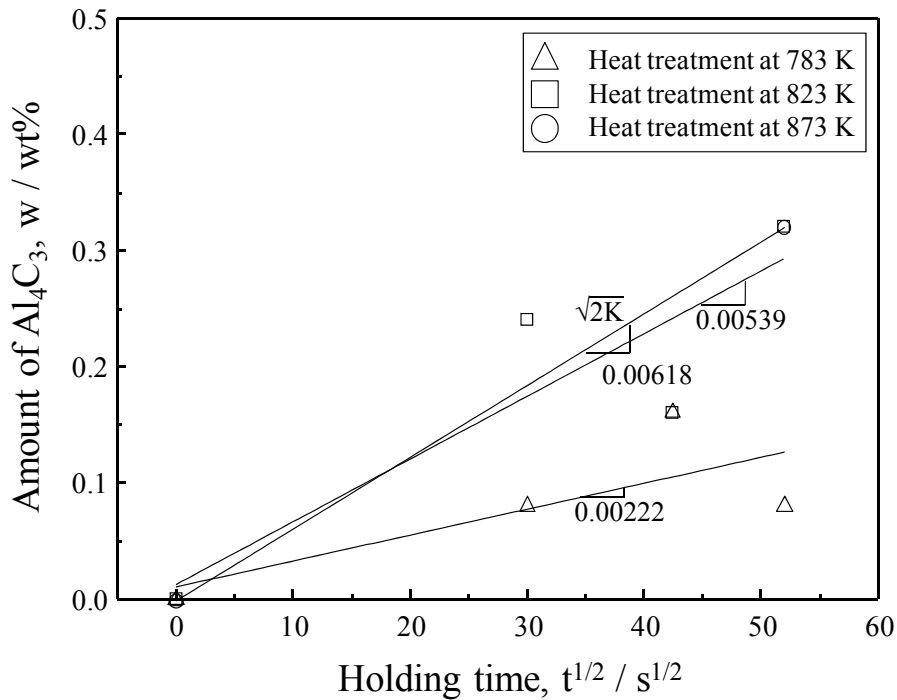
Fig. 4-6 Growth amount of aluminum carbide generated on CF surface as a function of the temperature and the holding time of heat treatment.
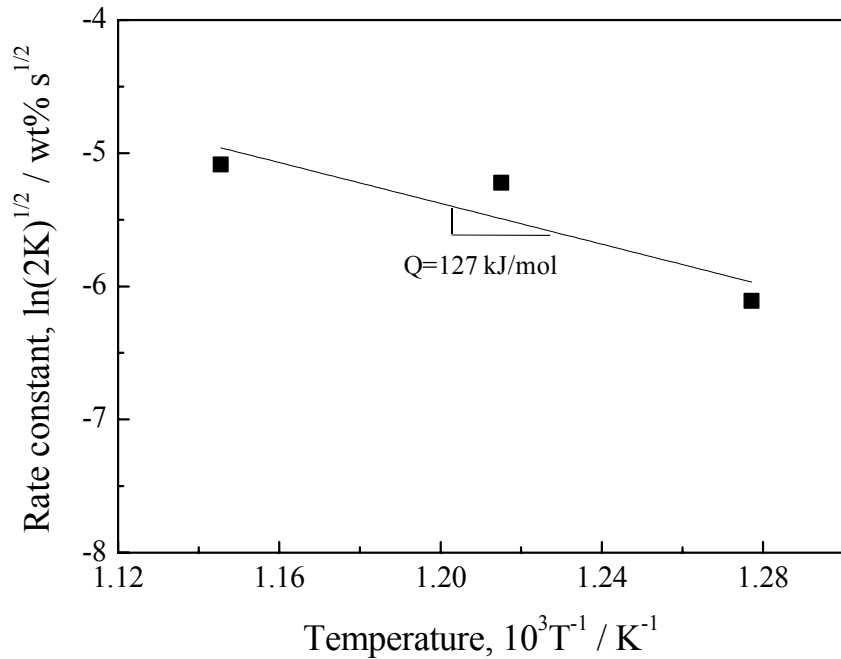
Fig. 4-7 Temperature dependence of the rate constant for the growth of aluminum carbide in Al-CF systems.

On the other hand, the growth amount of Al_4C_3 at the 'cooling process' is difficult to derive from the Arrhenius plot, due to the rapid and irregular change of the temperature at the cooling. Thus, the growth of Al_4C_3 in 'cooling process' is calculated from the weight loss of the CF/Al composites by venting CH_4 gas. Fig. 4-8 represents the growth amount of Al_4C_3 as a function of the cooling time at the LPI process. The growth amount of Al_4C_3 increased as 0.074, 0.158 and 0.284 wt% depending on the cooling time of 10, 20 and 30 min, respectively.

From these results, the growth amount of Al_4C_3 can be controlled according to changing both infiltration temperature and cooling time. Especially, the changing the cooling time is effective to control the generation of Al_4C_3.
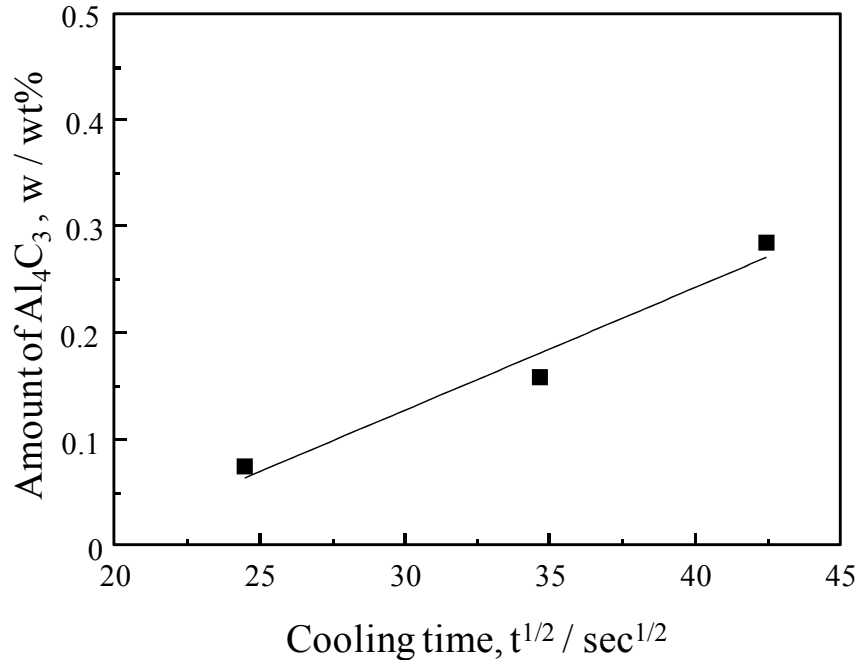
Fig. 4-8 Growth amount of aluminum carbide generated on CF surface depending on the cooling time at LPI process.

Fig.4-9 represents the thermal conductivity of unidirectional CF/Al composites as a function of cooling time at LPI process. With increasing cooling time, the longitudinal TC of composites was significantly decreased, whereas the transverse TC was not affected by cooling time mostly. It is assumed that the sufficiently generated Al_4C_3 can give a decisive effect on the TC of the CF/Al composites from the viewpoint of the CF degradation. In fact, the increase of CF-matrix reaction time led to increase the amount of Al_4C_3 and simultaneously decrease the weight of CF. The ratio of atomic weight between C and Al_4C_3 is 12:144. Thus, the weight loss of CFs can be calculated by using Eq. (4-4) and (4-5), as shown in Fig. 4-10. The weight loss of CFs was 0.09, 0.19 and 0.34 wt% according to the increasing cooling time of 10, 20 and 30 min, respectively. Since the unidirectional CF has high TC of parallel direction to the fiber axis (800 $Wm^{-1}K^{-1}$), the longitudinal TC is more sensitive on the weight loss of CFs than transverse

direction. In other words, it is doubtless that the weight loss of the CFs in composites is a main reason of decreasing longitudinal TC of composites.

Fig. 4-9 Thermal conductivity of longitudinal and transverse directions of unidirectional CF/Al composites depending on the cooling time at LPI process.
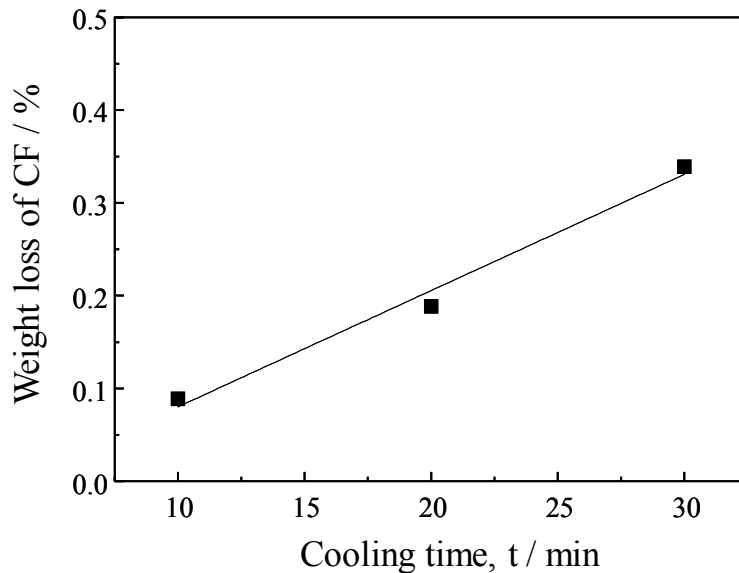
Fig. 4-10 Weight loss of carbon fibers in unidirectional CF/Al composites depending on the cooling time at LPI process.

88

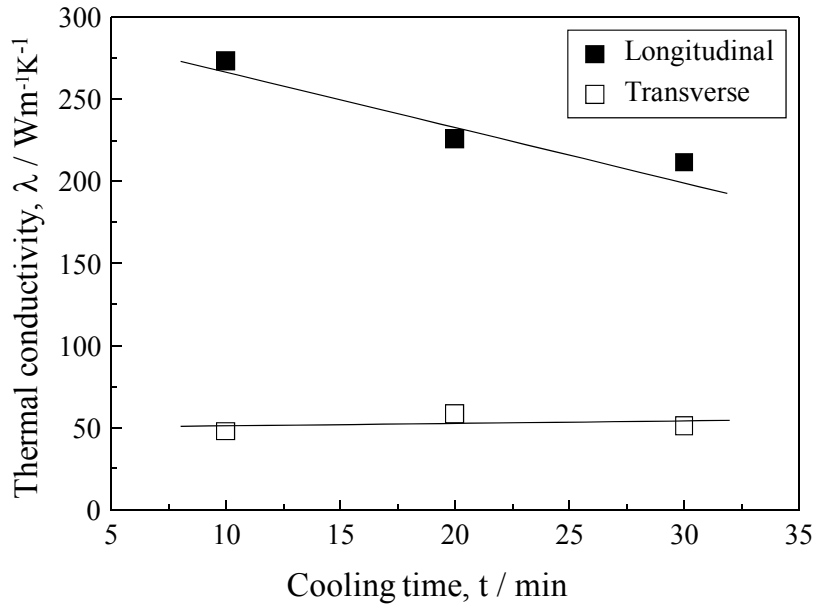However, the growth amount of Al_4C_3 was very little. That is, such little amount of Al_4C_3 cannot give significant effects on the longitudinal TC of the CF/Al composites. Meanwhile, the longitudinal TC was derived from area reduction of CFs according to the weight loss of CFs. Fig. 4-11 shows the calculated TC from the uniform radius reduction of CFs depending on the cooling time. The variation of TC from the radius reduction was not big difference, whereas the experimental values of TC shows significant decrease. Such assumption as uniform area reduction of CFs by generation of the uniform Al_4C_3 layer around CFs was not suitable to account for the significant loss of longitudinal TC.

Indeed, the Al_4C_3 by interfacial reaction did not created with the uniform layer form according to the SEM observation of the extracted CF from composites, as shown in Fig. 4-12. All of the CF surfaces (Fig. 4-12 (b)-(d)) depending on the cooling time of 10, 20 and 30 min were damaged by the generation of Al_4C_3, in comparison with the initial CF (Fig. 4-14 (a)). In case of Fig. 4-12 (b), the small and spot-like fiber damages at the local area of CF surface were observed because of the short duration of cooling time of 10 min. The spot-like fiber damage might be caused by the growth of the small group of the needle-like shaped Al_4C_3 from the CF surface to the Al matrix. Of course, the short duration of fiber-matrix reaction time is expected to limit the generation of Al_4C_3. Such small damages might not affect much to decrease the longitudinal TC of the CFs and further CF/Al composites significantly.
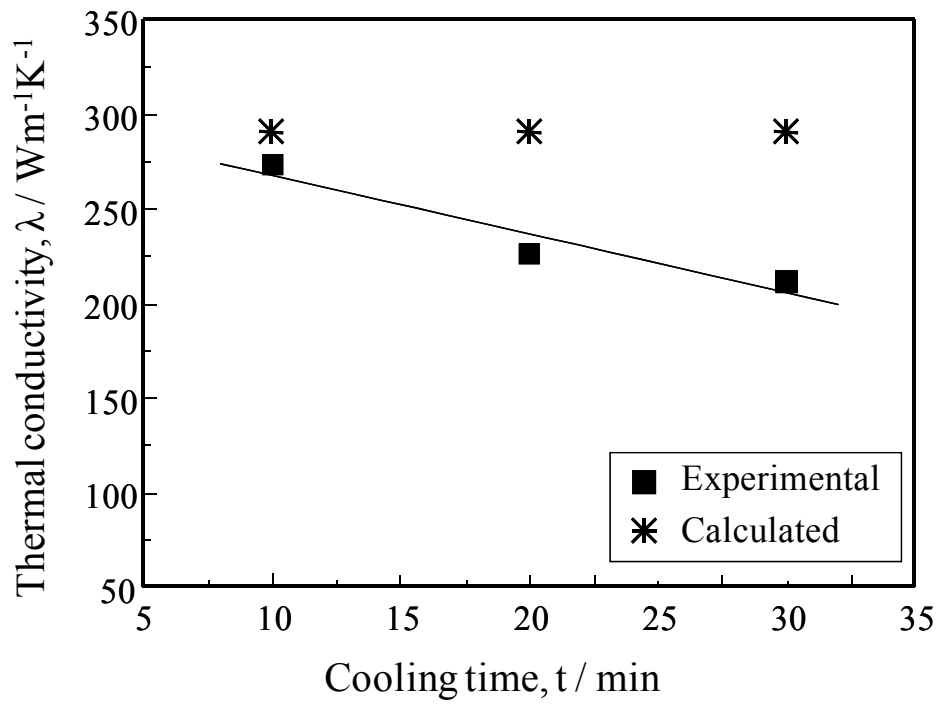
Fig. 4-11 Thermal conductivity by calculated uniform radius reduction of CFs and experimental depending on the cooling time at LPI process.
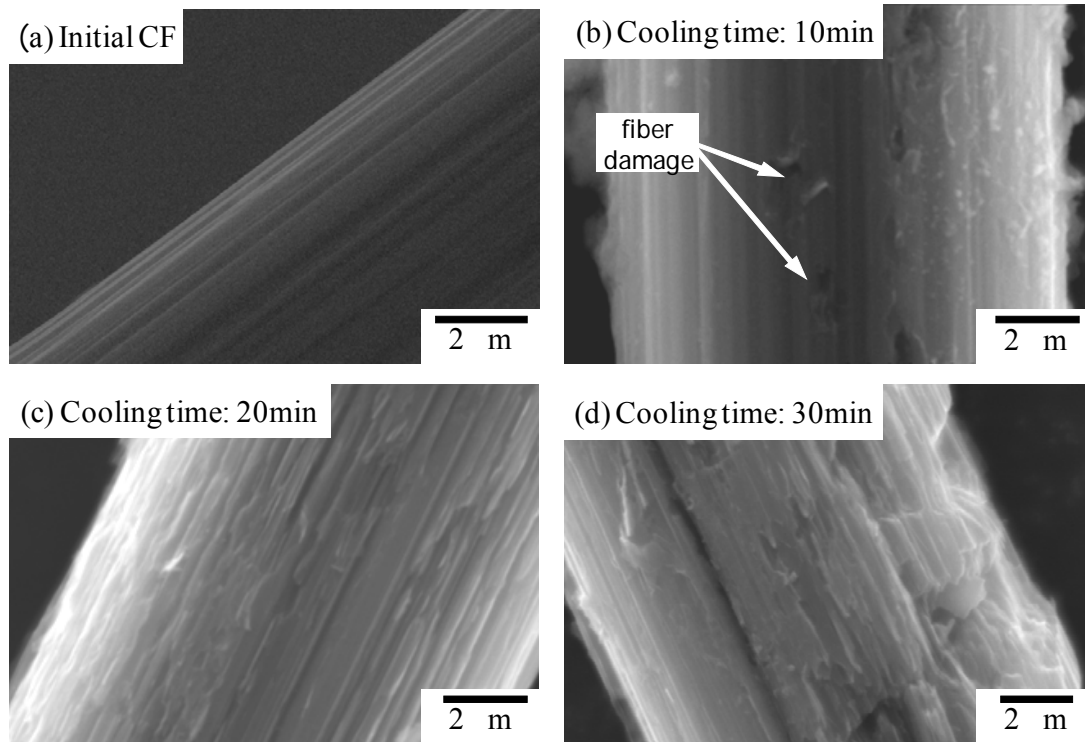
Fig. 4-12 Microstructure of carbon fiber surface; (a) initial fiber and (b), (c) and (d) damaged surfaces depending on the cooling time of (b) 10, (c) 20 and (d) 30 min at LPI process.

However, there were shown the remarkable fiber surface damages in Fig. 4-12 (c) and (d) according to increasing cooling time of 20 and 30 min. The locally and harshly damaged CF surface was able to disturb the effective heat flow to the parallel direction of the fiber axis such like Fig. 4-13, due to becoming the locally and drastically narrow cross-sectional area of the CF. The shrunken cross-sectional area of CF is considered a main reason of deteriorating longitudinal TC significantly. The longitudinal TCs of CF/Al composites are able to be recalculated by measuring the narrowed diameters of locally damaged CFs in the SEM images. Table 4-1 listed the diameter variation of the CFs, as a function of the cooling time at the LPI process. From the recalculation of TC by those data, the longitudinal TC decreased with increasing cooling time, as shown in Fig. 4-14. The calculation of longitudinal TC by locally narrowed CFs may not be

accurate because the measurement of damaged CF diameter was limited at the local SEM images. However, it is obvious that the prediction of TC from damaged TC was more sensitive on the cooling time than the calculation of the TC from the uniform radius reduction of CFs.

Table 4-1 Variation of local diameter of CFs depending on the cooling time at LPI process.

Cooling time (min)	Specimen No.	Diameter (μm)	Average diameter (μm)
10	1	10.81	10.784
	2	10.95	
	3	10.79	
	4	10.97	
	5	10.4	
20	1	10.15	10.318
	2	10.15	
	3	10.39	
	4	10.64	
	5	10.26	
30	1	9.97	9.966
	2	10.23	
	3	9.3	
	4	9.88	
	5	10.45	

Therefore, the local damage of CFs by generation of Al_4C_3 is able to be the main reason to decrease longitudinal TC of the unidirectional CF/Al composites. Furthermore, the short duration of cooling time on the LPI process is required in order to maintain the high performance of the TC through longitudinal direction.
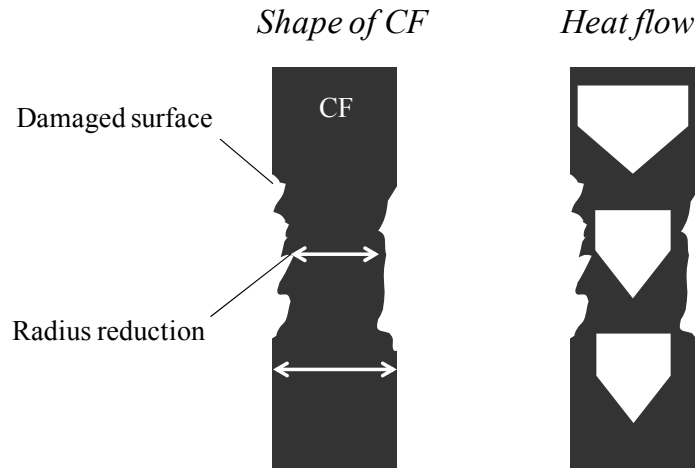

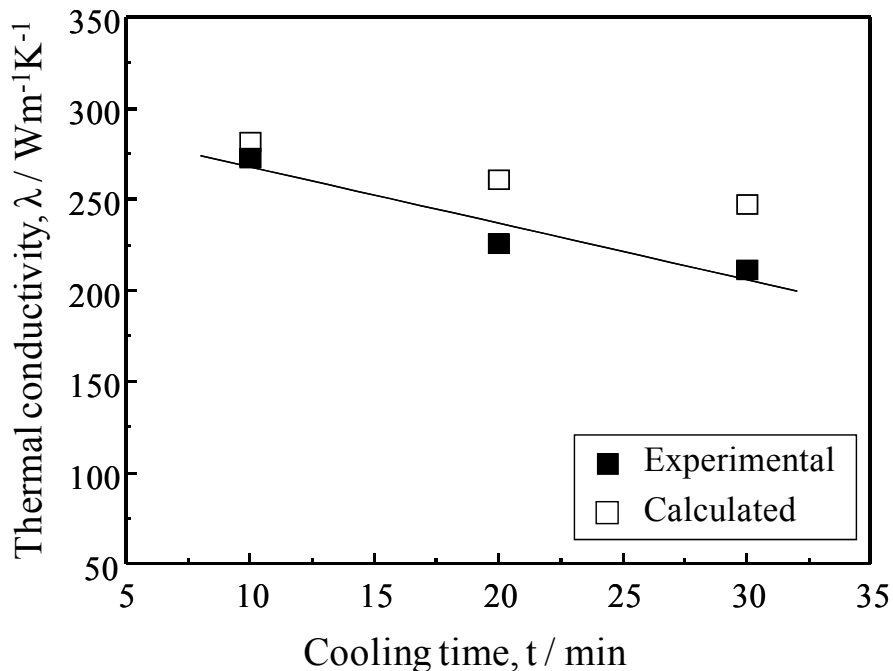Fig. 4-13 Schematic description of heat flow through the damaged CF.

Fig. 4-14 Thermal conductivity by calculated from the surface damage of CFs and experimental depending on the cooling time at LPI process.

4.3.2 Thermal conductivity of unidirectional CF/Al composites

The TC properties of the unidirectional CF/Al composites such as matrix and longitudinal and transverse direction have been investigated, in conjunction with their theoretical values calculated by well-known rule of mixture (ROM) of the CF and matrix. The ROM on the TC of CF/Al composites is expressed as follow:

$$\lambda_c = \lambda_m V_m + \lambda_f V_f \qquad (4\text{-}12)$$

where λ_c, λ_m and, λ_f are the TC of the composites, matrix and fiber, V_m and V_f are the volume fraction of matrix and fiber. The required properties in Eq. (4-12) were summarized in Table 4-2. Fig. 4-15 exhibits the TC of the CF/Al composites and the matrix by laser flash method at room temperature. The matrix and composites were fabricated with the cooling time of 10 min, at the temperature range from 1073 K to 773K after spark sintering and LPI process, respectively. The initial CF possessed the high longitudinal TC of about 800 $Wm^{-1}K^{-1}$ which was offered from company. Besides, the TC of the matrix such as Al- 35 wt% Cu alloy was as 71.7 $Wm^{-1}K^{-1}$ in this experiment.

The 30 vol% CF/Al composites represented the excellent longitudinal TC of 273.2 $Wm^{-1}K^{-1}$. The longitudinal TC of composites was corresponding to 94 % of the theoretical value. It can be supposed that the heat was individually conducted to CFs and matrix on longitudinal direction of composites without any remarkable heat loss by fiber-matrix interfacial reaction.

Table 4-2 Thermal conductivity of the raw materials used in this study.

Material	composition	Thermal conductivity ($Wm^{-1}k^{-1}$)		Volume fraction
CF (K13D2U)	99.9% C	Long.	800	0.3
		Trans.	2.4 (assume)	
Matrix	Al-35wt%Cu	71.7 (experiment)		0.7
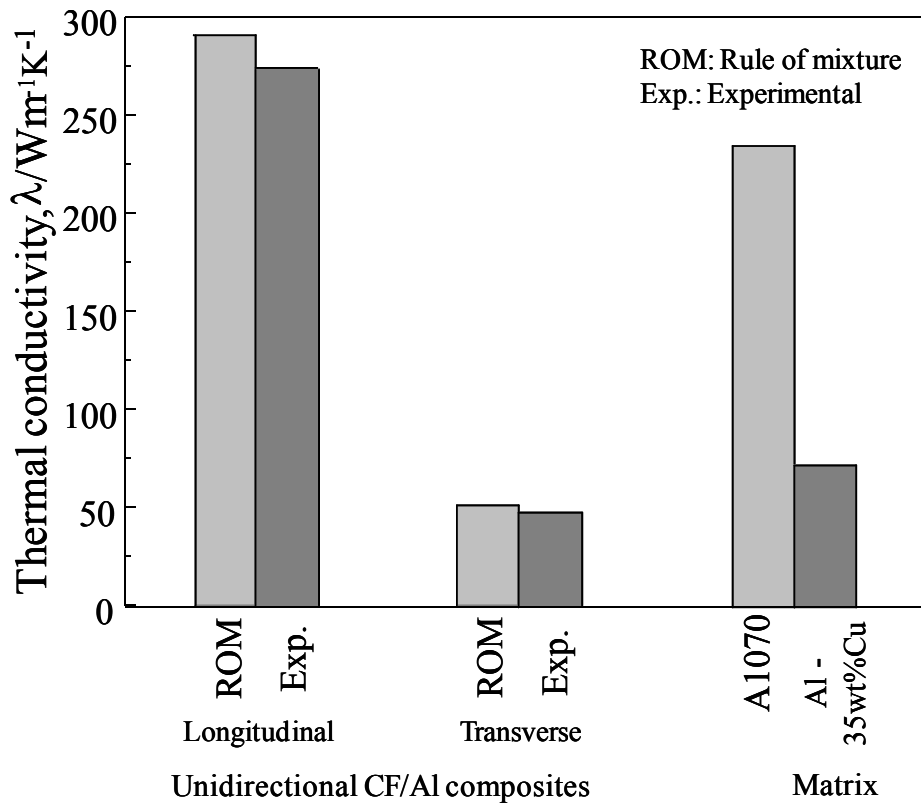
Fig. 4-15 Thermal conductivity of unidirectional CF/Al composites and matrix.

Moreover, the unidirectional CFs with high TC of 800 $Wm^{-1}K^{-1}$ is able to conduct the thermal flow most efficiently through the longitudinal direction. In the meantime, the transverse direction of CF/Al composites shows low TC of 48.0 $Wm^{-1}K^{-1}$. Although the transverse TC of K13D2U CFs was unknown from the company, that was assumed extremely low TC based on the K-1100 CFs (BP Amoco Chemicals) which had similar fiber internal structure with K13D2U CFs and represented extremely low transverse TC of 2.4 $Wm^{-1}K^{-1}$. The theoretical value of transverse TC was calculated by ROM with disregarding the transverse TC of the CFs. The experimental transverse TC was corresponding to 96 % of theoretical value. This can be explained that the heat flow was mainly conducted through the matrix. The schematic diagram for the heat flow into the CF/Al composites is shown in Fig. 4-16. One important thing is that there were not any

95

bad effects by the interfacial reactant on the TCs of both directions. From these results, it is confirmed that the short cooling time at LPI process enables to maintain high longitudinal TC of the unidirectional CF/Al composites.

(a) Longitudinal Direction   (b) Transverse Direction
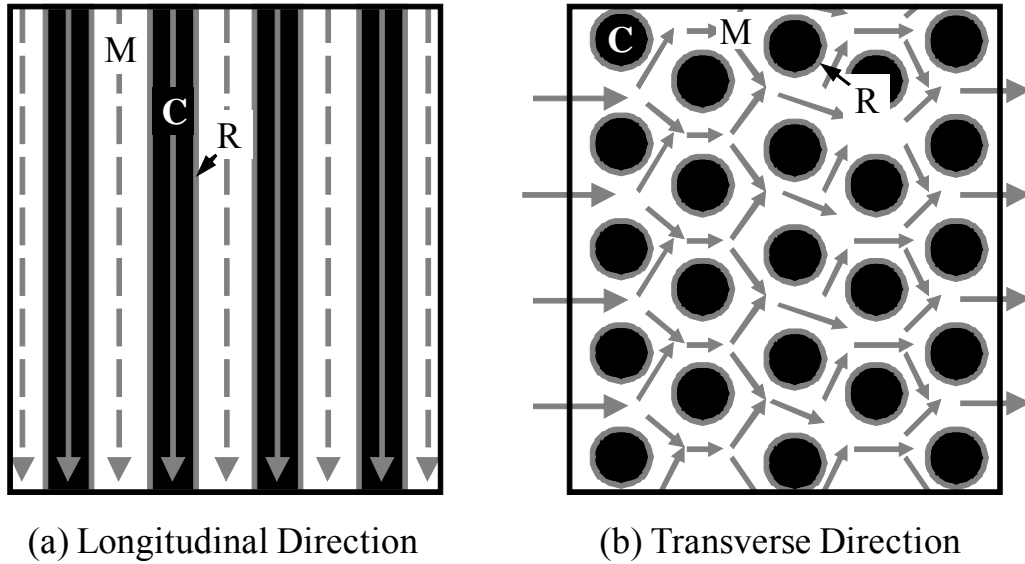
Fig. 4-16 Description of thermal conduction in (a) longitudinal and (b) transverse direction of unidirectional CF/Al composites. (C; carbon fiber, M; matrix, R; layer of reactant)

4.3.3 Coefficient of thermal expansion of unidirectional CF/Al composites

The thermal dissipation materials have been required to match their CTE with the heat generated components especially electronic parts in order to avoid the thermal history. The CTE of the unidirectional CF/Al composites was evaluated by measuring thermal strain with the strain gage method. Fig. 4-17 shows the thermal strain of CF/Al composites, as a function of exposure temperature from room temperature to 393 K. The exposure temperature was determined with the general operating temperature range of electronic components as well as strain gage. The thermal strain of soda-lime glass also measured to calculate the CTEs by the Eq (4-3). The thermal strain of soda-lime glass at the exposure temperature corresponds to CTE of 9.2×10^{-6} K^{-1}. The CTEs of the CF/Al composites were measured with the Eq. (4-3).
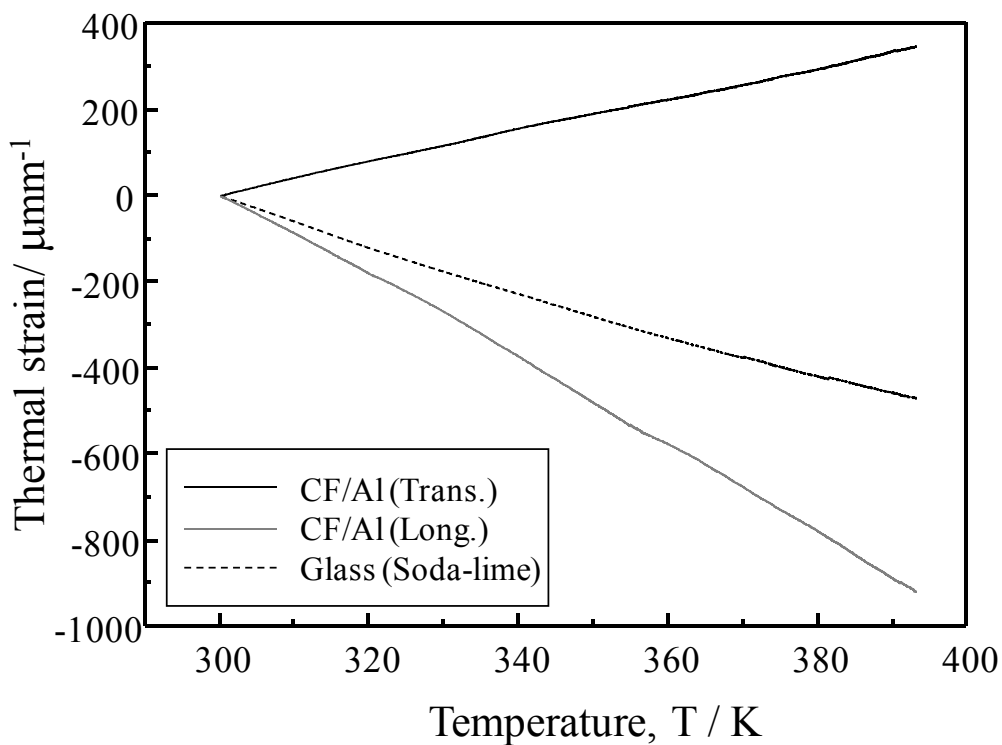
Fig. 4-17 Thermal strain of longitudinal and transverse directions of unidirectional CF/Al composites at the temperature from room temperature to 393 K.
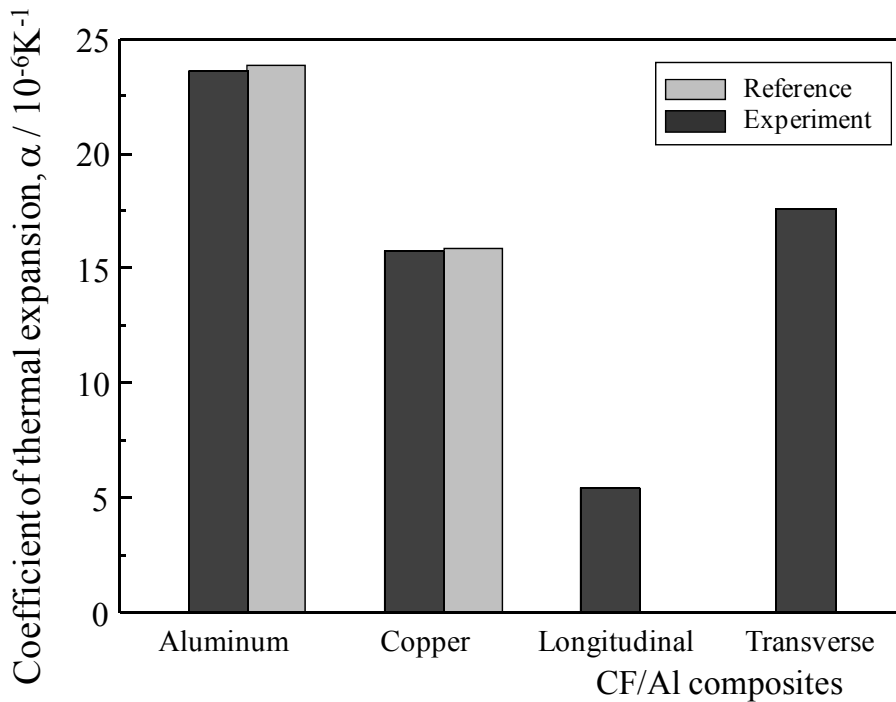
Fig. 4-18 Coefficient of thermal expansion of aluminum, copper and unidirectional CF/Al composites.

Fig. 4-18 represents the results of the measured CTEs of the CF/Al composites by the strain gage method. The thermal strain of the longitudinal direction of CF/Al composites is smaller than that of soda-lime glass, whereas the thermal strain of the transverse direction larger than that of soda-lime glass. The CTEs of Cu and Al, in particular, were also measured by strain gage method in order to compare the experimental and theoretical CTEs of them. The strain gage method for CTEs showed high accuracy on the Al and Cu. The experimental CTEs corresponded to about 98 and 95 % of theoretical values of Cu (24×10^{-6} K^{-1}) and Al 16.5×10^{-6} K^{-1}), respectively. On the other hand, the CTE of longitudinal direction of CF/Al composites represented very low value of 5.5×10^{-6} K^{-1}, meanwhile that of transverse direction showed relatively high CTE of 17.6×10^{-6} K^{-1}. There were many kinds of thermal management materials developed to apply to the highly heat generated electronic components especially semiconductors as shown in Fig. 1-1. Although the thermal dissipation materials are required high TC to exchange the generated heat efficiently, the CTE

matching with the heat generating components is primary to avoid the thermal history because the thermal history can degrade the mechanical properties of both materials. In case of the longitudinal CTE of the CF/Al composites in this study, it is well-matched with the semiconductor materials. Besides, the longitudinal TC of CF/Al composites is also excellent comparing to recently actively studied SiC/Al composites, even if the CF/Al composites had low content of the CFs such as 30 vol % and low TC of matrix. From these result, the unidirectional CF/Al composites fabricated by LPI process is expected to apply to the industrial field of thermal management materials with high TC and low cost fabrication process.

4.3.4 Mechanical property of unidirectional CF/Al composites

The strength properties of the unidirectional CF/Al composites were evaluated to consider the suitability as heat sink materials. Table 4-3 represents the flexural strength of the several commercial heat sink materials. The commercial heat sink materials showed their strength range from 159 to 500 MPa. It can be known that the heat sink materials are not required much about strength properties.

Table 4-3 Flexural strength of commercial heat sink materials

Company	A.M. Tech[50]	Nihon ceratec[51]	MMCC[52]
Material	SiC/Al	SiC/Al, SiC/Si, B_4C/Si, Al_2O_3/Al	Al MetGraf, Cu MetGraf
Flexural strength (MPa)	380 - 500	280 - 380	159 - 186

On the other hand, the evaluated strength properties of the unidirectional CF/Al composites, in this study, are listed in Table 4-4. The CF/Al composites exhibited the

99

flexural strength of 360 MPa in the longitudinal direction. Moreover, such levels of the modulus and strain in Table 4-4 can be considered sufficient as heat sink materials.

Table 4-4 Flexural properties of the unidirectional CF/Al composites

Material	Unidirectional CF/Al composites	
	K13D2U	0.3
Volume fraction	Al1070	0.6
	Pure Cu	0.1
Fabrication route	Low pressure infiltration	
Flexural srength (MPa)	360	
Flexutral strain (%)	6.2	
Modulus (Gpa)	63	

From the characterization of the thermal and mechanical properties, the unidirectional CF/Al composites fabricated by LPI process are expected to apply to the heat generation components as heat sink materials.

4.4 Summary

(1) The interfacial reaction between CF and Al in the unidirectional CF/Al composites was occurred at the infiltrating and cooling stage during LPI process. However, the generation amount of Al_4C_3 can be controlled according to changing both infiltration temperature and cooling time. Besides, the decrease of the cooling time decreased the interfacial reactant Al_4C_3, remarkably.

(2) The longitudinal TC of the unidirectional CF/Al composites significantly decreased with increasing amount of Al_4C_3 generated by increasing cooling time. In other words, the generation of Al_4C_3 affected the degradation of longitudinal TC of CFs. Moreover, the Al_4C_3 generated not uniformly but locally on the CF surfaces. The local generation of Al_4C_3 affected the surface damage of CFs due to the decrease of C content. The local radius reduction by surface damage of CFs was main reason to cause the significant decrease of longitudinal TC. On the other hand, the unidirectional CF/Al composites with the short cooling time of 10 min accomplished high TC level of 273 $Wm^{-1}K^{-1}$.

(3) The unidirectional CF/Al composites showed excellent CTE of 5.5 × 10^{-6} K^{-1} which can be suitable to applications. Moreover, the strength properties of the composites were also acceptable level for heat sink materials.

(4) The unidirectional CF/Al composites fabricated by LPI process are expected to apply to the heat generation components as heat sink materials with the advantages of the thermal and mechanical properties.

References

[1] C. Zweben: JOM, **44** (1992) 15-23.

[2] J.M. Molina, J. Narciso, L. Weber, A. Mortensen, E. Louis: Mater. Sci. Eng. A, **480** (2008) 483-488.

[3] Y. B. Choi, G. Sasaki, K. Matsugi, O. Yanagisawa: Mater. Trans., **46** (2005) 2156-2158.

[4] Y. B. Choi, G. Sasaki, K. Matsugi, N. Sorida, S. Kondoh, T. Fujii, O. Yanagisawa: J SME A, **49** (2006) 20-24.

[5] Y. B. Choi, K. Matsugi, G. Sasaki, K. Arita, O. Yanagisawa: Mater. Trans., **47** (2006) 1227-1231.

[6] Y. B. Choi, K. Matsugi, G. Sasaki, S. Kondoh: Mater. Trans., **49** (2008) 390-392.

[7] K. Matsugi, Y. B. Choi, K. Arita, O. Yanagisawa, G. Sasaki: J. Jpn. Inst. Light Met., **58** (2008) 71-80.

[8] I. H. Khan: Metall. Trans. A, **7** (1976) 1281-1289.

[9] G. H. Rinehart, R. G. Behrens: J. Chem. Thermodynamics, **12** (1980) 205-215.

[10] A. Okura, K. Motoki: Compo. Mater. Tech., **24** (1985) 243-252.

[11] M. Yang, V. D. Scott: Carbon, **29** (1991) 877-879.

[12] S. G. Warrier, R. Y. Lin: Scripta Metal. Mater., **29** (1993) 1513-1518.

[13] M. V. Gurjar, G. S. Murty, G. S. Upadhyaya: J. Mater. Sci. **28** (1993) 5654-5657.

[14] M. D. Sanctis, S. Pelletier, Y. Bienvenu, M. Guigon: Carbon, **32** (1994) 925-930.

[15] C. Qiu, R. Metselaar: J. Alloy. Compd., **216** (1994) 55-60.

[16] H. -D. Steffens, B. Reznik, V. Kruzhanov, W. Dudzinski: J. Mater. Sci., **32** (1997) 5413-5417.

[17] M. H. Vidal-Sétif, M. Lancin, C. Marhic, R. Valle, J. -L. Raviart, J. -C. Daux and M. Rabinovitch: Mater. Sci. Eng. A, **272** (1999) 321-333.

[18] M. Lancin, C. Marhic: J. Euro. Cera. Soc., **20** (2000) 1493-1503.

[19] E. Pippel, J. Woltersdorf, M. Doktor, J. Blucher, H. P. Degischer: J. Mater. Sci., **35** (2000) 2279-2289.

[20] S. Li and C. -G. Chao: Metall. Mater. Trans. A, **35** (2004) 2153-2160.

[21] S. -H. Li, C. -G. Chao: Metall. Trans. A, **35** (2004) 2153-2160.

[22] A. N. Streletskii, I. V. Povstugar, A. B. Borunova, S. F. Lomaeva, Pu. Y. Butyagin: Colloid Journal, **68** (2006) 470-480.

[23] A. N. Streletskii, S. N. Mudretsova, I. V. Povstugar, Pu. Y. Butyagin: Colloid Journal, **68** (2006) 623-631.

[24] M. Besterci: Mater. Design, **27** (2006) 416-421.

[25] T. Etter, P. Schulz, M. Weber, J. Metz, M. Wimmler, J. F. Löffler, P. J. Uggowitzer: Mater. Sci. Eng. A, **448** (2007) 1-6.

[26] B. Bhav Singh and M. Balasubramanian: . J. Mater. Proc. Tech., **209** (2009) 2104-2110.

[27] S. Kanagaraj, S. Pattanayak: Cryogenics, **43** (2003) 399-424.

[28] D. Bijl, H. Pullan: Physica., **21** (1955) 285-298.

[29] J. R.G. Keyston, J. D. Macpherson, E. W. Guptill: Rev. Sci. Instrum., **30** (1959) 246-248.

[30] R. F. Robbins, D. H. Weitzel, R. N. Herring: Adv. Cryog. Eng., **7** (1962) 343-352.

[31] R. H. Carr, C. A. Swenson: Cryogenics, **4** (1964) 76-82.

[32] M. D. Campbell: Adv. Cryog. Eng., **10** (1965) 154-162.

[33] W. O. Hamilton, D. B. Greene, D. E. Davidson: Rev. Sci. Instrum., **39** (1968) 645-648.

[34] J. D. Foster, I. Finnie: Rev. Sci. Instrum., **39** (1968) 654-657.

[35] N. Waterhouse, B. Yates: Cryogenics, **8** (1968) 267-271.

[36] A. F. Clark: Cryogenics, **8** (1968) 282-289.

[37] F. N. D. D. Pereika, C. H. Barnes, G. M. Graham: J. Appl. Phys., **41** (1970) 5050-5054.

[38] G. K. White, J. G. Collins: J. Low Temp. Phys., **7** (1972) 43-75.

[39] F. R. Kroegner, C. A. Swenson: J. Appl. Phys., **48** (1977) 853-864.

[40] H. N. Subrahmanyam, S. V. Subramanyam: Pramana- J. Phys., **27** (1986) 647-660.

[41] S. S. Tompkins, D. E. Bowles, W. R. Kennedy: Exp. Mech., **26** (1986) 1-6.

[42] G. Schwarz: Cryogenics, **28** (1988) 248-254.

[43] G. Schwarz, F. Krahn, G. Hartwig: Cryogenics, **31** (1991) 244-247.

[44] M. Okaji, N. Yamada, K. Nara, H. Kato: Cryogenics, **35** (1995) 887-891.

[45] M. Rotter, M. Muller, E. Gratz, M. Doerr M. Loewenhaupt: Rev. Sci. Instrum., **69** (1998) 2742-2746.

[46] M. D. Strycker, L. Schueremans, W. V. Paepegem, D. Debruyne: Optic. Laser. Eng., **48** (2010) 978-986.

[47] F. L. Scalea: Experi. Mechanic., **38** (1998) 233-241.

[48] Vishay Micro-Measurements: Strain gage thermal output and gage factor variation with temperature. Technical Note tn-504-1 (2007).

[49] Vishay Micro-Measurements: Measurement of thermal expansion coefficient using strain gages. Technical Note tn-513-1 (2007).

[50] A.M. Tech Co., Ltd., Japan, Available at. http://www.amtech.co.jp/sitemap.htm (Accessed 11.11.04).

[51] Nihon Ceratec Co., Ltd., Japan, Available at. http://www.ceratech.co.jp/product/ 01 _03.html (Accessed 11.11.04).

[52] MMCC, LLC., USA, Available at. http://www.mmccinc.com/APIC.htm (Accessed 11.11.04).

Conclusions

The purpose of this thesis is to develop the unidirectional CF/Al composites of high thermal conductivity with the cost effective fabrication process, in order to replace the conventional heat sink materials applying to the high heat generation components. In this study, the unidirectional CF/Al composites were fabricated by low pressure infiltration process which enables complex/large shape and cost saving fabrication. Besides, the fabrication conditions for the unidirectional CF preform and CF/Al composites were investigated to accomplish the high performance. Meanwhile, the influence of the CF-Al interfacial reaction on the thermal conductivity of unidirectional CF/Al composites was examined. Moreover, the suitability of the unidirectional CF/Al composites for the heat sink materials was evaluated in conjunction with the characterization of their thermal and mechanical properties. The conclusions of this thesis are summarized as follows:

1. The study on the fabrication route and conditions for the high performance unidirectional CF preform and CF/Al composites (Chapter 2, 3)

Prior to the fabrication of unidirectional CF/Al composites by the low pressure infiltration process, the decision of the fabrication conditions for the unidirectional CF preform by spark sintering process was studied. The Cu particles were selected as spacers between CFs to maintain the porous CF arrays for the smooth infiltration of molten Al into the preform and appropriate compressive strength against the applied infiltration pressure. Moreover, the appropriate sintering temperature led to accomplish

both excellent fiber bridging and Cu coating on the CFs. From these results, the unidirectional CF preform possessed the proper strength against the infiltration pressure and an advantage of wettability to Al infiltration hence it enabled the fabrication of unidirectional CF/Al composites by low pressure infiltration.

In the low pressure infiltration process, the variables such as capillary resistance pressure, internal friction, back pressure, gravity were considered to predict the initial infiltration pressure. The infiltration of molten Al into the CF preform initiated over the calculated infiltration pressure and was invigorated with increasing pressure. However, non-uniform distribution of CF arrays disturbed the smooth infiltration. Thus, the appropriate sizes of the Cu particles for the uniform distribution of CF arrays were considered. However, the addition of the nearly theoretical Cu sizes for the uniform distribution of CF arrays was not completely resolved the non-uniform distribution in the practical fabrication step. The newly decided sizes of Cu particles reflected both theory and practice, as a countermeasure to prevent such CF clustering, permitted the uniform distribution of the CF arrays and high density of the unidirectional CF/Al composites. From these results, the unidirectional CF/Al composites with the high density and uniform CF distribution could be obtained by the low pressure infiltration process of 0.8 MPa.

2. The influence of the CF-Al interfacial reactants on the thermal conductivity of the unidirectional CF/Al composites. (Chapter 4)

The generation of the CF-Al interfacial reactants Al_4C_3 was reported at the exposure temperature above 773 K. Thus, the generation of Al_4C_3 was considered at the 'infiltration process' and 'cooling process' in low pressure infiltration process. The growth amount of Al_4C_3 was derived by measurement of the activation energy at the 'infiltration process' and experiment of the weight loss of CFs from the 'cooling process'. Especially, the amount of Al_4C_3 was remarkably controlled by controlling the cooling time. However, the increase of Al_4C_3 amount led to decrease the longitudinal thermal conductivity of unidirectional CF/Al composites significantly. It was confirmed that the locally generated Al_4C_3 narrowed the local diameters of the CFs, thus the thermal flow

through the high thermal conductivity CFs was disturbed. On the other hand, the thermal conductivity of the unidirectional CF/Al composites exhibited high levels by reducing the cooling time at the 'cooling process'.

3. The study on the thermal expansion and mechanical properties of the unidirectional CF/Al composites. (Chapter 4)

The longitudinal direction of the unidirectional CF/Al composites showed very low coefficient of thermal expansion which can be matched to high heat generation components such as semiconductors avoiding thermal stress. Moreover, their flexural strength also exhibited the stable levels as heat sink materials. In other words, the unidirectional CF/Al composites by low pressure infiltration achieved high thermal conductivity with matching the coefficient of thermal expansion and appropriate mechanical properties to high heat generated applications.

From these comprehensive results, the unidirectional CF/Al composites are look forward to replace the conventional materials in the field of thermal management.